AN INTEGRATED APPROACH FOR TRANSPORTATION FUELS PRODUCTION: FAST PYROLYSIS AND BIO-OIL ELECTROCATALYTIC UPGRADING

By

Zhenglong Li

A DISSERTATION

Submitted to
Michigan State University
in partial fulfillment of the requirements
for the degree of

DOCTOR OF PHILOSOPHY

Biosystems Engineering
Chemical Engineering

2012

ABSTRACT

AN INTEGRATED APPROACH FOR TRANSPORTATION FUELS PRODUCTION: FAST PYROLYSIS AND BIO-OIL ELECTROCATALYTIC UPGRADING

By

Zhenglong Li

Fast pyrolysis is a thermochemical approach for biomass liquefaction in which biomass is heated without oxygen to produce pyrolysis gas and char. The majority of the pyrolysis gas can be condensed to bio-oil with a bulk density greater than the feedstock biomass. Deployment of fast pyrolysis near the source of harvest will increase bulk density and reduce the cost of transportation prior to upgrading in a central refinery. However, bio-oil corrosiveness and reactive instability pose significant barriers to the adoption of pyrolysis systems. Catalytic stabilization is needed to produce an energy dense fuel intermediate that is compatible with common infrastructure materials such as carbon steel. Several catalysis approaches, including hydrotreatment and catalytic cracking, are being considered to stabilize and upgrade bio-oil. However, these approaches face high cost, catalyst deactivation and the high cost of producing molecular hydrogen in the regional biomass processing depots. In this context, electrocatalytic hydrogenation (ECH) is proposed to stabilize bio-oil by hydrogenation with *in situ* atomic hydrogen created by reducing protons in the electrolyte solution. Instead of fossil-based electricity, solar or wind energy can be employed to supply the reducing equivalent. The energy contents of the liquid products are enhanced by addition of solar or wind reducing equivalent. Moreover, this method allows bio-oil stabilization at very mild conditions (25-100°C, 1atm), with little to no evidence of catalyst deactivation.

In this dissertation, a 1 Kg/hr screw-conveyor fast pyrolysis reactor was designed and

operated to produce bio-oil from poplar biomass. Bio-oil from this reactor was characterized by GC/MS, HPLC, size exclusion chromatography, proximate analysis and ultimate analysis. Bio-oil stability was also studied by performing an accelerated aging test at 80°C. Stabilization of the bio-oil was then investigated using electrocatalytic hydrogenation. The transformation of a bio-oil model compound, furfural, was studied using a nickel sacrificial anode in an undivided cell. Product yields and electrochemical efficiency as functions of electrode type, pH, reactant concentration and current density were examined. To further upgrade the phenolic compounds, a new electrocatalyst, ruthenium supported on activated carbon cloth (Ru/ACC), was invented. The effects of electrode type, electrolyte composition, support property, temperature and current density were investigated. Reaction network was also studied and compared with catalytic hydrodeoxygenation of guaiacol. This catalyst was used to perform electrocatalytic stabilization of water-soluble bio-oil. The majority of the carbonyl groups were hydrogenated to the related alcohols. After the electrocatalytic hydrogenation treatment, bio-oil became more stable compared with the bio-oil without electrocatalytic stabilization. The outcome of this research reveals an advanced understanding of integrated fast pyrolysis and ECH systems for bio-oil stabilization. Pyrolysis followed by electrocatalytic hydrogenation shows significant potential for creating a stable bio-oil that is suitable for further upgrading at central refineries. This integrated approach can help solve the energy deficiency, biomass supply and bio-oil upgrading challenges.

Dedicated to my family.

ACKNOWLEDGEMENTS

I would love to express my sincerest gratitude to my advisor, Dr. Chris Saffron, for his strong support during this work and for his guidance in my future research career. I also want to thank Dr. James Jackson to be a great mentor during the entire project. The guidance and support from him are greatly acknowledged. Thanks to my co-advisor in Chemical Engineering, Dr. Dennis Miller, for his strong support in my work. I would also like to thank Dr. Wei Liao for the guidance and serving as my Ph.D. committee member.

Special thanks to group members and friends Shantanu Kelkar, Mahlet Garedew, Lauren Raycraft, Chai Li, Jon Bovee, Tom Stucken, Dr. Lars Peereboom, Xianfeng Ma, Dr. Ambareesh Murkute, Chun Ho Lam, Dr. Mikhail Redko and Souful Bhatia for their help during this work.

I would love to offer my heartfelt thanks to my wife, my parents and my whole family for their support during my education and my life.

TABLE OF CONTENTS

LIST OF TABLES

LIST OF FIGURES

LIST OF SCHEMES

Chapter 1 Introduction and Background

1.1 Introduction

Renewable energy plays an increasingly important role in enhancing the energy security and solving the environmental problems caused by traditional fossil fuels. Bioenergy is one potential renewable energy source to provide the energy needs for both developing and developed areas in the world.[1] Due to the carbon neutral or carbon negative benefits of bioenergy, it can contribute greatly to reducing greenhouse gas emissions and alleviating global warming.

According to U.S. Energy Information Administration, about 1 billion tons/year of oil was used in U.S. in 2010.[2] Assuming the energy content of the oil is 45 MJ/Kg, the total energy content of the oil consumed is 4.5×10^{13} MJ/year. According to the billion ton vision of DOE, about 1.5 billion tons/year of non-food biomass can be used for bioenergy, including agricultural residues, forestry residues and energy crops.[3] If the biomass energy content is estimated as 15 MJ/Kg, the total energy content of the biomass is 2.3×10^{13} MJ/year. Even if we assume 100% energy conversion during biomass utilization, the energy content of the biomass is just about half of that from the consumed oil. To displace the petroleum oil with biofuel in the future, we need to enhance the energy content of the biofuel by using other renewable resources, such as solar and wind. These renewable energy techniques can be integrated with bioenergy to produce hydrocarbon fuels.

Low bulk density and dispersed geographic distribution pose additional barrier to the adsorption of bioenergy systems. These bring difficulty for biomass collection and high transportation cost is required for long distance delivery to central refineries. High land use

and high storage cost are also required.[4] It is essentially critical to solve this biomass supply issue for biofuels development. Regional biomass processing depots (RBPDs) have been proposed to solve this biomass supply challenge.[4] Fast pyrolysis, a thermochemical conversion method, can convert biomass to a liquid product (bio-oil) at about 500°C in the absence of oxygen. Due to much higher density of the bio-oil compared to biomass, fast pyrolysis can be used in the RBPDs to convert biomass to bio-oil, resulted in reduced transportation and storage costs.[5] Deployment of fast pyrolysis near the source of biomass harvest will also ease the collection of biomass.

Bio-oil, the liquid product from fast pyrolysis, is reactive and unstable because of the presence of carboxylic acids, aldehydes, ketones and phenols. Bio-oil polymerizes during its storage even at room temperature, causing problems for further upgrading, such as coke formation and catalyst deactivation. Carboxylic acids existing in the bio-oil also corrode metal surfaces. This requires high cost materials for storage and transportation. Thus stabilization and neutralization of bio-oil are required before transport to the central refinery. Recently low temperature hydrogenation using hydrogen has been used to stabilize bio-oil and works as the first-stage upgrading ahead of a high temperature deoxygenation. However, this low temperature hydrogenation still employs temperatures (125-175°C) that are high enough to cause bio-oil polymerization.[6] These conditions also result in a significant loss of carbon to the gas phase and reduce the carbon yield of the final liquid products. Hydrogen is another issue because: 1) currently it is a fossil-based reducing agent. Since the goal is to replace the petroleum oils, fossil based reducing agents should be avoided; 2) hydrogen production is expensive and thus it may not be available in the regional biomass processing

depots. To effectively stabilize bio-oil in the RBPDs, a new method should be explored to provide a much milder condtion and use alternative reducing equivalent instead of hydrogen.

To solve the aforementioned energy deficiency, biomass supply and bio-oil upgrading issues, we propose a new biofuels development approach, integration of fast pyrolysis and electrocatalytic hydrogenation for bio-oil stabilization/partial upgrading. Biomass is first converted to a high bulk density bio-oil in the RBPDs by fast pyrolysis; electrocatalytic hydrogenation is used to upgrade the bio-oil to a stable fuel intermediate, which can be used directly or can be further upgraded with electrocatalytic hydrodeoxygenation in the central refinery. Electricity from solar or wind energy is employed as the reducing agent to avoid the use of fossil-based hydrogen. Using this method, the energy content of the biofuel is enhanced by adding energy from solar or wind. Moreover, this method allows bio-oil stabilization at very mild conditions (25-100°C, 1atm). Thus bio-oil polymerization and carbon loss to the gas products can be greatly reduced under these conditions.

1.2 Research objectives

(1) Design, build and test a screw-conveyor fast pyrolysis reactor; characterize bio-oil using GC/MS, HPLC, size exclusion chromatography, proximate analysis and ultimate analysis; assess bio-oil stability by performing aging studies;

(2) Develop catalysts to study electrocatalytic hydrogenation and hydrodeoxygenation of bio-oil model compounds, including furfural and phenolic compounds;

(3) Perform stabilization and upgrading of bio-oil with electrocatalytic hydrogenation.

1.3 Fast pyrolysis

1.3.1 Principles

Fast pyrolysis usually happens at moderate temperature (450-550°C), ambient pressure [7] and in the absence of oxygen, generating three products: bio-oil, non-condensable gas and char. Important characteristics of fast pyrolysis include:[1] 1) pyrolysis reaction temperature should be carefully kept at around 500°C; 2) heat transfer rates should be high enough, which usually requires biomass feed particle size smaller than 2mm;[8] 3) vapor residence time should be less than one second; 4) the pyrolysis vapor should be rapidly cooled down to low temperature, such as -10°C.

Bio-oil, char and non-condensable gas are the three generated products of fast pyrolysis processes. The mass yields of these three products are usually 60-75 wt %, 15-25 wt %, and 10-20 wt %, respectively. The yields vary among different biomass feedstock. This process does not generate any waste, because the non-condensable gas can be burned to provide heat for this process, and bio-oil and char can potentially be sold as commercial fuels.[9]

1.3.2 Fast pyrolysis reactors

A wide range of reactor configurations have been operated, including fluidized-bed reactor, circulating fluidized-bed reactor (CFB), transported bed reactor, rotating cone reactor, ablative reactor, auger reactor, vacuum moving bed reactor and entrained flow reactor, etc (Table 1.1) . Among these reactors, fluidized-bed reactor and circulating fluidized-bed reactor are the most popular configurations due to their ease of operation and ready scale-up. However, these two types of reactors require a heat transfer medium (sand) to increase the

heat transfer rate and need high amounts of inert gas to fluidize the biomass. The operation cost is increased due to energy input for heating the sand and the cost from using inert gas.

Table 1.1 Overview of fast pyrolysis reactor characteristics for bio-oil production[1]

Property	Status	Bio-oil (wt%)	Complexity	Feed size	Inert gas need	Specific size	Scale Up
Fluid bed	Comm	75	Medium	Small	High	Medium	Easy
CFB	Pilot	75	High	Medium	High	Large	Easy
Entrained	None	65	High	Small	High	Large	Easy
Rotating cone	Demo	70	High	Very small	Low	Small	Medium
Ablative	Lab	75	High	Large	Low	Small	Hard
Vacuum	Demo	60	High	Large	Low	Large	Hard

Comm: commercial (>3000 Kg-h^{-1}). Demo: demonstration (300-3000 Kg-h^{-1}). Pilot: pilot plant (30-300 Kg-h^{-1}). Lab: laboratory (1-30 Kg-h^{-1}).

1.3.3 Bio-oil characterization

Bio-oil is a complicated mixture of organic acids, aldehydes, ketones, alcohols, phenols, esters, furans, sugars and many other oxygenated compounds. It requires to be characterized physically and chemically in order to identify the bio-oil quality and carry out further upgrading. Some researches for physcial and chemical characterization of bio-oil are discussed below.

Extensive research on analyzing physical properties of bio-oil has been carried out since the 1980s at PNNL, NREL, and former British Columbia Research, Canada.[10] Table 1.2 shows the typical properties of wood pyrolysis bio-oil. Compared with heavy fuel oil, bio-oil contains more water, higher oxygen content, lower heating value and low pH.

Complete chemical composition of bio-oil is very difficult because it contains more than 400 compounds. Until now, there is no precise description of the bio-oil composition, so

that it is very hard to understand detailed bio-oil chemical changes during upgrading.

Table 1.2 Typical properties of wood pyrolysis bio-oil and heavy fuel oil [6]

Property		Pyrolysis oil	Heavy fuel oil
Moisture content, wt%		15-30	0.1
pH		2.5	
Specific gravity		1.2	0.94
Element composition, wt%	Carbon	54-58	85
	Hydrogen	5.5-7.0	11
	Oxygen	35-40	1.0
	Nitrogen	0-0.2	0.3
Ash		0-0.2	0.1
Higher heating value, MJ/Kg		16-19	40
Viscosity (50°C), cP		40-100	180
Solids, wt%		0.2-1	1
Distillation residue, wt%		Up to 50	1

According to Garcia-Perez, bio-oil contains "around 20 mass percent of water, around 40 mass percent of GC-detectable compounds, around 15 mass percent of non-volatile HPLC detectable compounds and around 15 mass percent of high molecule weight non-detectable compounds."[11] Due to the complexity of bio-oil, chemical analysis requires the combined use of more than one analytical technique. The analytical methods usually include: "GC-MS (volatile compounds), HPLC (nonvolatile compounds), Fourier transform infrared spectroscopy (FTIR) (functional groups), gel permeation spectroscopy (GPC) (molecular weight distributions), nuclear magnetic resonance (NMR) (types of hydrogen or carbon in specific structural groups, bonds)".[9] "Matrix assisted laser desorption ionization time-of-flight mass spectrometry (MALDI-TOF-MS), laser desorption/ionization time-of-flight mass spectrometry (LDI-TOF-MS), and pyrolysis field ionization mass spectrometry (Py-FIMS)" are used to evaluate the molar mass characteristics of the water-insoluble fraction.[12]

Bio-oil compounds have a wide range of properties, varying from non-polar to polar,

from small molecule to large molecule and from volatile to nonvolatile. Fractionation is usually needed to separate bio-oil into different fractions to carry out the chemical characterization. Garcia-Perez et al.[11] developed a method to categorize the chemical composition of bio-oils into eight chemical families. Bio-oils were extracted using various solvents, including toluene, methanol, water, dichloromethane and diethylether. Six fractions were obtained and several techniques, including GC-MS, TGA and GPC, were used to characterize these fractions. This procedure clearly described bio-oil composition as a mixture of "water, monolignols, polar compounds with moderate volatility, sugars, extractive-derived compounds, heavy polar and non-polar compounds, methanol-toluene insolubles and volatile organic compounds."[11] Sipila et al.[13] fractionated bio-oil with water first and extracted the water-soluble fraction using diethyl ether. The relationship between the physical characteristics and chemical compositions of the bio-oil was established. The pH was affected mainly by volatile acids and diluting effect of water. Higher water content, lower proportion of water-insoluble fraction and the presence of alcohols resulted in lower viscosity. The pour point was lower for lower amount of water-insoluble fraction and higher total amount of volatiles and water.

1.4 Bio-oil stability and evaluation methods

Bio-oil stability is an important aspect to be considered during fast pyrolysis research. Two types of stability have been studied, thermal stability and oxidative stability. To evaluate bio-oil stability, various researchers have measured viscosity, molecular weight distribution, water content and the content of carbonyl groups.

1.4.1. Bio-oil thermal stability

Thermal stability is measured by storing bio-oil in a container (closed or open) for a period of time at a specific temperature (up to 90°C). Samples are taken during storage, and samples are analyzed to evaluate changes. The container to store the bio-oil can be open or closed. In open containers, the evaporation of small molecules will result in viscosity changes. Exposure to oxygen can also accelerate aging. The storage temperature is another important variable to consider when performing stability measurements as it has great effect on the thermal stability and it will determine how long the storage will be. If the storage is at room temperature, at least several months are needed, while only several days are required for 90°C. According to Oasmaa et al.[10], in order to observe significant viscosity changes, bio-oils are stored for 12 months, 12 months, 2 months and 1 week for storage temperature 20°C, 35°C, 50°C and 80°C, respectively. When the temperature reaches 80°C, only 1 week is needed, and this is called accelerated aging test.[14]

(1) Viscosity measurement

Stability can also be evaluated by measuring the change in viscosity during storage. Several different equipments have been used, e.g., Bohlin rheometer with the coaxial cyclinders geometry[14] and Brookfield digital viscometer.[15, 16] As bio-oil polymerizes, viscosity will increase, but the increasing rate is different for different biomass varieties,[17] different storage temperatures and different viscosity measurement temperatures.[14] Bio-oil from manure has an aging rate of 1.3 cP/day, while bio-oil from a mixture of 50% manure and 50% pine wood aged at 7.3 cP/day when stored at room temperature and measured at 60°C.[17] The storage temperature also influences the aging rate. As shown in the paper from

Boucher et al.,[14] the aging rate changed from 0.42 cP/day to 29.79 cP/day as the storage temperature increased from 40°C to 80°C. The viscosity measurement temperature is very important because the aging rate is a function of the measurement temperature. As shown by Boucher et al.,[14] the aging rate at 30 °C is 0.50 cP/day, while it decreases to 0.47 cP/day and 0.11 cP/day at 50°C and 80°C with the storage temperature at 40°C.

For the accelerated aging test, there is a concern about losing volatiles during sample transfer, so a real-time viscosity measurement was carried out in a pressure cell-fitted rheometer.[18] This method was proved to give similar results to the traditional method that analyzes samples after the aging was completed.

(2) Molecular weight distribution

The molecular weight distribution of the bio-oil can be measured by gel permeation chromatography (GPC) using ultraviolet (UV) or refractive index (RI) detector.[11] Carbohydrate and lignin fractions can be detected with UV and RI detectors, repectively. Usually more than two columns are used in series to get an accurate large range of distribution.[15] Average molecular weight can be calculated to compare the weight distribution of different samples.

(3) Chemical characterization during bio-oil aging

Chemical reactions are responsible for bio-oil aging, such as reactions between aldehydes and phenols, acids with alcohols.[19] During bio-oil aging tests, chemical characterization is necessary to understand the chemical changes. Because of the complexity of bio-oil, fractionation methods have been used to characterize the changes during bio-oil storage.[20, 21] Bio-oil is first extracted with water to form water-soluble and water-insoluble

fractions. The water-insoluble fraction was further extracted with dichloromethane, while the water-soluble fraction was extracted using diethyl ether. The evaporation residues were used as the weight for each fraction. During 12 months of storage at 9°C of forestry residue bio-oil, high-molecular-mass lignin fraction of the water-insoluble fraction increased, while the sugar and ether-soluble fractions decreased. Solid phase separation of bio-oil can also be used to evaluate chemical changes with silica gel and five solvents (pentane, benzene, dichloromethane, ethyl acetate and methanol).[22]

GC/MS, GC/FID, HPLC,[23] NMR[24] and FTIR[25,26] can be used to study chemical changes. Oasmaa and Kuoppala [20] showed that aldehydes and ketones decreased significantly during 12 months storage of forestry residue bio-oil. Oasmaa et al.[27] shows the chemical changes by GC/FID during bio-oil storage at -16.5°C, 9°C and 22°C for 4 years. Acetaldehyde, methanol, glycoaldehyde, furfural and 5-(hydroxymethyl) furfural show the most significant changes.

Among the functional groups existing in bio-oil, carbonyl groups are the most reactive ones and change greatly during bio-oil aging. Analysis of the carbonyl group is usually performed by oximation with hydroxylamine hydrochloride in pyridine followed by titration of the pyridinium hydrochloride with a 1.0 N standardized NaOH solution using a dosimat.[28] Moens et al.[28] show that bio-oil typically has 4-6 mol carbonyl groups per Kg of bio-oil using this method. Carbonyl content exhibits a linear relationship with viscosity, thus its measurement is a good indicator of bio-oil stability.[27]

(4) Water content

Many condensation reactions occur during bio-oil polymerization, that releases water

as a byproduct. Therefore, an increase of water content may be another indicator of bio-oil aging. According to Oasmaa and Kuoppala,[20] pine and brown forestry residue bio-oil produced more water than green forestry residue bio-oil during storage.

(5) Microstructure evolution

Pyrolytic lignin has important relationship with bio-oil stability. Fratini et al.[29] applied small-angle neutron scattering (SANS) to detect the microstructural changes during bio-oil storage. Lignin oligomers polymerize during storage, and this process continues until the heaviest lignin-rich fraction separates out as a viscous sludge. Usually the polymerization occurs during the first 6-7 months of aging, but the sludge formation typically happens after one year of storage, depending on the water content.

1.4.2. Bio-oil oxidative stability

Besides the thermal stability, oxidative stability is used to evaluate bio-oil stability.[30] The oxidative stability can be assessed by measuring solids formation or oxidation onset temperature (OOT). In the first method, a known amount of pre-filtered bio-oil in a pressure vessel is pressurized to 800 kPa with oxygen and heated to 90°C for 16 h. The amount of insolubles formed is used to determine the stability. In the second method, a bio-oil sample is tested in a differential scanning calorimetry (DSC) to determine the oxidation onset temperature. The samples with higher OOT are more stable.

1.5 Bio-oil stabilization

Chemical reactions of abundant unsaturated chemicals have been proposed as a main reason for bio-oil instability, such as, polymerization, esterification and etherification. These reactions increase bio-oil viscosity and molecular weight. To increase the stability of bio-oil,

several methods have been used, including adding methanol, filtration and low temperature hydrogenation.

Methanol or short chain alcohols can be added into bio-oil to reduce bio-oil aging.[15] Boucher et al.[14] found that stability of bio-oil can be greatly increased by adding methanol. The dissolution of some structured components by methanol was explained as the reason for increasing bio-oil stability. Reaction of methanol with the reactive components in bio-oil was proposed as another reason to reduce bio-oil aging using methanol.[15] Methanol can react with the oligomers, terminate the chain reaction and prevent viscosity increase. It can also react with aldehydes or ketones to form acetals and ketals, and the latter are more stable.

Char or minerals in the char can catalyze bio-oil polymerization and cause a viscosity increase.[19] Filtration of fine char particles using microfiltration and nanofiltration was tested as a method to stabilize bio-oil.[31] With microfiltration, char particles above 1 um can be removed, thus ash content was reduced. However, microfiltration did not improve the bio-oil stability. Nanofiltration of bio-oil with 5 nm pore size membrane was shown to work for bio-oil stabilization probably due to the reduction in the average molecular weight of bio-oil and the reduction in the concentration of oligomers.

Low temperature hydrogenation was another effective method for bio-oil stabilization.[6] With hydrogenation, most of the C=O groups can be reduced to CH-OH groups, which are more thermally stable. However, a relatively high temperature is needed (125-175°C) when using a heterogeneous catalyst for hydrogenation.[6] To carry out hydrogenation under milder conditions, homogeneous ruthenium catalysts have been used to hydrogenate bio-oil at 90°C and 40 bar.[32]

A thorough literature search showed that there is no report on electrocatalytic stabilization or upgrading of bio-oil. The use of ECH provides a new method for bio-oil stabilization and upgrading at very mild conditions.

1.6 Electrocatalytic hydrogenation

1.6.1 Principle of electrocatalytic hydrogenation

As shown in Scheme 1.1, there are several steps involved in electrocatalytic hydrogenation, including atomic hydrogen generation, adsorption of organic compounds, hydrogenation and desorption of the hydrogenated products. Hydrogen evolution is competitive with electrocatalytic hydrogenation, which affects the electrochemical efficiency (the electrons used for products generation/total electrons passed).

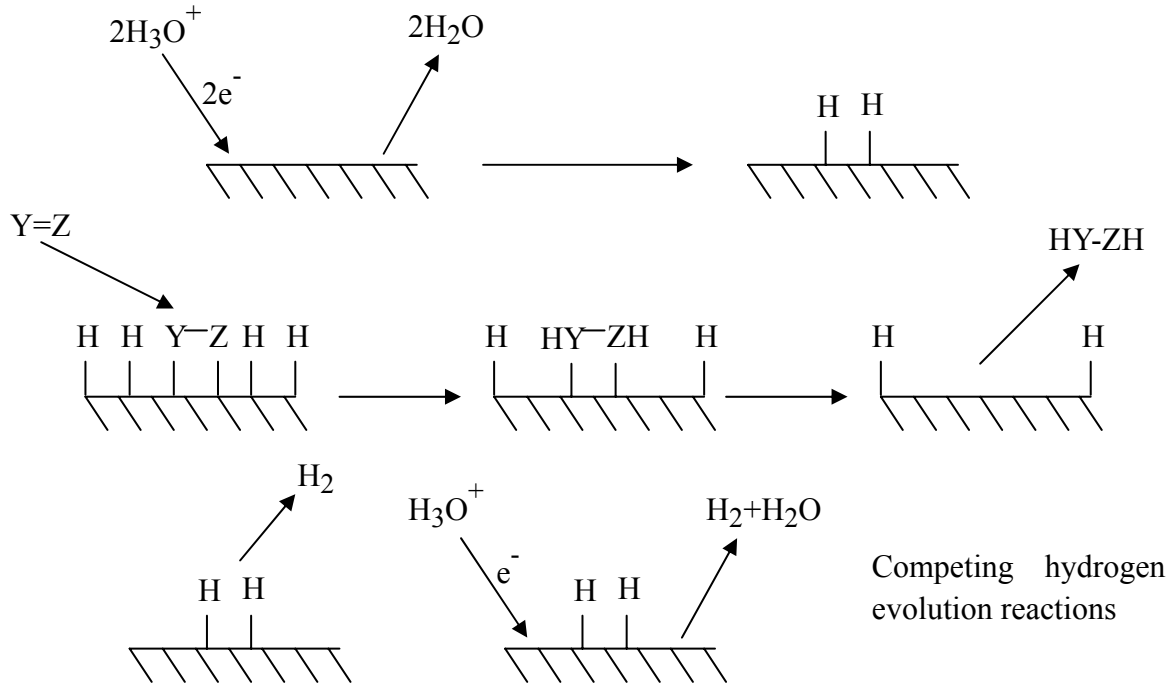

Scheme 1.1 Electrocatalytic hydrogenation and competitive hydrogen evolution. Data was taken from reference 33.

1.6.2 Electrocatalytic hydrogenation of various organic compounds

There are many studies on the electrocatalytic reduction of single organic compounds

or mixtures, such as carbonyl groups,[34-38, 39, 40] carboxylic acids,[33] aromatics,[41-43] lignin[44-47] and edible oils[48-57]. Some examples on the investigation of these organic compounds are discussed in the following text, which is very useful for this dissertation research on bio-oil model compound studies.

Carbonyl groups in adehydes and ketones can be reduced to alcohols or hydrocarbons depending on the pH of the medium. Sekine et al.[35] showed that hydrocarbons could be formed in the electrolytic reduction of acetone in aqueous sulfuric acid. In the research of electrocatalytic hydrogenation of benzylideneacetone, three products are found in large quantity, including 4-phenylbutene-3-ol-2 (7.2%), a mixture of 4-phenylbutanol-2 and 4-phenyl-2-butanone (75%).[36] Parpot et al.[34] showed that furfuryl alcohol was obtained by electroreduction of furfural in a 55% yield on Cu cathodes at pH 10 and 30 mA cm^{-2}. The carbonyl group in benzophenone was successfully reduced in aqueous ethanol on 10% Pd-alumina supported catalyst.[37] Electrocatalytic hydrogenation of cyclohexanone was examined over Pd catalysts in aqueous solution using acetic acid as the electrolyte and cyclohexanol was the only product.[38] ECH of the carbonyl groups in sugars was also very successful to produce sugar alcohols when using powder Raney nickel cathode.[39, 40]

The carboxyl group can be reduced to carboxylate anion, the aldehyde, the alcohol, or the hydrocarbon. Dalavoy et al.[33] showed that the major product from electrocatalytic hydrogenation of lactic acid was lactaldehyde with small quantity of propylene glycol when using 5% Ru/C powder catalyst. Popp and Schultz [58] reviewed electrochemical reduction of organic acids using various cathodes, C, Pb, Hg, Ni, Cd, Ti and Cu-Hg.

For aromatics reduction, the benzene ring is usually first saturated with hydrogen if

there is no other unsaturated bonds. Brisach-Wittmeyer et al.[42] studied electrocatalytic hydrogenation of catechol using Rh-Al_2O_3 powder catalyst in aqueous media within different pH ranges. It was shown that the final products are 1,2-cyclohexanediol (cis and trans isomers) and several intermediates, including 1,2-cyclohexanedione, 2-hydroxycyclohexan-1-one, depending on the pH of the solution. Electrocatalytic hydrogenation of phenanthrene was carried out at Raney nickel electrodes under medium pressure of nitrogen at 80 and 110 °C.[59] The asymmetric and symmetric octahydrophenanthrenes were obtained with high yield (91%) and current efficiency (94-96%). Miller and Christensen [60] showed that different phenols, anisole, aniline, benzoic acid, cumene and tert-butylbenzene were successfully converted to the corresponding cyclohexyl compounds with carbon supported precious metal cathodes. The electrocatalytic hydrogenation of benzene, aniline and nitrobenzene was studied using a Raney nickel powder cathode.[61] Benzene was hydrogenated to cyclohexane with tetraethylammonium p-toluenesulphonate (TEATS) as electrolyte. Aniline was converted to cyclohexylamine only in the presence of a quaternary ammonium ion supporting electrolyte. Only the nitro group was reduced during ECH of nitrobenzene with a sodium p-toluenesulphonate.

Surfactant was shown to improve the electrochemical efficiency of ECH of phenols. Ilikti et al.[62] showed that the electrochemical efficiency of 2,6-dimethylphenol and 2-*tert*-butylphenol was significantly improved by adding low amounts of didodecyldimethylammonium bromide (DDAB). The yield of alkylcyclohexanols was also increased by adding the DDAB surfactant. The electrochemical efficiency was also increased to 30% during ECH of limonene with cationic micelles cetyltrimethylammonium bromide

(CTAB).[63]

Electrocatalytic hydrogenation of lignin is to break the ether bond and produce lower molecular weight phenolics. There are several papers about ECH of lignin model compounds. Cyr et al.[44] showed that the electrocatalytic hydrogenolysis of β-O-4 lignin model compounds took place at Raney nickel and palladium cathodes in sodium hydroxide solution at temperatures of 25 to 75°C. Electrocatalytic hydrogenolysis of benzyl phenyl ether was also studied at Raney nickel cathodes in aqueous ethanol.[45] A 4-O-5 type linkage model compound, 4-phenoxyphenol, was also investigated in aqueous sodium hydroxide solution using Raney nickel, nickel boride, and precious metals supported on activated carbon or alumina.[46] Electrocatalytic hydrogenation of real lignin showed that hydrogen content increased by 1.7% and the softening temperature decreased by 24°C.[47]

Electrocatalytic hydrogenation of unsaturated fatty acids in edible oil can saturate the C=C and produce a more oxidatively stable product. Unlike reactions at high temperatures, the mild temperature used by ECH avoids the side reactions that produce trans isomers and cyclic aromatic fatty acids.[38] Soybean oil was shown to be hydrogenated on a Raney nickel powder cathode at 70°C in a flow-through electrochemical reactor. Mixture of water and t-butanol was used as solvent, and tetraethylammonium p-toluenesulfonate was used as the supporting electrolyte.[38] To avoid the use of the electrolyte, a solid polymer electrolyte reactor was used to hydrogenate the soybean oil with water as the anode feed and source of hydrogen. The membrane electrode assembly was composed of a precious metal-black cathode, a RuO_2 powder anode and a Nafion® 117 membrane. Different metals show different electrochemical efficiencies, with the trend Pd > Pt > Rh > Ru >Ir.[50]

1.6.3 Cathodes for electrocatalytic hydrogenation

Hydrogen overpotential is a very important parameter for evaluating the cathode. Average hydrogen overpotentials for various cathodes are shown in Table 1.3.

Table 1.3 Average hydrogen overpotential on various cathodes. Data was taken from the reference 58.

Cathode	Overpotential, V	Cathode	Overpotential, V
Platinized platinum	0.03	Copper	0.67
Tungsten	0.27	Iron	0.71
Smooth platinum	0.29	Graphite	0.77
Antimony	0.43	Aluminum	0.80
Gold	0.48	Mercury	0.89
Nickel	0.56	Tin	0.92
Palladium	0.59	Zinc	0.94
Silver	0.62	Lead	1.00
Carbon	0.64	Cadmium	1.22

For the cathodes with high hydrogen overpotential (potential difference between a half-reaction's thermodynamically determined reduction potential and the potential at which the redox event is experimentally observed), direct electron transfer to the organic compounds and solvent protonation are the reaction pathways. This type of cathode is and electron conductor and not considered as catalyst. Usually hydrogenation with these cathodes results in different products selectivities compared with electrocatalytic hydrogenation. Electrochemical reduction of benzene with non-catalytic cathodes can be used to generate partially reduced products. A patent from Hatayama et al.[64] shows that 1,4-cyclohexadiene and cyclohexene are two products from electrochemical reduction of benzene using an aqueous solution of quaternary ammonium salts. The selectivity of 1,4-cyclohexadiene is larger than 90% in all cases. Coleman and Wagenknecht[65] also found that 1,4-cyclohexadiene was obtained with 90% selectivity during the ECH of benzene in an undivided cell with

quaternary ammonium hydroxide as electrolyte. ECH of benzene in methylamine solution containing lithium chloride with a carbon cathode also generates cyclohexadiene with 95% selectivity.[66] Usually more reduced products will be expected with catalytic cathode during electrocatalytic hydrogenation. Pintauro and Bontha[61] show that ECH of benzene with Raney nickel cathode only leads to cyclohexane using t-butanol and water as solvent and with hydrotropic salt as electrolyte. The partially reduced intermediates, cyclohexene and cyclohexadiene, are not observed.

With the high hydrogen overpotential cathode, dimerization or polymerization takes place very often due to the radicals generated from the direct electron transfer. Furthermore, those cathodes are not environmentally friendly. To prevent or reduce polymerization, ECH with low hydrogen overpotential cathodes are usually preferred, such as Ni, Pd, Au, Pt and Ru. Most of the results and discussion in this dissertation is focused on these types of cathodes.

REFERENCES

REFERENCES

1. A. V. Bridgwater, International Journal of Global Energy Issues, 2007, **27**, 160-203.

2. U. S. E. I. Administration, *Annual Energy Outlook 2012*, Report DOE/EIA-0383(2012), U.S. Department of Energy, Washington, DC, 2012.

3. U. S. D. o. energy, *U.S. Billion-Ton Update: Biomass Supply for a Bioenergy and Bioproducts Industry.* , Report ORNL/TM-2011/224, Oak Ridge National Laboratory, Oak Ridge, 2011.

4. P. L. Eranki, B. D. Bals and B. E. Dale, Biofuels, Bioproducts and Biorefining, 2011, **5**, 621-630.

5. P. C. Badger and P. Fransham, Biomass & Bioenergy, 2006, **30**, 321-325.

6. T. P. Vispute and G. W. Huber, Green Chem., 2009, **11**, 1433-1445.

7. A. V. Bridgwater and G. V. C. Peacocke, Renewable & Sustainable Energy Reviews, 2000, **4**, 1-73.

8. M. Garcia-Perez, X. S. Wang, J. Shen, M. J. Rhodes, F. J. Tian, W. J. Lee, H. W. Wu and C. Z. Li, Industrial & Engineering Chemistry Research, 2008, **47**, 1846-1854.

9. D. Mohan, C. U. Pittman and P. H. Steele, Energy & Fuels, 2006, **20**, 848-889.

10. A. Oasmaa, E. Leppamaki, P. Koponen, J. Levander and E. Tapola, *Physical characterization of biomass-based pyrolysis liquids: application of standard fuel oil analyses*, Technical Research Center of Finland, Espoo, 1997.

11. M. Garcia-Perez, A. Chaala, H. Pakdel, D. Kretschmer and C. Roy, Biomass and Bioenergy, 2007, **31**, 222-242.

12. R. Bayerbach, V. D. Nguyen, U. Schurr and D. Meier, Journal of Analytical and Applied Pyrolysis, 2006, **77**, 95-101.

13. K. Sipilae, E. Kuoppala, L. Fagern s and A. Oasmaa, Biomass and Bioenergy, 1998, **14**, 103-113.

14. M. E. Boucher, A. Chaala, H. Pakdel and C. Roy, Biomass and bioenergy, 2000, **19**, 351-361.

15. S. Czernik, D. K. Johnson and S. Black, Biomass and Bioenergy, 1994, **7**, 187-192.

16. R. N. Hilten, B. P. Bibens, J. R. Kastner and K. C. Das, Energy & Fuels, 2009, **24**,

673-682.

17. O. D. Mante and F. A. Agblevor, Waste Management, 2012, **32**, 67-76.

18. M. W. Nolte and M. W. Liberatore, Energy & Fuels, 2011, **25**, 3314-3317.

19. J. P. Diebold, *A review of the chemical and physical mechanisms of the storage stability of fast pyrolysis bio-oils*, Thermalchemie, Inc, Lakewood, 1999.

20. A. Oasmaa and E. Kuoppala, Energy & fuels, 2003, **17**, 1075-1084.

21. R. H. Venderbosch, A. R. Ardiyanti, J. Wildschut, A. Oasmaa and H. J. Heeres, Journal of Chemical Technology and Biotechnology, 2010, **85**, 674-686.

22. T. Ba, A. Chaala, M. Garcia-Perez and C. Roy, Energy & fuels, 2004, **18**, 188-201.

23. P. Bhattacharya, P. S. El Barbary Hassan and L. L. Ingram, BioResources, 2010, **5**, 908-919.

24. X. Junming, J. Jianchun, S. Yunjuan and L. Yanju, Biomass and Bioenergy, 2008, **32**, 1056-1061.

25. B. Scholze, Ph.D. dissertation, University of Hamburg, 2002.

26. B. Scholze and D. Meier, Journal of Analytical and Applied Pyrolysis, 2001, **60**, 41-54.

27. A. Oasmaa, J. Korhonen and E. Kuoppala, Energy & Fuels, 2011, **25**, 3307-3313.

28. L. Moens, S. K. Black, M. D. Myers and S. Czernik, Energy & Fuels, 2009, **23**, 2695-2699.

29. E. Fratini, M. Bonini, A. Oasmaa, Y. Solantausta, J. Teixeira and P. Baglioni, Langmuir, 2006, **22**, 306-312.

30. R. N. Hilten and K. C. Das, Fuel, 2010, **89**, 2741-2749.

31. T. Vispute, Ph.D., University of Massachusetts - Amherst, 2011.

32. F. H. Mahfud, F. Ghijsen and H. J. Heeres, Journal of Molecular Catalysis a-Chemical, 2007, **264**, 227-236.

33. T. S. Dalavoy, J. E. Jackson, G. M. Swain, D. J. Miller, J. Li and J. Lipkowski, Journal of Catalysis, 2007, **246**, 15-28.

34. P. Parpot, A. P. Bettencourt, G. Chamoulaud, K. B. Kokoh and E. M. Beigsir, Electrochimica Acta, 2004, **49**, 397-403.

35. T. Sekine, A. Yamura and K. Sugino, Journal of The Electrochemical Society, 1965,

112, 439.

36. U. B. Bekenova, S. V. Do, N. M. Ivanova, O. A. Sivolobova and I. V. Kirilyus, Russian Journal of Electrochemistry, 2006, **42**, 393-397.

37. C. M. Cirtiu, A. Brisach-Wittmeyer and H. Menard, Catalysis Communications, 2007, **8**, 751-754.

38. C. M. Cirtiu, A. Brisach-Wittmeyer and H. Menard, Journal of Catalysis, 2007, **245**, 191-197.

39. V. Anantharaman and P. N. Pintauro, Journal of the Electrochemical Society, 1994, **141**, 2742-2752.

40. V. Anantharaman and P. N. Pintauro, Journal of the Electrochemical Society, 1994, **141**, 2729.

41. F. Laplante, L. Brossard and H. Menard, Canadian journal of chemistry, 2003, **81**, 258-264.

42. D. Tountian, A. Brisach-Wittmeyer, P. Nkeng, G. Poillerat and H. Menard, Journal of applied electrochemistry, 2009, **39**, 411-419.

43. K. Amouzegar and O. Savadogo, Journal of applied electrochemistry, 1997, **27**, 539-542.

44. A. Cyr, F. Chiltz, P. Jeanson, A. Martel, L. Brossard, J. Lessard and H. Menard, Canadian Journal of Chemistry, 2000, **78**, 307-315.

45. B. Mahdavi, A. Lafrance, A. Martel, J. Lessard, H. Menard and L. Brossard, Journal of applied electrochemistry, 1997, **27**, 605-611.

46. P. Dabo, A. Cyr, J. Lessard, L. Brossard and H. Menard, Canadian journal of chemistry, 1999, **77**, 1225-1229.

47. J. Zhang, X. Zhang, D. Xie, D. Liu and Z. Li, The Canadian Journal of Chemical Engineering, 2002, **80**, 1-5.

48. G. J. Yusem and P. N. Pintauro, Journal of the American Oil Chemists' Society, 1992, **69**, 399-404.

49. G. Yusem, P. N. Pintauro, P. C. Cheng and W. An, Journal of applied electrochemistry, 1996, **26**, 989-997.

50. W. An, J. K. Hong and P. N. Pintauro, Journal of applied electrochemistry, 1998, **28**, 947-954.

51. K. Mondal and S. B Lalvani, Chemical engineering science, 2003, **58**, 2643-2656.

52. P. N. Pintauro, M. P. Gil, K. Warner, G. List and W. Neff, Industrial & engineering chemistry research, 2005, **44**, 6188-6195.

53. W. An, J. K. Hong, P. N. Pintauro, K. Warner and W. Neff, Journal of the American Oil Chemists' Society, 1998, **75**, 917-925.

54. P. N. Pintauro, *US Pat.*, 5225581, 1993.

55. K. Warner, W. E. Neff, G. R. List and P. Pintauro, Journal of the American Oil Chemists' Society, 2000, **77**, 1113-1118.

56. K. Mondal and S. B. Lalvani, Journal of the American Oil Chemists' Society, 2003, **80**, 1135-1141.

57. K. Mondal and S. Lalvani, Journal of Food Engineering, 2008, **84**, 526-533.

58. F. D. Popp and H. P. Schultz, Chemical Reviews, 1962, **62**, 19-40.

59. R. Menini, A. Martel, J. Lessard and O. Vittori, Electrochimica acta, 1998, **43**, 1697-1703.

60. L. L. Miller and L. Christensen, The Journal of Organic Chemistry, 1978, **43**, 2059-2061.

61. P. N. Pintauro and J. R. Bontha, Journal of applied electrochemistry, 1991, **21**, 799-804.

62. H. Ilikti, N. Rekik and M. Thomalla, Journal of applied electrochemistry, 2004, **34**, 127-136.

63. P. Chambrion, L. Roger, J. Lessard, V. Beraud, J. Mailhot and M. Thomalla, Canadian journal of chemistry, 1995, **73**, 804-815.

64. T. Hatayama, Y. Hamano and T. Yamamoto, *US Pat.,* 3700572, 1972.

65. J. P. Coleman and J. H. Wagenknecht, Journal of the Electrochemical Society, 1981, **128**, 322-326.

66. R. A. Benkeser, E. M. Kaiser and R. F. Lambert, Journal of the American Chemical Society, 1964, **86**, 5272-5276.

Chapter 2 Fast Pyrolysis of Hybrid Poplar in a Screw-conveyor Pyrolysis Reactor: Bio-oil Characterization and Stability Analysis

Zhenglong Li[a,b], Shantanu Kelkar[a,b], Mahlet Garedew[a], Lauren Raycraft[a], Jon Bovee[a], Thomas Stuecken[c], Christopher M. Saffron[a,b,d,*]

A paper to be submitted

Abstract

Fast pyrolysis is a thermochemical method for converting biomass into a liquid product, known as bio-oil. Because of bio-oil's high bulk density, the deployment of fast pyrolysis in the regional biomass processing depots (RBPDs) may be feasible. A compact and transportable screw-conveyor pyrolysis reactor was designed for application in RBPDs. The bio-oil produced from this reactor was characterized using proximate analysis, ultimate analysis, GC/MS, HPLC and fractionation. Water content of the bio-oil was higher than that of the bio-oils made in other types of reactors and this resulted in lower HHV, density and carbon content. However, chemical characterization results showed that the major chemicals in this bio-oil were very similar with those in typical bio-oils. Bio-oil stability was also evaluated by performing the accelerated aging test and the aged bio-oil was analyzed by a viscometer and by measuring the content of carbonyl groups. During 2 days' aging, viscosity increased at a rate of 17 cP/day. The carbonyl groups decreased from 3.3 mol/Kg to 2.3

a.Department of Biosystems & Agricultural Engineering, Michigan State University, East Lansing, MI 48824, US; b. Department of Chemical Engineering & Materials Science, Michigan State University; c. Department of Mechanical Engineering, Michigan State University.; d. Department of Forestry, Michigan State University.
* Corresponding author at: Department of Biosystems & Agricultural Engineering, Michigan State University, East Lansing, MI, 48824, United States. Tel.: +1 517 432 7414; fax: +1 517 432 2892. E-mail address: saffronc@egr.msu.edu (C.M. Saffron).

mol/Kg within 23 h. As the bio-oil yield was still lower than those reported in the literature, further optimization of the reactor operation is suggested as future work.

2.1 Introduction

Renewable energy plays an increasingly important role in enhancing the energy security and solving the environmental problems caused by traditional fossil fuels. Bioenergy is one potential renewable energy source to provide the energy needs for both developing and developed areas in the world.[1] Due to the carbon neutral or carbon negative benefits of bioenergy, it can contribute greatly to reducing greenhouse gas emissions and alleviating global warming.

Due to the low bulk density and dispersive geographic distribution, biomass is difficult to collect and requires high transportation cost for long distance delivery to central refineries, high land use and storage cost. It is essentially critical to solve this biomass supply issue for biofuels development. Regional biomass processing depots (RBPDs) have been proposed to solve this biomass supply challenge.[2] Fast pyrolysis, a thermochemical technique, can be used in the RBPDs to convert biomass to high density liquid biofuels (bio-oil) with potential to reduce transportation cost and storage cost.[3]

Fast pyrolysis reactor is the key component for the whole pyrolysis plant. Currently, there are several types of designs, including fluidized bed, circulating fluidized bed, transported bed, rotating cone, ablative, auger, vacuum moving bed and entrained flow reactors.[1] Among these reactors, fluid bed reactor and circulating fluid bed reactor are the most popular configurations due to their ease of operation and ready scale-up. However, these two types of reactors require a heat transfer medium (sand) to increase the heat transfer rate

and need high amount of inert gas to fluidize the biomass. The operation cost is increased due to the energy input for heating the sand and separating sand from the product, and due to cost from using inert gas.

To apply fast pyrolysis in the RBPDs, pyrolysis reactor system should be compact and transportable. Firstly, the size of the reactor system should be compact, and it's better to use as few accessories as possible. Secondly, continuous consumables should be avoided, such as the large use of inert gas. Heating media, such as sand or metal beads, are also not desirable because additional separation cost is added. To satisfy these requirements, we developed a new compact screw-conveyor pyrolysis reactor. Inert gas is not needed continuously, and only very little amount is required at the beginning to purge the air out from the reactor. Unlike the fluidized bed reactor, the non-condensable gas is much more concentrated without the inert gas, thus it can be effectively combusted to provide heat for the pyrolysis reactor. Auger pyrolysis reactors, developed in several groups,[4-6] were shown to have similar advantages with this screw-conveyor reactor. However, according to Brown JN and Brown RC,[7] heat carrier is mandatory for commercial-scale auger reactors to provide high heat transfer rates. This screw-conveyor pyrolysis reactor with varying flight depths can press biomass closely to the heating barrel in the end of the reactor to provide high heating rate. With the heating from inside of the screw, heating media may not be considered necessary even in the large-scale screw-conveyor pyrolysis system.

One of the important questions related to this new screw-conveyor pyrolysis reactor is whether there are differences between the bio-oil from this reactor and the other bio-oils. Several different physical and chemical characterization methods were performed to

investigate this bio-oil, including proximate analysis, ultimate analysis, GC/MS, HPLC, fractionation. Bio-oil stability was also investigated using the accelerated aging test. Viscosity measurement and size exclusion chromatography were used to analyze the aged bio-oil.

2.2 Experimental

2.2.1 Biomass feedstock

Hybrid poplar (Populus deltoides×Nigra, DN34) is used as the biomass feedstock for this research because it is among the fast-growing trees in North America and is well suited for biofuels and chemicals production.[8] The biomass sample was dried to less than 10% moisture by weight and milled to a particle size of 1 mm using a hammer mill.

2.2.2 Pyrolysis reactor

Figure 2.1 is a depiction of the screw-conveyor pyrolysis reactor system. The actual pyrolysis system used in this investigation is shown in Figure 2.2. The pyrolysis system is comprised of a reactor unit and associated auxiliary systems for biomass feeding and products collection. The detailed design features are discussed herein.

(1) Reactor unit

The reactor unit consists of a stainless steel barrel, a screw shaft for conveying biomass, six band heaters, and a feed cooling system between the feed hopper and the band heaters to prevent biomass preheating. The shaft was driven by a variable speed electric motor connected to a gear box. The screw with variable flight depth pressurizes the biomass against the barrel towards the end of the reactor and enhances the heat transfer from the reactor wall to biomass. Argon was used only for purging oxygen from the system to provide an inert atmosphere before each run. Sometimes it was also used to facilitate the biomass feeding to

maintain solids flow. The six band heaters were divided into three heating zones (1st, 2nd, 3rd), where each zone comprised of two band heaters. Each zone can be operated at different temperatures for the optimum products production. The temperatures of the three different zones were monitored by thermocouples and controllers maintained set points of 350, 450 and 450°C over the course of reaction.

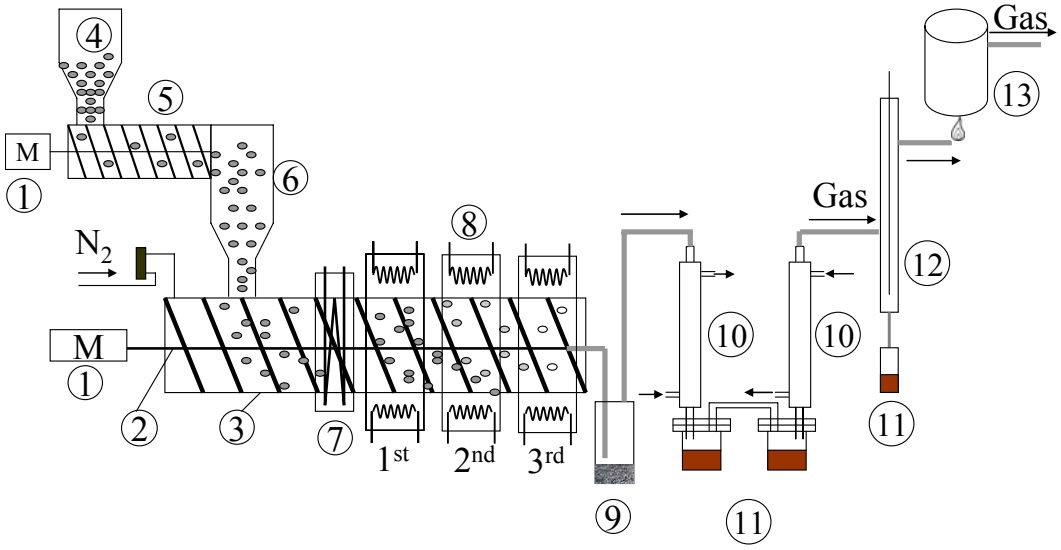

Figure 2.1 Schematic diagram of the bench-scale screw-conveyor pyrolysis reactor with downstream product recovery constructed in MSU Pyrolysis Laboratory. 1. screw motor, 2. screw conveyor, 3. pyrolysis reactor, 4. biomass feed hopper, 5. auger feeder, 6. feeding connection, 7. cooler, 8. heat source, 9. char collector, 10. condenser, 11. bio-oil container, 12. electrostatic precipitator, 13. gas flame calorimeter. "For interpretation of the references to color in this and all other figures, the reader is referred to the electronic version of this dissertation."

Biomass feeder and reactor | Condenser and collection vessels | Electrostatic precipitator | Gas flame calorimeter

Figure 2.2 The bench-scale screw-conveyor pyrolysis reactor parts

(2) Feed unit

A Mechatron® gravimetric feeder was used to meter biomass into the reactor by controlling the mass or volume flow rate. One example of the biomass feeding test was shown in Figure 2.3, with feeding variability less than 4%.

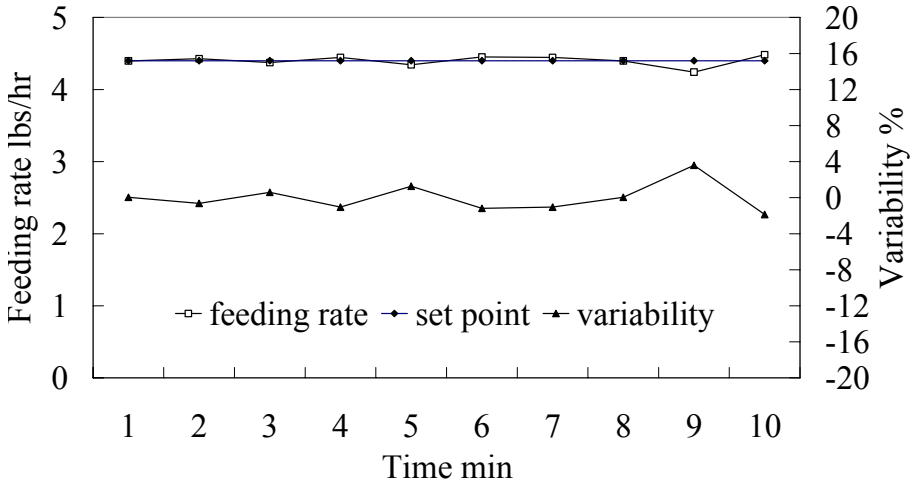

Figure 2.3 Biomass feeding testing using a Mechatron® gravimetric feeder

(3) Product collection unit

The product collection unit consists of a char trap, two bio-oil condensers, an electrostatic precipitator and a gas flame calorimeter. The char trap has a plate and holes array

inside of the char canister to remove large particles from the pyrolysis gas. Most of the pyrolysis gas was condensed in the following two bio-oil condensers, and the bio-oil was collected in two glass jars. The two condensers were controlled at room temperature and -17°C respectively, with most of the bio-oil collected in the first condenser. Electrostatic precipitator is used to further collect bio-oil, however, it was not operated during the production of the poplar derived bio-oil. After that, the non-condensable gas was burned and the combustion heat was measured by the flame calorimeter. Usually it's very hard to measure the gas heating value. With the gas flame calorimeter, it allows us to close the energy balance.

2.2.3 Products analyses

The ultimate analysis of the biomass and the bio-oil were carried out using combustion with automatic analyzers in the Atlantic Microlabs in Georgia. The minerals Fe, Ca, P, Mg, K, and Na were analyzed at Dairyone Labs (Ithaca, NY) using inductively coupled plasma (ICP) spectrometry after microwave digestion. Chloride ion concentration was determined using potentiometric titration. Moisture content in the grass species was determined using ASTM D4442-07 method and the ash content was determined using the ASTM D1102 method. The high heating value of biomass was determined using a Parr 1341 Plain Jacket Calorimeter (Parr Instrument Co., Moline, IL) and method elaborated in ASTM D2105.

Neutral detergent fiber (NDF), acid detergent fiber (ADF), and acid detergent lignin (ADL) of samples were performed in the Van Soest Fiber Analysis System.[9] NDF, ADF, and ADL were used to calculate cellulose, hemicellulose, and lignin contents, respectively.

Cellulose and hemicellulose can be determined by the differences of %ADF–%ADL and %NDF–%ADF, respectively. Lignin content was obtained from ADL. Lignin content was also determined using ASTM E 1721-01 method. About 0.3 g of biomass was placed in a 100 ml sealed bottle. To this flask, 3 ml 72% H_2SO_4 was added. The mixture was maintained at a temperature of 30°C for 2 hrs with continuous stirring. At the end of 2 hrs, the mixture was diluted to 4% H_2SO_4 by adding 84.0 ml of deionized water. This mixture was heated in oven at 110°C for 1 hour. At the end of this reaction, mixture was cooled, filtered under vacuum followed by washing with hot deionized water. The residue was dried at 105°C and weighed to determine the lignin content.

Table 2.1 Analytical methods summary

Characteristic	Method	Remarks
Moisture	ASTM E1756-01	
Ash	ASTM D1102	Wet ashing
	ASTM E1755-01	Dry ashing
High Heating Value	ASTM D2015	Bomb calorimetry
Elemental analysis	Combustion	C-H-O-N
Elemental analysis	ICP-AES, titration	Cl-K-Na-Ca
Viscosity	Viscometer	
pH	pH meter	
Density	Densitometer	

Pyroprobe-GC/MS (Py-GC/MS) Analytical pyrolysis experiments were conducted using a microscale pyrolysis unit, CDS Pyroprobe 5250 (CDS Analytical Inc, Oxford, PA) interfaced to a Shimadzu QP-5050A gas chromatograph/mass spectrometer (Shimadzu Corp, Columbia, MD). Approximately 0.5 mg of ground biomass sample was packed between quartz wool in a quartz tube with a filler rod. Three replicates of each sample were run. The pyroprobe was set at 600°C with a hold time of 10 s at a heating rate of 1000°C/s. The GC used a Restek Rtx-1701 column (Restek, Bellefonte, PA), 60 m x 25 mm with a 0.25 mm film

thickness. The column gas flow was 1 cm/s with a split ratio of 1:100. The GC oven temperature program began with a 1 minute hold at 40 °C followed by heating at 8 °C/min to 270 °C. The injector and detector temperature was set at 280 °C. The mass spectra were recorded in electron ionization mode for m/z 28 to 400. Identification of compounds was performed by comparing the mass spectra of the peaks with standard spectra of other compounds using the NIST library to obtain the most probable matches. Pure compounds (Sigma-Aldrich Co., St Louis, MO) were then used to confirm some of the peak identities based on matching of retention times and mass spectra.

GC/MS Liquid samples were analyzed using GC/MS (Shimadzu Corp, Columbia, MD), with the conditions same as above. Quantification was performed using external standards in methanol. A four-point calibration curve was constructed relating concentration to peak area response. The amount of a certain chemical produced was determined with the calibration curves.

HPLC Sugars in the bio-oil (levoglucosan, glucose and xylose) were determined using an Agilent 1100 HPLC system equipped with a Bio-rad Aminex HPX-87H analytical column and a refractive index detector. The mobile phase was 0.005 M sulfuric acid with a flow rate of 0.6 mL/min. Column temperature was set as 65°C for sugar analysis. External standards were used to identify and quantify these sugars.

Thermogravimetric analysis (TGA) Thermogravimetric analysis was performed using Mettler Toledo TGA. Temperature was held at 30°C for 10 min, and then increased to 600°C using 10°C/min. Nitrogen was used with a flow rate of 20 mL/min.

Bio-oil fractionation Fractionation scheme of poplar derived bio-oil was shown in

Figure 2.4. Bio-oil (60 g) was added dropwise into 1 L cooled DI water with strong stirring. Two fractions were obtained, water-soluble fraction and water-insoluble fraction (pyrolytic lignin). After water separation of the bio-oil, water-soluble fraction was further extracted with diethyl ether into ether-soluble fraction and ether-insoluble fraction.

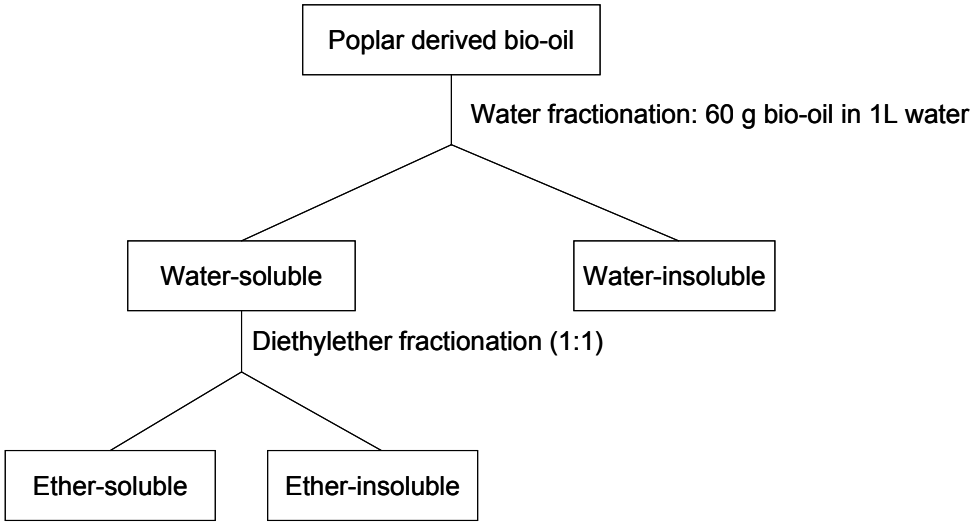

Figure 2.4 Bio-oil fractionation scheme[10]

Carbonyl group measurement Carbonyl group concentration in the bio-oil during aging was analyzed using the oximation method. Bio-oil samples were weighed into an erlenmeyer flask. The samples were mixed with 50 mL hydroxylamine hydrochloride in ethanol (8.75 g hydroxylamine hydrochloride in 40 mL DI water and dilute to 250 mL using ethanol) and 100 mL pyridine in ethanol (10 mL pyridine in 500 mL ethanol). These mixtures were stirred for more than 20 hours at room temperature. After that, 1 M sodium hydroxide was used to titrate the released hydrochloric acid. The amount of carbonyl groups can be calculated according to the following reaction equation:

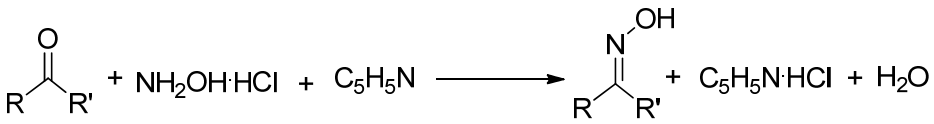

2.3 Results and discussion

2.3.1 Biomass (poplar DN 34) characterization

The proximate and ultimate analyses of poplar DN34 are shown in Table 2.2. The elemental analysis shows slightly different results from those reported in other literatures.[8,11,12] Carbon and nitrogen contents are smaller, while the oxygen, sulfur, potassium and calcium contents are higher, which may be due to the different soil conditions for the plantation.

Table 2.2 Proximate analysis and ultimate analysis of poplar DN 34

Analysis (wt% dw)	Poplar (DN-34)	
	This research	Literature[8,11,12]
Cellulose	54.60	43.67
Hemicellulose	13.50	19.55
Lignin [a]	27.2	27.23
ADL (Lignin)	11.40	
Ash	0.55	0.43-2.07
Elemental composition (wt% dw)		
%C	47.50	48.45-51.73
%H	6.20	4.47-6.45
%O	46.10	35.11-43.69
%N	0.16	0.19-0.60
%S	0.22	0.01-0.03
%Na	0.01	0.01
%K	0.02	0.24
%Ca	0.20	0.56
%Mg	0.04	0.05
Fe (ppm)	38	
%Cl	0.06	
%P	0.04	0.08

[a]This lignin was measured according to ASTM E 1721-01 method.

Figure 2.5 shows the TG and differential thermogravimetry (DTG) curves of poplar DN34 performed at heating rates of 10°C/min. The thermal degradation of poplar shows

separated regions. A shoulder, appearing at 309°C, is attributed to the thermal degradation of hemicellulose. The peak observed at 359°C corresponds to the thermal degradation of cellulose. Similar results were reported by Garcia-Perez et. al. for oil mallee biomass and sugarcane bagasse.[13, 14] The thermal degradation of the lignin spans over a wide range of temperature, overlapping with the peaks of hemicellulose and cellulose. The final solid residue is 20% as the temperature reached 600°C, leaving the char and ash in the residue.

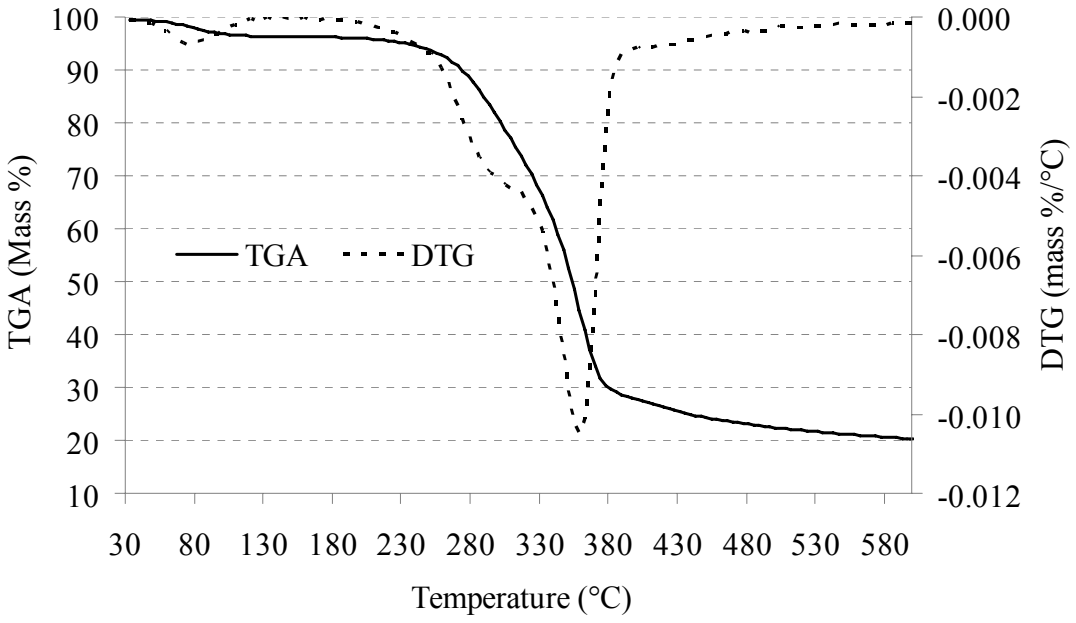

Figure 2.5 Thermogravimetric analysis of poplar DN34

2.3.2 Pyrolysis products

(1) Product yields from pyrolysis of poplar DN34

Pyrolysis of poplar DN34 was performed in the screw-conveyor reactor without the operation of the electrostatic precipitator. As shown in Table 2.3, the yield of bio-oil is 47-50%, comparable to the auger reactor,[5] but lower than that reported in the fluidized bed reactor (up to 69%).[11] One of the reasons is the loss of mass to the non-condensable gas (NCG) as we can see that the yield of NCG is much higher than those in the fluidized bed

reactor (Table 2.3). Without the electrostatic precipitators, aerosols in the non-condensable gas can not be removed only using the condensers. Temperature may not be high enough for high bio-oil yield as usually the optimum temperature is around 500°C.[15] Residence time of the pyrolysis products in the reactor could be too long because there was no inert gas purging the products out. According to Kim et al.,[11] longer residence time resulted in lower bio-oil yield in the fluidized bed reactor. In the future, further optimization of the reactor operation is required to increase the bio-oil yield and lower the char and non-condensable gas yield.

Table 2.3 Products yield for pyrolysis of poplar using screw-conveyor pyrolysis reactor and fluidized bed reactor

Yield, wt%			Temp.	Residence time	Reactor	Feed	Reference
Bio-oil	Char	NCG					
47-50	20-22	28-33	450°C	~30s (solid)	Screw-conveyor	Poplar	This research
50	27	23	450°C	--	Auger	Pine	5
50	28	22	400°C	1.2s	Fluidized bed	Poplar	11
66	12	22	450°C	1.2s	Fluidized bed	Poplar	11
69	10	21	500°C	1.2s	Fluidized bed	Poplar	11
64	8	28	550°C	1.2s	Fluidized bed	Poplar	11

NCG: non-condensable gas. Non-condensable gas is calculated by difference.

(2) Physical characterization of the products

Physical characterization of the bio-oil was shown in Table 2.4 and its properties were compared with other bio-oils. It is notable that the carbon content and oxygen content are very different from most of other bio-oils except poplar derived bio-oil in a fluidized bed reactor. This is most likely due to the loss of lignin fraction in aerosol form and also due to high water content of this bio-oil, which also resulted in lower density and HHV. Several factors may influence water content, including starting biomass moisture content, pyrolysis temperature and biomass particle size, etc. Westerhof et al.[16] found that 12wt % water content was produced at 400°C, while 7% water was generated at 325°C and 575°C during

pyrolysis of pine wood in a fluidized bed reactor. Garcia-Perez et al.[13] also showed that water content was reduced from 28% to 16% by reducing pyrolysis temperature from 580°C to 450°C for pyrolysis of mallee woody biomass in a fluidized bed reactor. Pyrolysis temperature is the most important factor that may influence the water content for this study. Future optimization of the reactor operation can be done to solve this problem.

Table 2.4 Physical characterization of the bio-oil

Reactor	Feed	Elements, wt%			Water Content wt%	pH	Density g/ml	HHV MJ/Kg	Ref
		C	H	O					
Screw-conveyor	Poplar	34.3	8.20	57.5	36.6	2.8	1.11	10.4	--
Auger	Pine	--	--	--	21	--	1.16	19.1	5
Auger	Pine	52.6	7.53	39.5	16	3.1	1.19	18.7	6
Auger	Oak	47.2	4.51	48.0	22.5	3.1	1.20	21.9	6
Fluidized bed	Poplar	39.9	5.6	54.2	24.9	2.3	--	16.8	11
Ensyn flash pyrolysis	Hard-wood	58.4	6.0	35.5	23.3	2.8	1.23	--	10
Typical wood pyrolysis		54-58	5.5-7.0	35-40	15-30	2.5	1.2	16-19	17

(3) Chemical characterization of bio-oil

Currently, Py-GC/MS is a common tool to study the pyrolysis behavior of different biomass.[18-20] However, the analytical reactor is very different from the screw-conveyor pyrolysis reactor in several aspects, such as the sample size (mg vs Kg) and pyrolysis conditions (fixed bed vs continuous flow). Thus there may be some differences between the products from the analytical and large scale reactors. The chromatogram from pyrolysis of poplar DN34 in the Py-GC/MS was compared with that from the GC/MS of the bio-oil (generated from the screw-conveyor reactor) (Figure 2.6). It is clear that these two chromatograms look very similar to each other. There are only differences for some small

peaks, such as peaks 3-6, 8 and 12. Thus, the volatile fractions of these two pyrolysis products are qualitatively similar, consistent with the results from Azeez et al.[21]

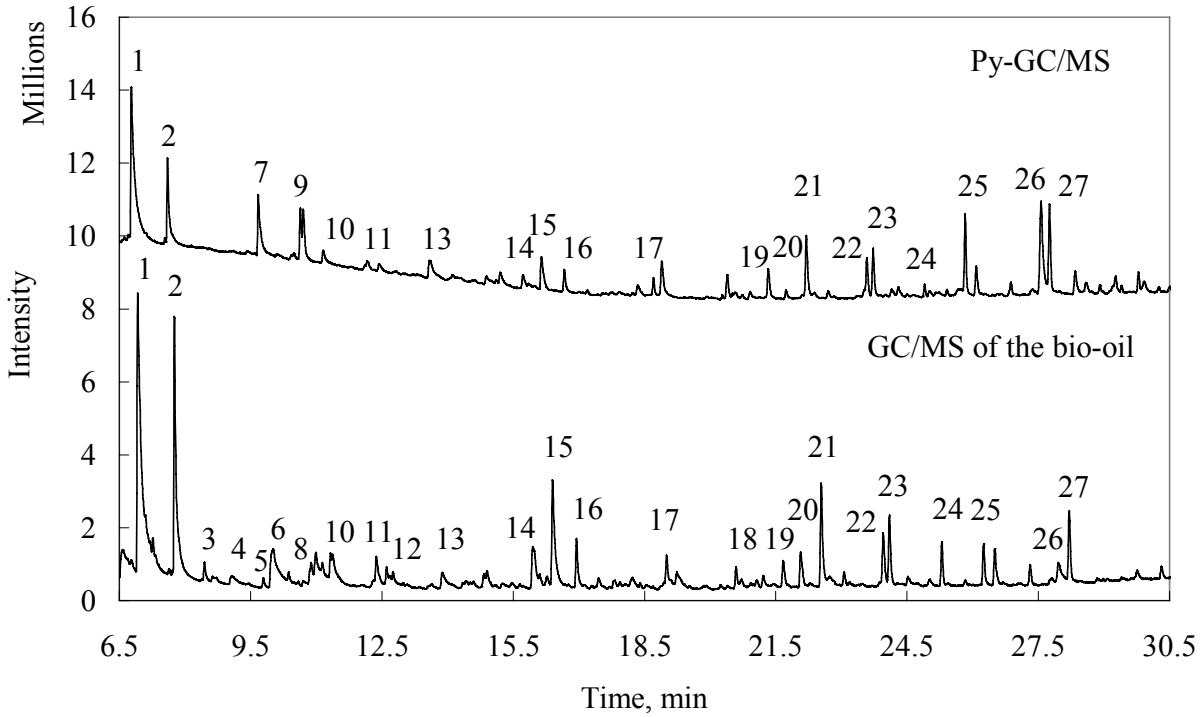

Figure 2.6 Comparison of the chromatograms from Py-GC/MS of the poplar and GC/MS of the poplar derived bio-oil. (1) acetic acid, (2) acetol, (3) 3-hydroxy-2-butanone, (4) propanoic acid, (5) cyclopetanone, (6) 2,3-Pentanedione, (7) 1-hydroxy-2-butanone, (8) 2,5-dimethoxytetrahydrofuran, (9) acetic anhydride, (10) furfural, (11) acetol acetate, (12) 2-methyl-2-cyclopentenone, (13) cyclohexanone, (14) 3-methyl-1,2-cyclopentanedione, (15) phenol, (16) guaiacol, (17) 2-methoxy-4-methylphenol, (18) 4-ethyl-2-methoxyPhenol, (19) 2-methoxy-4-vinylphenol, (20) eugenol, (21) syringol, (22) 2-methoxy-4-(1-propenyl)-phenol, (23) 1,2,4-trimethoxybenzene, (24) 5-tert-Butylpyrogallol, (25) 3',5'-dimethoxyacetophenone, (26) levoglucosan, (27) 2,6-dimethoxy-4-(2-propenyl)-phenol.

As is seen in Figure 2.6, there are many peaks showing up in GC/MS analysis. It is very difficult to quantify all of the peaks. Thus quantification was done only on some major compounds using GC/MS and HPLC (summarized in Table 2.5). The major groups are carboxylic acids, misc. oxygenates, furans, ketones, sugars and phenols. These analysis results were also compared with the compound concentrations in the typical bio-oils summarized by Diebold.[22] Most of these compounds are in the similar ranges with the other

bio-oils.[23, 24] The only exception is levoglucosan, which has higher concentration than the other bio-oils. However, this reported levoglucosan range may be lower since several studies show larger than 3 wt% levoglucosan.[21, 25]

Carboxylic acids are the main reason for bio-oil corrosiveness, so low levels of them are preferred for bio-oil with better quality. Usually the carboxylic acids concentration ranges from 0.5% to 12%,[26] so poplar derived bio-oil from this reactor has medium acids level. The acids concentration is very similar with the poplar bio-oil from the other type of reactor.[8]

The oxygenated organic compounds are possible reasons for the bio-oil instability[27] and coke formation during bio-oil upgrading.[28] Possible reactions between them include esterification, condensation and polymerization, etc.[29] To improve the bio-oil stability, reduction of the some of the unsaturated bonds is required.

The reaction pathway for forming the major compounds from pyrolysis of the woody biomass has been studied for several years. One proposed mechanism was summarized by Kim et al.[11] Acetic acid is considered as the product from deactylation of the hemicellulose. Low molecular ketones, aldehydes are from the ring opening of cellulose and hemicellulose, while furans and levoglucosan come from the dehydration of the sugars. Most of the phenolic compounds are proposed from the degradation of lignin, including side chain cleavage, C-O ether bond breakage and C-C bond breakage, etc.

Table 2.5 Quantification of some major compounds in bio-oil with GC/MS and HPLC

Compounds in bio-oil	Group	Method	wt% in whole bio-oil	
			This study	Typical Bio-oil Ref. 22
Cellulose/hemicellulose derived compounds				
Acetic acid	Acids	GC/MS	6.2	0.5-12
Propanoic acid	Acids	GC/MS	0.6	0.1-1.8
Sum			**6.8**	
Acetol	Misc. Oxygenates	GC/MS	5.6	0.7-7.4
1-Hydroxy-2-butanone	Misc. Oxygenates	GC/MS	3.1	
Sum			**8.7**	
Furfural	Furans	GC/MS	0.4	0.1-1.1
Furfuryl alcohol	Furans	GC/MS	0.3	0.1-5.2
Sum			**0.7**	
Cyclopentanone	Ketones	GC/MS	0.3	--
3-Methyl-2-cyclopentenone	Ketones	GC/MS	0.4	0.1-0.6
3-Methyl-1,2-cyclopentanedione	Ketones	GC/MS	1.1	
Sum			**1.8**	
Levoglucosan	Sugars	GC/MS	3	0.4-1.4
Glucose	Sugars	HPLC	0.3	0.4-1.3
Xylose	Sugars	HPLC	0.3	0.1-1.4
Sum			**3.6**	
Lignin derived compounds				
Phenol	Phenols	GC/MS	1	0.1-3.8
2-Methylphenol	Phenols	GC/MS	0.3	0.1-0.6
Guaiacol	Phenols	GC/MS	0.5	0.1-1.1
Cresol	Phenols	GC/MS	0.5	0.1-1.9
4-Ethyl-guaiacol	Phenols	GC/MS	0.4	0.1-0.6
Eugenol	Phenols	GC/MS	0.2	0.1-2.3
Isoeugenol	Phenols	GC/MS	1.2	0.1-7.2
Methoxyeugenol	Phenols	GC/MS	2.3	0.1-0.3
Syringol	Phenols	GC/MS	1.4	0.7-4.8
Sum			**7.8**	
Sum of all the quantified chemicals			29.4	

Due to the complexity of the bio-oil, it's very difficult to analyze the whole bio-oil with one or two analysis tools. Fractionation is usually used to separate bio-oil into several fractions and different analytical instruments can be used to understand the properties for different fractions. A typical fractionation scheme was used to separate poplar derived bio-oil (Figure 2.4).[10]

These fractions were analyzed using GC/MS. The total ion chromatograms (TIC) are shown in Figure 2.7, Figure 2.8 and Figure 2.9, and the TIC area percentage is listed in Table 2.6. From the comparison of the chromatograms between the whole bio-oil (Figure 2.6) and water-soluble bio-oil, we can see that most of the volatile compounds are retained in the water-soluble fraction. The lignin oligomers are separated from the water-soluble fraction due to their low solubility in water.

Part of the organic acids, like acetic acid, was extracted into ether-soluble fraction. Most of furan type of compounds and lignin derived phenols were extracted into ether-soluble fraction. Much fewer compounds were detected in the ether-insoluble fraction with GC/MS, mainly organic acids, misc. oxygenates and levoglucosan. According to Sipila et al.,[10] this fraction was mainly sugars, such as levoglucosan and cellobiosan. The fractionation of the poplar derived bio-oil shows very similar results with that from the hardwood pyrolysis oil.[10]

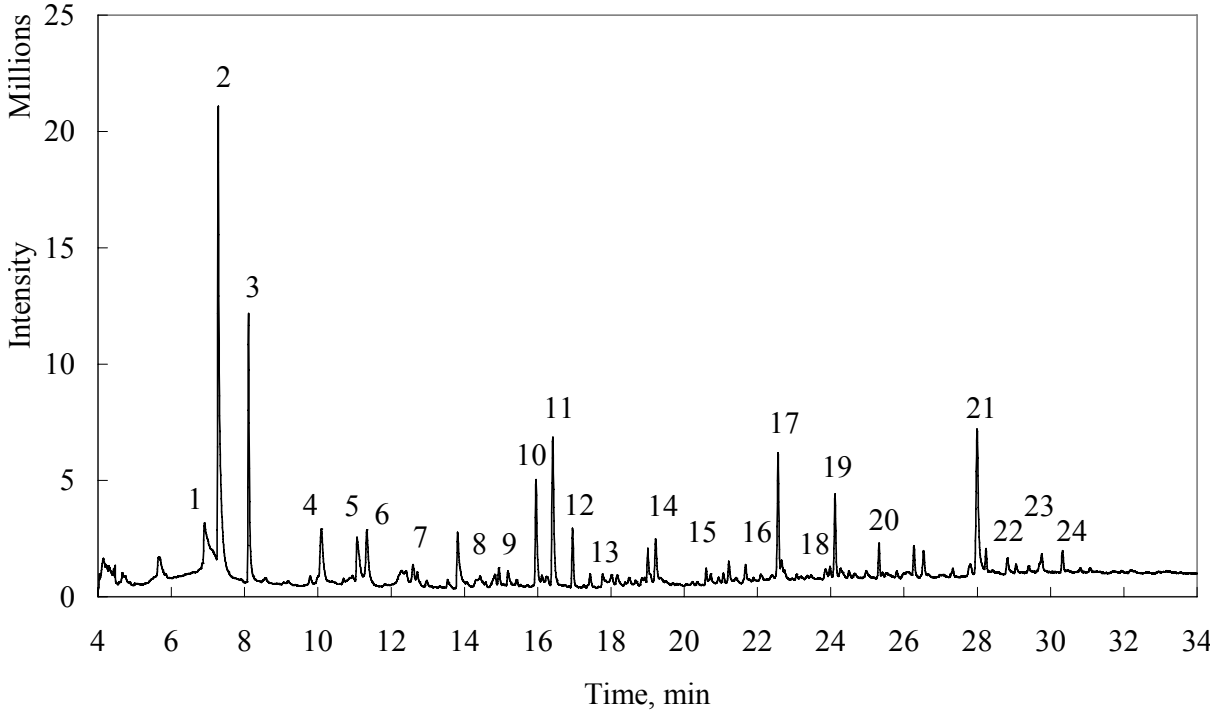

Figure 2.7 Total ion chromatograms of water-soluble fraction from poplar bio-oil. (1) Glycolaldehyde; (2) Acetic acid; (3) Acetol; (4) Ethyl pyruvate; (5) Butanedial; (6) Furfural; (7) 2-Methyl-2-cyclopentenone; (8) Butyrolactone; (9) 2(5H)-Furanone; (10) 3-Methyl-1,2-cyclopentanedione; (11) Phenol; (12) Guaiacol; (13) o-Cresol; (14) 2-Methoxy-4-methylphenol; (15) 4-Ethyl-2-methoxyphenol; (16) 2-Methoxy-4-vinylphenol; (17) Syringol; (18) Isoeugenol; (19) 1,2,4-Trimethoxybenzene; (20) 5-tert-Butyl-1,2,3-benzenetriol; (21) Levoglucosan; (22) Methoxyeugenol; (23) Syringylaldehyde; (24) Acetosyringone.

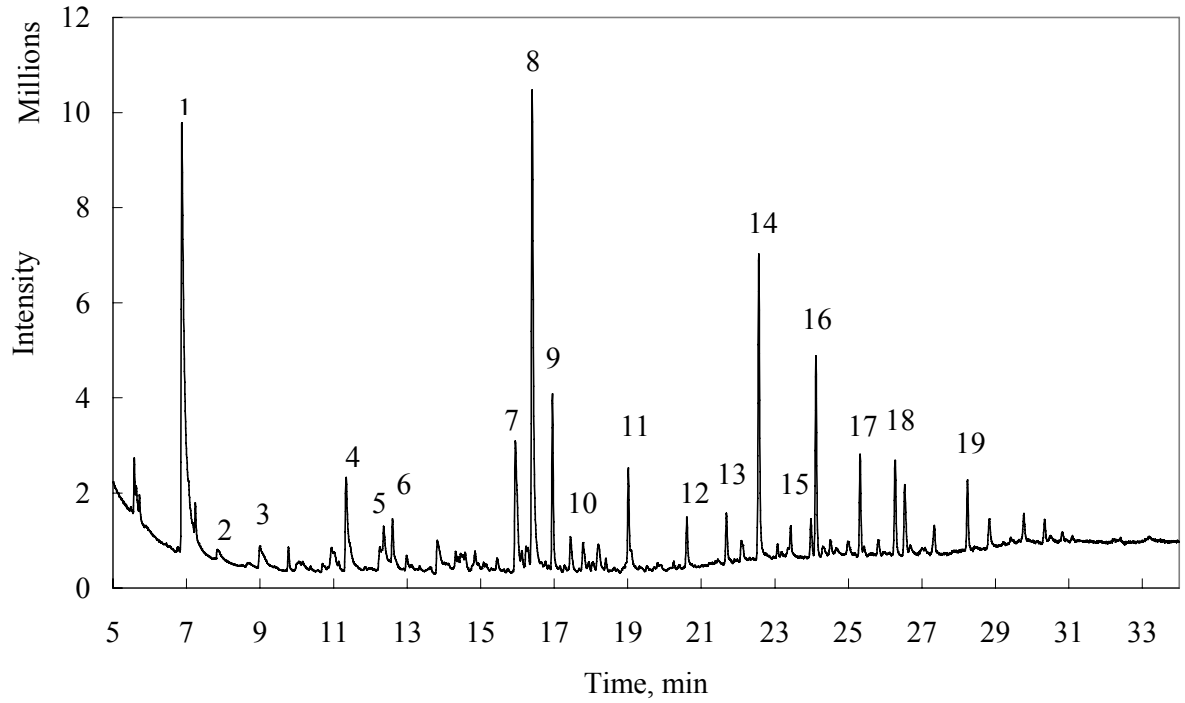

Figure 2.8 Total ion chromatograms of ether-soluble fraction from poplar bio-oil. (1) Acetic acid; (2) Acetol; (3) Propanoic acid; (4) Furfural; (5) Furfuryl alcohol; (6) 2-Methyl-2-cyclopentenone; (7) 3-Methyl-1,2-cyclopentanedione; (8) Phenol; (9) Guaiacol; (10) o-Cresol; (11) 4-Methyl-2-methoxyphenol; (12) 4-Ethyl-2-methoxyphenol; (13) 2-Methoxy-4-vinylphenol; (14) Syringol; (15) Isoeugenol; (16) 1,2,4-Trimethoxybenzene; (17) 5-tert-Butyl-1,2,3-benzenetriol; (18) 3,4-Dimethoxyacetophenone; (19) Methoxyeugenol.

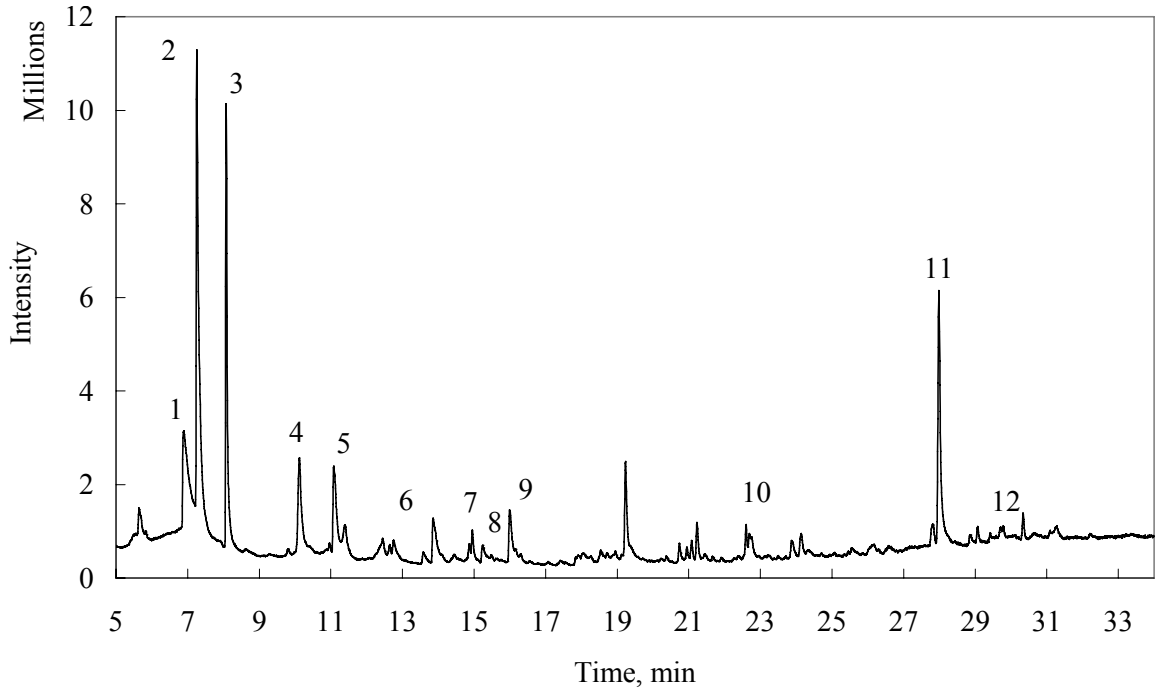

Figure 2.9 Total ion chromatograms of ether-insoluble fraction. (1) Glycolaldehyde; (2) Acetic acid; (3) Acetol; (4) Ethyl pyruvate; (5) Butanedial; (6) 2-Methyl-2-cyclopentenone;

Figure 2.9 (cont'd)
(7) Butyrolactone; (8) 2(5H)-Furanone; (9) 3-Methyl-1,2-cyclopentanedione; (10) Syringol; (11) Levoglucosan; (12) Acetosyringone.

Table 2.6 TIC area percentage of compounds in different bio-oil fractions

Compounds	Retention time (min)	Water-soluble Fraction %	Ether-soluble Fraction %	Ether-insoluble Fraction %
Glycolaldehyde	6.91	3.24	-	11.57
Acetic acid	7.28	22.95	23.54	26.84
Acetol	8.11	9.68	0.55	13.43
Ethyl pyruvate	10.09	3.84	-	5.64
Butanedial	11.07	3.60	-	5.82
Furfural	11.34	4.19	2.78	-
2-Methyl-2-cyclopentenone	12.60	0.87	1.03	1.04
Butyrolactone	14.94	0.77	-	1.13
3-Methyl-1,2-cyclopentanedione	15.96	4.86	4.80	2.44
Phenol	16.41	7.74	14.84	-
Guaiacol	16.95	2.51	4.35	-
o-Cresol	17.43	0.55	-	-
2-Methoxy-4-methylphenol	19.01	1.06	2.10	-
4-Ethyl-2-methoxyphenol	20.60	0.54	1.19	-
2-Methoxy-4-vinylphenol	21.67	0.63	1.31	-
Syringol	22.56	4.94	8.27	0.75
Isoeugenol	23.98	0.48	1.07	-
1,2,4-Trimethoxybenzene	24.12	3.74	5.15	-
5-tert-Butyl-1,2,3-benzenetriol	25.32	1.33	2.46	-
Levoglucosan	28.00	9.54	-	11.88

The water-insoluble fraction was analyzed with Py-GC/MS (Figure 2.10). The majority of the pyrolysis products are lignin-derived compounds, confirming that the water-insoluble fraction is lignin derived oligomers (pyrolytic lignin).

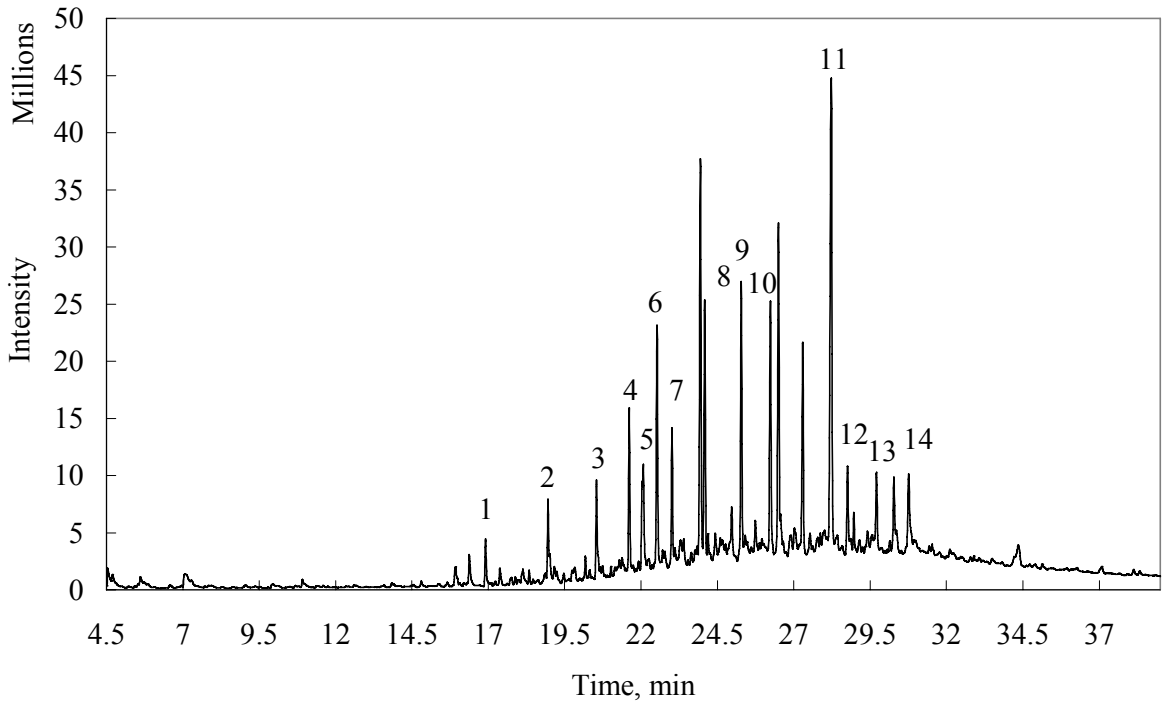

Figure 2.10 Pyrogram for pyroprobe-GC/MS analysis of the water-insoluble fraction. (1) Guaiacol; (2) p-Creosol; (3) p-Ethylguaiacol; (4) 2-Methoxy-4-vinylphenol; (5) Eugenol; (6) Syringol; (7) 2-Methoxy-4-propenylphenol; (8) 1,2,3-Trimethoxybenzene; (9) 5-tert-Butylpyrogallol; (10) 3,5-Dimethoxyacetophenone; (11) Methoxyeugenol; (12) Syringaldehyde; (13) Acetosyringone; (14) Desaspidinol

2.3.3 Bio-oil stability

Bio-oil stability is a very important characteristic for its application. The stability of the bio-oil from pyrolysis of poplar DN34 was evaluated by accelerated aging test, heating the bio-oil in a sealed pressure tube at 80°C for 48 h. The original and the aged bio-oil were analyzed by the viscosity measurement and carbonyl group measurement. The stability of this bio-oil was also compared with the other bio-oils.

(1) Viscosity change during accelerated aging test

Viscosity change is a good indication for bio-oil aging[30, 31] because of the formation of larger molecules from various reactions, condensation and polymerization. As shown in Figure 2.11, viscosity of the original bio-oil and the aged bio-oil depend on the shear rates, indicating they are non-Newtonian fluid. After aging for 2 days, viscosity of the bio-oil

increased significantly. The maximum increase of the viscosity (64 cP) was at the shear rate of 2.4 s^{-1}, with the viscosity increase rate of 17 cP/day.

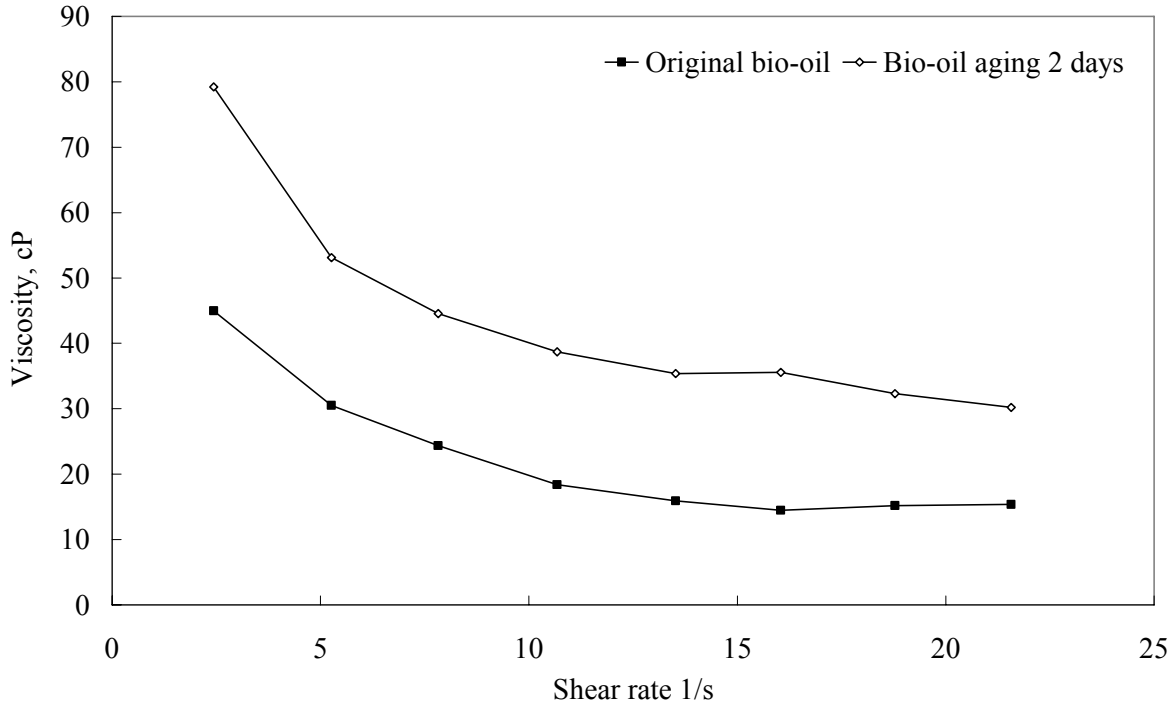

Figure 2.11 Viscosity vs shear rate measured at 25°C for original bio-oil and bio-oil aging 2 days at 80°C.

(2) Carbonyl group measurement

Carbonyl group is one of the most reactive functional groups in bio-oil. The change of functional group can also be an indication for the bio-oil aging. As shown in Figure 2.12, carbonyl group concentration (t=0) is 3.3 mol/Kg, decreased to 2.3 mol/Kg at 23 hr. Then it does not change very much from 23 hr to 48 hr, indicating the majority of the polymerization reaction related to carbonyl group takes place at the first 23 hr.

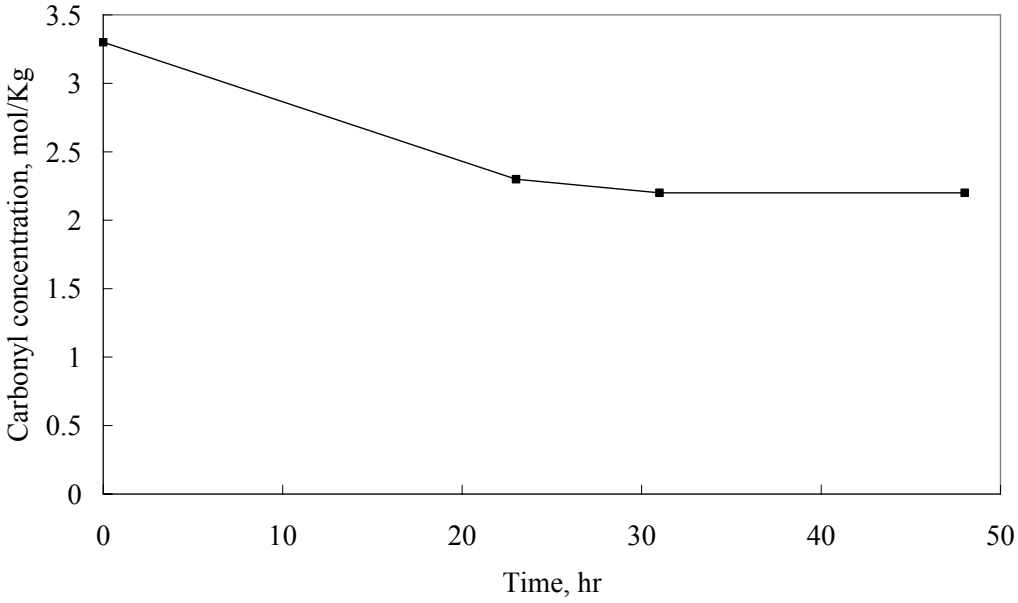

Figure 2.12 Carbonyl group concentration changes during bio-oil aging at 80 °C for 48 hrs.

2.4 Conclusions

The screw-conveyor pyrolysis reactor provides several advantages, including no requirement for heating media and no large requirement for inert gas, compact size and easy transportability. Poplar derived bio-oil from this reactor shows different physical properties compared with other bio-oils because of the high water content. Similar chemical properties were obtained compared with bio-oils from the other reactors. Accelerated aging test showed that the bio-oil viscosity increase rate was 17 cP/day at 80°C. Carbonyl group measurement also indicated that the majority of the polymerization reaction related to carbonyl group takes place at the first 23 hr. The low bio-oil yield (50 wt%) suggests that optimum operation of the reactor is required in the future.

Acknowledgements

The authors would like to thank the Michigan State University Foundation and AgBioResearch for financial support.

REFERENCES

REFERENCES

1. A. V. Bridgwater, International Journal of Global Energy Issues, 2007, **27**, 160-203.

2. P. L. Eranki, B. D. Bals and B. E. Dale, Biofuels, Bioproducts and Biorefining, 2011, **5**, 621-630.

3. P. C. Badger and P. Fransham, Biomass & Bioenergy, 2006, **30**, 321-325.

4. N. Puy, R. Murillo, M. V. Navarro, J. M. Lopez, J. Rieradevall, G. Fowler, I. Aranguren, T. Garcia, J. Bartroli and A. M. Mastral, Waste management, 2011, **31**, 1339-1349.

5. S. Thangalazhy-Gopakumar, S. Adhikari, H. Ravindran, R. B. Gupta, O. Fasina, M. Tu and S. D. Fernando, Bioresource technology, 2010, **101**, 8389-8395.

6. L. Ingram, D. Mohan, M. Bricka, P. Steele, D. Strobel, D. Crocker, B. Mitchell, J. Mohammad, K. Cantrell and C. U. Pittman Jr, Energy & Fuels, 2007, **22**, 614-625.

7. J. N. Brown and R. C. Brown, Bioresource technology, 2012, **103**, 405-414.

8. P. Sannigrahi, A. J. Ragauskas and G. A. Tuskan, Biofuels Bioproducts & Biorefining-Biofpr, 2009, **4**, 209-226.

9. G. HK and V. S. PJ, in *Agriculture handbook*, ed. M. EK, Beltsville, 1970.

10. K. Sipila, E. Kuoppala, L. Fagernas and A. Oasmaa, Biomass and Bioenergy, 1998, **14**, 103-113.

11. K. H. Kim, I. Y. Eom, S. M. Lee, D. Choi, H. Yeo, I. G. Choi and J. W. Choi, Journal of Analytical and Applied Pyrolysis, 2011, **92**, 2-9.

12. P. J. Tharakan, T. A. Volk, L. P. Abrahamson and E. H. White, Biomass & Bioenergy, 2003, **25**, 571-580.

13. M. Garcia-Perez, X. S. Wang, J. Shen, M. J. Rhodes, F. Tian, W. J. Lee, H. Wu and C. Z. Li, Industrial & Engineering Chemistry Research, 2008, **47**, 1846-1854.

14. M. Garcia-Perez, A. Chaala, J. Yang and C. Roy, Fuel, 2001, **80**, 1245-1258.

15. M. Garcia-Perez, S. Wang, J. Shen, M. Rhodes, W. J. Lee and C. Z. Li, Energy & Fuels, 2008, **22**, 2022-2032.

16. R. J. M. Westerhof, D. W. F. Brilman, W. P. M. Van Swaaij and S. R. A. Kersten, Industrial & Engineering Chemistry Research, 2009, **49**, 1160-1168.

17. S. Czernik and A. V. Bridgwater, Energy & Fuels, 2004, **18**, 590-598.

18. S. Thangalazhy-Gopakumar, S. Adhikari, R. B. Gupta and S. D. Fernando, Energy & Fuels, 2011, **25**, 1191-1199.

19. P. R. Patwardhan, D. L. Dalluge, B. H. Shanks and R. C. Brown, Bioresource technology, 2011, **102**, 5265-5269.

20. P. R. Patwardhan, R. C. Brown and B. H. Shanks, ChemSusChem, 2011, **4**, 636-643.

21. A. M. Azeez, D. Meier, J. Odermatt and T. Willner, Energy & Fuels, **24**, 2078-2085.

22. J. P. Diebold, I. Thermalchemie and L. National Renewable Energy, *A review of the chemical and physical mechanisms of the storage stability of fast pyrolysis bio-oils*, National Renewable Energy Laboratory Golden, CO, 2000.

23. A. M. Azeez, D. Meier, J. Odermatt and T. Willner, Energy & Fuels, 2010, **24**, 2078-2085.

24. C. A. Mullen and A. A. Boateng, Energy & Fuels, 2008, **22**, 2104-2109.

25. C. A. Mullen and A. A. Boateng, Energy & Fuels, 2008, **22**, 2104-2109.

26. J. P. Diebold, in *Fast Pyrolysis of Biomass: A Handbook*, ed. A. V. Bridgwater, CPL Scientific Publishing, Newbury, 2003, pp. 135-163.

27. J. P. Diebold, *A review of the chemical and physical mechanisms of the storage stability of fast pyrolysis bio-oils*, Thermalchemie, Inc, Lakewood, 1999.

28. T. P. Vispute, H. Y. Zhang, A. Sanna, R. Xiao and G. W. Huber, Science, 2010, **330**, 1222-1227.

29. A. S. Pollard, M. R. Rover and R. C. Brown, Journal of Analytical and Applied Pyrolysis, 2012, **93**, 129-138.

30. R. N. Hilten and K. C. Das, Fuel, 2010, **89**, 2741-2749.

31. A. Oasmaa and E. Kuoppala, Energy & fuels, 2003, **17**, 1075-1084.

Chapter 3 Aqueous Electrocatalytic Hydrogenation of Furfural Using a Sacrificial Anode

A paper published in *Electrochimica Acta*

Zhenglong Li[a,b], Shantanu Kelkar[a,b], Chun Ho Lam[c], Kathryn Luczek[d], James E. Jackson[c], Dennis J. Miller[b], Christopher M. Saffron[a,b,*]

Abstract

Electrocatalytic hydrogenation (ECH) of furfural to furfuryl alcohol and 2-methylfuran was studied. Experiments were run in an undivided cell in aqueous solution with a sacrificial Ni or Ni-Fe alloy anode. Aluminum (Al), Iron (Fe), Nickel (Ni), Copper (Cu), and stainless steel (SS) 308 were used as cathode materials. As expected, the cathode metal, which serves as the hydrogenation catalyst, was found to have a large effect on the ECH of furfural. Among the cathode metals studied, the Ni and Fe cathodes gave the greatest product yield and electrochemical efficiency. Effects of electrolyte solution pH on product yield and electrochemical efficiency were also investigated. The yield of furfuryl alcohol was highest at pH=5.0, while that of 2-methylfuran was favored at pH=1.0. To differentiate between the catalytic roles of the original cathode material and the Ni being dynamically deposited on the cathode by reduction of anode-derived Ni ions, ECH of furfural in a divided cell was compared with that in the undivided cell. Without pre-electrolysis during electrocatalytic hydrogenation of furfural, both the original cathode material and the

a. Department of Biosystems & Agricultural Engineering, Michigan State University, East Lansing, MI 48824, US; b. Department of Chemical Engineering & Materials Science, Michigan State University, US; c. Department of Chemistry, Michigan State University, US; d. Catholic Central High School, Grand Rapids, MI, US

* Corresponding author. Tel.: +001 517 432 7414; Fax: +001 517 432 2892. Email address: saffronc@egr.msu.edu (C.M. Saffron).

deposited nickel contributed to the catalytic effect. The initial furfural concentration and the current density also strongly affected the product yield and electrochemical efficiency.

Keywords: electrocatalytic hydrogenation; furfural; furfuryl alcohol; 2-methylfuran; sacrificial anode

3.1 Introduction

Furfural is a furan derivative that can serve as a building block for fuels and chemicals [1] or as a liquid fuel itself. Interestingly, it is also known to be inhibitory in alcohol production by *Saccharomyces cerevisiae* [2]. Reduction of furfural's aldehyde moiety forms primarily furfuryl alcohol and small amounts of 2-methylfuran,[3] valuable intermediates in the perfumery, pharmaceutical and polymer industries.[4, 5] In particular, furfuryl alcohol has wide application in a variety of synthetic fibers, rubbers, thermostatic resins and farm chemicals.[4] It can serve as a solvent for furan resins and pigments of low solubility [6] and also as a component in rocket fuel.[7] 2-Methylfuran is an intermediate in syntheses of crysanthemate pesticides, perfume intermediates and chloroquine lateral chains in medical polymers.[5] It may serve as a fuel itself, or as an octane enhancer that reduces CO and volatile hydrocarbon emissions.[8]

The main method for preparation of furfuryl alcohol and 2-methylfuran is vapor-phase catalytic hydrogenation (CH) of furfural.[3, 4, 9, 10] This approach requires high reaction temperatures (573-673K) and pressurized hydrogen,[3] a gaseous reagent not always available where furfural is produced. In this study, we explored furfural reduction via electrocatalytic hydrogenation (ECH) as a mild, efficient alternative to CH.[11] This approach is usually performed at atmospheric pressure and temperatures below 100°C with electricity as the

reducing agent. The main difference between CH and ECH is the way to generate atomic hydrogen: the CH process requires externally supplied hydrogen gas and splits molecular hydrogen to atomic hydrogen (Eq.1), while ECH reduces hydronium ions to form atomic hydrogen in situ on the catalytic cathode surface using external electrons (Eq.2).[12]

$$H_2 + 2M \rightarrow 2(H)_{ads}M \quad (1)$$

$$H_3O^+ + e^- + M \rightarrow (H)_{ads}M + H_2O \quad (2)$$

Here, M is the metal active site for hydrogen and $(H)_{ads}M$ is the chemisorbed hydrogen.

The other reactions involved in the ECH process include adsorption of unsaturated compounds (Eq. 3), the hydrogenation reaction between the adsorbed unsaturated compounds and the adsorbed hydrogen (Eq. 4), and desorption of the hydrogenated product (Eq. 5).

$$(Y=Z)_{aq} + A \rightarrow (Y=Z)_{ads}A \quad (3)$$

$$2(H)_{ads}M + (Y=Z)_{ads}A \rightarrow (YH\text{-}ZH)_{ads}A + 2M \quad (4)$$

$$(YH\text{-}ZH)_{ads}A \rightarrow (YH\text{-}ZH)_{aq} + A \quad (5)$$

Here, Y=Z is an unsaturated organic reactant, A is the adsorption sites for organic substrate, $(Y=Z)_{ads}A$ is the adsorbed organic compound, and $(YH\text{-}ZH)_{ads}A$ is the adsorbed hydrogenated product.

During ECH, hydrogen (H_2) is commonly formed as a side product from the cathode's chemisorbed hydrogen via the Tafel (Eq. 6) or Heyrovsky (Eq. 7) reactions. These processes compete with hydrogenation of organics and negatively affect the electrochemical efficiency (E.E.) of ECH.[13, 14] However, the hydrogen byproduct has value and can be further used in other catalytic processing.

$$(H)_{ads}M + (H)_{ads}M \rightarrow H_2 + 2M \quad (6)$$

$$(H)_{ads}M + (H^+)_{aq} + e^- \rightarrow H_2 + M \quad (7)$$

A few electrocatalytic hydrogenation studies of furfural to furfuryl alcohol have been reported at room temperature. Chu obtained 61.7% of furfuryl alcohol using a nano TiO_2 film electrode.[6] But earlier studies by Parpot et al.[15] explored electroreduction of furfural on Pt and Pb cathodes in 0.1 M $HClO_4$ and 0.1 M H_2SO_4, and on Cu in an alkaline medium. Interestingly, they noted 2-methylfuran in some of their final product mixtures, but reported neither yields nor optimized conditions for this little-discussed reaction. With the Pt cathode, the selectivity from furfural to furfuryl alcohol was 98% but the conversion remained very low (7.8%) after 24.5 h of electrolysis. With Cu in a carbonate buffer (pH 10), 80% of the furfural was selectively reduced to furfuryl alcohol and the conversion reached 90% within 5.5 h; this result echoed an earlier finding by Chamoulaud et al.[16], which showed that furfuryl alcohol was formed with 95% selectivity using a copper-modified graphite felt cathode in a flow cell.

The present investigation explored ECH of furfural to furfuryl alcohol and 2-methylfuran in aqueous solution in a simple undivided cell with a sacrificial anode. This approach avoided the need for proton exchange membranes, lowering both electrical resistance and equipment costs relative to most literature studies, where divided cells and anodes made of noble metals, usually Pt, were used. In this work, different anode and cathode materials as well as varying pH conditions were studied and their effects on the product yield and electrochemical efficiency were examined. Effect of starting furfural concentration and current density were also investigated. The continuous cathode reactivation via nickel ion

reduction and deposition was verified using a divided cell. Furthermore, the competitive reaction kinetics for ECH of furfural and benzaldehyde were investigated.

3.2 Experimental

3.2.1 Reagents and electrodes

Furfural (F) (≥98%), furfuryl alcohol (FA) (≥98%), 2-methylfuran (2-MF) (≥98%) and n-octane (>99%) were purchased from Sigma-Aldrich and used as received without further purification. Deionized (DI) water and methanol (>99.9%) from Sigma-Aldrich were used as solvents. The cathode material, including pure copper (Cu), pure aluminum (Al), pure iron (Fe), pure nickel (Ni) and stainless steel (SS) 308 were obtained from McMaster-Carr. Nickel alloy (80% Ni, 20% Fe) and pure nickel were used as sacrificial anodes and were purchased from The Science Company.

3.2.2 Electrochemical cell setup

The bench-scale electrocatalysis unit consisted of a simple undivided cell, configured in a manner similar to that of Navarro et al.[17] (Figure 3.1). It was constructed using a 75 mL thin layer chromatography (TLC) developing chamber, capped by a rubber stopper with holes for the anode and the cathode. To avoid oxidation of substrates on the anode side, a strip of nickel (2.8 cm×3 cm ×0.1 cm) was used as the sacrificial anode. Two types of nickel strips were used: nickel alloy and pure nickel. Several cathode materials were tested, including Fe, 308 SS, Cu, Al and pure Ni.

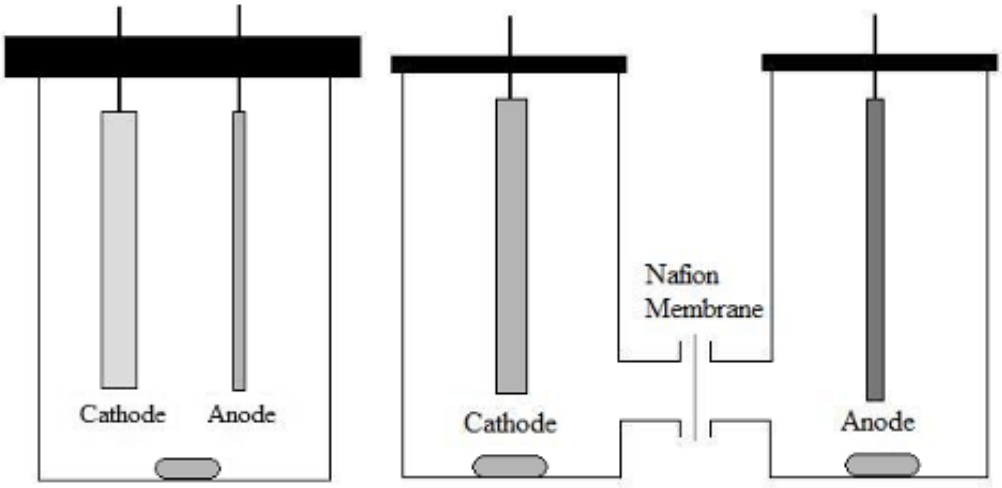

Figure 3.1 Laboratory scale undivided electrochemical cell (left) and divided H-cell (right)

Pretreatment of the electrodes was carried out to remove the metal oxides, which can deactivate the reaction when existing on the electrode surface. After polishing with sand paper, Ni, Cu, and SS electrodes were acid washed with 6.0 M HCl solution while Fe was immersed in glacial acetic acid for 1 hour. The electrode made of Al required no acid wash. After pretreatment, all electrodes were rinsed with DI water.

Base case experiments used 50 mL of 100 mM furfural solution in 4:1 mixture of water and methanol, a good solvent for both electrolyte and organic substrates.[18] Unless otherwise stated, 260% equivalent of electrons (1254 coulombs, 130% hydrogen equivalent) based on 100 mM of furfural was passed to ensure sufficient conversion for all experiments. Ammonium chloride (0.2 M) was selected as the electrolyte because it was previously shown to promote reactant conversion with good electrochemical efficiency.[19]

A dual channel power supply from Lambda (Model: LPD 422A FM) was used to provide a constant current to the cells with the positive and negative leads connected to anode and cathode electrodes, respectively. Multimeters from Omega (Model: HHM34) were used to measure current and voltage. Unless otherwise stated, a current density of 600 mA/dm^2 was used for most of the experiments. The voltage varied between 1.6 V and 2.1 V,

depending upon the cathode materials and the distance between electrodes.

To investigate effects of nickel re-deposition on the product yield, a divided H-cell was used (Figure 1) with a Nafion membrane separating the two chambers. Iron and pure nickel were used as the cathode and the anode. The catholyte was the same as in the undivided cell. There was only solvent (methanol : water, 1:4) and 0.2 M electrolyte in the anolyte.

3.2.3 Product analyses

Aqueous samples were diluted ten-fold with acetonitrile, filtered through 0.22 μm filters, and analyzed on a Shimadzu QP-5050A GC/MS. The GC used a Restek Rtx-1701 capillary column, 60 m × 0.25mm with a 0.25 μm film thickness, helium running at 1.0 ml/min as carrier gas, and a split ratio of 1:100. The injector temperature was set at 270 °C. The GC oven program started at 40°C for 1 min, then heated at 8 °C/min to 80 °C, then at 15 °C/min to 260 °C. The mass spectrometer was operated in the Electron Ionization (EI) mode at an ionization energy of 80 eV, a m/z ranging from 40 to 400, and a sampling interval of 0.34 s. The identification of species associated with each chromatographic peak was done by comparing the observed mass spectrum with the NIST library and then confirmed by injection of authentic samples. External standards were used to quantify furfural and the products of furfural reduction.

3.2.4 Calculations

The conversion, selectivity, yield and electrochemical efficiency were calculated according to the following equations:

$$\text{Conversion} = ([F]_{t=0} - [F]_t)/[F]_{t=0} \times 100 \quad (8)$$

$$\text{Selectivity} = ([FA]_t \text{ or } [2\text{-MF}]_t)/([FA]_t + [2\text{-MF}]_t) \times 100 \quad (9)$$

$$\text{Yield} = ([FA]_t \text{ or } [2\text{-MF}]_t)/[F]_{t=0} \times 100 \quad (10)$$

$$\text{E.E.} = (m_1 \times n_1 + m_2 \times n_2) / (f \times m \times n) \times 100 \quad (11)$$

Here, m_1, m_2 and m (mol) are the numbers of moles for furfuryl alcohol, 2-methylfuran and starting furfural, respectively; n_1 and n_2 are the numbers of electrons transferred during the reaction to furfuryl alcohol and 2-methylfuran, respectively (n_1=2, n_2=4), n is the number of electrons transferred during furfural reduction to furfuryl alcohol (n=2), f is the number of H_2 equivalent and it's equal to 130%. E.E. is calculated based on all the products (furfuyl alcohol and 2-methylfuran) unless otherwise stated.

3.3 Results and discussion

3.3.1 Material balance in ECH of furfural using iron as the cathode

The selectivity and material balance were investigated by hydrogenating furfural using iron as the cathode and nickel alloy as the sacrificial anode in aqueous solution (Table 3.1). Furfuryl alcohol was the major product formed under these conditions, along with small quantities of 2-methylfuran. Pathway to these two products is shown in Schemes 1.[15]

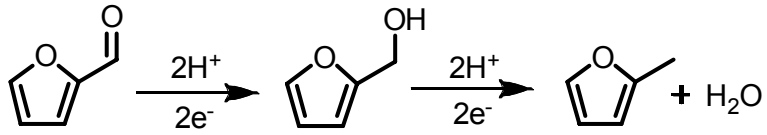

Scheme 3.1 Reaction scheme for ECH of furfural to furfuryl alcohol and 2-methylfuran

Table 3.1 ECH of furfural using iron (cathode) and nickel alloy (anode) with different starting concentrations. 260% equiv. of electrons based on the nominal starting concentration was passed.

Furfural concentration (mM)	Current density (mA/dm^2)	Run time (hr)	Selectivity (FA) (%)	Selectivity (2-MF) (%)	E.E.[a] %	Mass balance
20	175	2	100±0.0	b	26±5.0	71±3.1
100	600	5	98±0.1	2.0±0.1	29±3.5	64±0.3
140	900	5	97±1.2	3.0±1.2	18±0.7	68±5.3

a: electrochemical efficiency based on FA. b: not detected. Solvent and electrolytes: 0.2 M NH_4Cl in 50 mL water + methanol (4:1, V/V); pH: 5.0.

As Table 3.1 shows, complete material balance closure was not achieved in any of the experiments. Poor material balances for reactions in undivided ECH cells have been previously observed but were not clearly explained.[18] Figure 3.2 shows the results of three control experiments, performed without passing current, to quantify mass losses due to simple evaporation and chemical adsorption onto the electrodes: (1) substrate/electrolyte solution in cell without electrodes; (2) substrate/electrolyte solution in cell with electrodes; (3) substrate/electrolyte solution in cell with electrodes and a layer of octane on top to trap hydrophobic and volatile reaction species. There was no significant difference between controls (1) and (2) because the amount of organic compounds absorbed on the electrodes was small, on the order of 10^{-5} mmol. Controls (2) and (3) showed that evaporation contributed to the loss of reaction species as evidenced by less chemical loss with an octane layer trap. The relatively hydrophobic and volatile 2-methylfuran in particular was not very soluble in the aqueous electrolyte, so without the octane layer present as a trap, it separated from the aqueous phase and evaporated quickly.

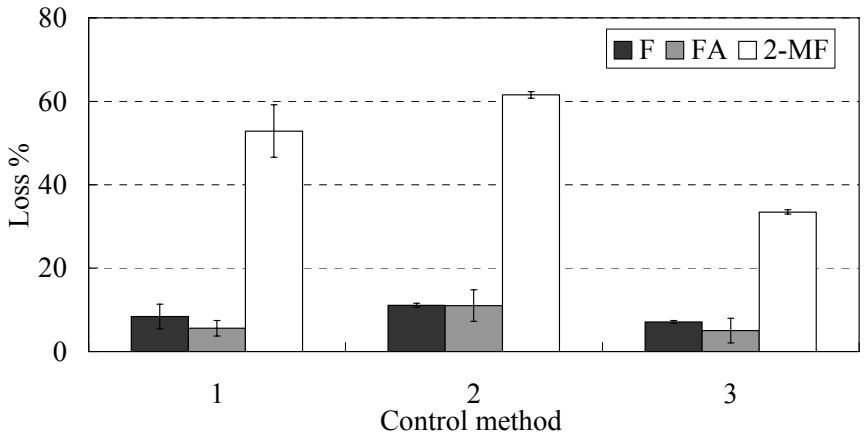

Figure 3.2 Control experiments. The solutions for the control experiments: 40 mM furfural, 40 mM furfuryl alcohol and 20 mM 2-methylfuran, 0.2 M NH_4Cl in 50 mL water + methanol (4:1, V/V).

Table 3.2 presents results for the ECH of furfural, with and without the octane layer to enhance the recovery of furfuryl alcohol and 2-methylfuran. Reactant furfural was partially extracted into the octane layer, so its extent of conversion was less (78% vs 97% conversion) with octane present than in the octane-free run. Conversely, the improved product recovery with the octane-trap increased both the electrochemical efficiency (from 29% to 43%) and the material balance (from 64% to 85%). Control experiment (3) suggested that even with the octane layer, there was still significant material loss because of the evaporation and the experimental variability, which can be considered as one of the loss mechanisms for the remaining 15% of unaccounted material. Precipitate observed during the ECH of furfural was identified as a mixture of nickel metal and nickel hydroxide based on the analysis results from inductively coupled plasma optical emission spectrometer (ICP-OES) and energy-dispersive X-ray spectroscopy (EDS) (not shown). Ongoing oxidation of the nickel anode (Eq. 12) raised the nickel ion (Ni^{2+}) concentration while cathodic proton consumption raised the OH^- concentration during electrolysis, leading to precipitation of nickel hydroxide. In addition, it was noted that under vigorous stirring conditions, nickel deposited on the

cathode surface (Eq. 13) could flake off to become part of the precipitated particles.

$$Ni(anode, s) \rightarrow Ni^{2+} + 2e^{-} \quad (12)$$

$$Ni^{2+} + 2e^{-} \rightarrow Ni(cathode, s) \quad (13)$$

Table 3.2 ECH of furfural (100 mM) without and with octane trap (12mL) using iron (cathode) and nickel alloy (anode)

Method	Conversion (%)	Selectivity (FA) (%)	Selectivity (2-MF) (%)	Yield (FA) (%)	E.E.[a] %	Mass balance (%)
without octane	97±1.4	98±0.1	2.0±0.1	61±1.2	29±3.5	64±0.3
with octane	78±4.2	98±0.3	2.0±0.3	63±3.8	43±1.0	85±7.8

a: Electrochemical efficiency based on FA. Solvent and electrolytes: 0.2 M NH_4Cl in 50 mL water + methanol (4:1, V/V); Current density: 600 mA/dm^2; pH: 5.0. Electrode areas were chosen to achieve 260% equiv. of electrons.

After filtration, the precipitate was suspended into methanol and the solution was sonicated. Analysis of the resulting solution by GC/MS showed that organic species were adsorbed onto this precipitate, another reason for the mass loss. Despite incomplete closure of the mass balance, the data in Table 2 suffice to demonstrate the utility of ECH of furfural. In the following experiments, only the organic compounds in the solution were used in mass balance calculations.

3.3.2 Effect of electrodes

Both pure nickel and nickel-iron alloy were tested as sacrificial anodes for the ECH of furfural. Iron is the more easily oxidized metal, and the alloy's behavior might differ from that of the pure metals.[20] However, the results (Figure 3.3) for the two anode materials revealed no obvious differences in performance. Therefore, to avoid irrelevant complexity, pure nickel was used as anode material in all subsequent investigations.

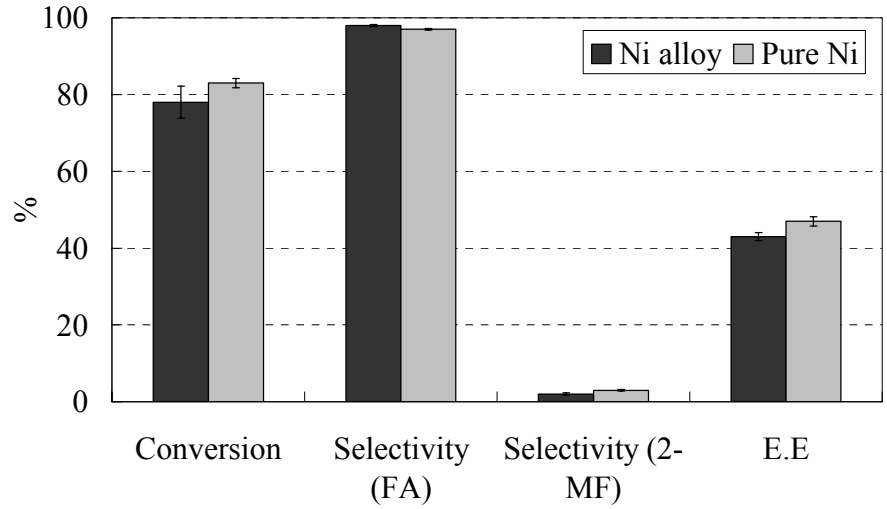

Figure 3.3 ECH of furfural (100 mM) in 50 mL water + methanol (4:1, V/V) with 0.2 M NH_4Cl using two different Ni anode materials: Ni alloy and pure Ni. Current density: 600 mA/dm^2; pH: 5.0; E.E.: electrochemical efficiency based on FA.

For ECH of organic compounds, the catalytic cathode material was the key component in terms of product selectivity and electrochemical efficiency. In an undivided cell with a nickel sacrificial anode, nickel deposit was formed onto the cathode surface due to the reduction of nickel ion (Ni^{2+}), as shown in Eq. 13. Thus, both the original cathode surface material and the new deposited nickel layer may affect the ECH of furfural.

To differentiate between the original cathode material and the influence of the nickel deposition, a divided H-cell was used with iron as the cathode and pure nickel as the anode. A Nafion membrane 117 was used to separate the two chambers and thus prevent nickel deposition on the Fe cathode. The divided H-cell had significantly lower furfuryl alcohol yield and electrochemical efficiency than the undivided cell (Figure 3.4). In the undivided cell, the nickel deposits, examined by SEM, were in the μm range, resulting in relatively large surface area compared with the plain iron cathode in the divided cell. This is a possible reason for the better performance of the undivided cell. Important information can be

obtained from this experiment: (a) the iron cathode alone without deposited nickel was electrochemically active for ECH of furfural, and (b) the deposition of nickel clearly enhanced the cathode's activity.

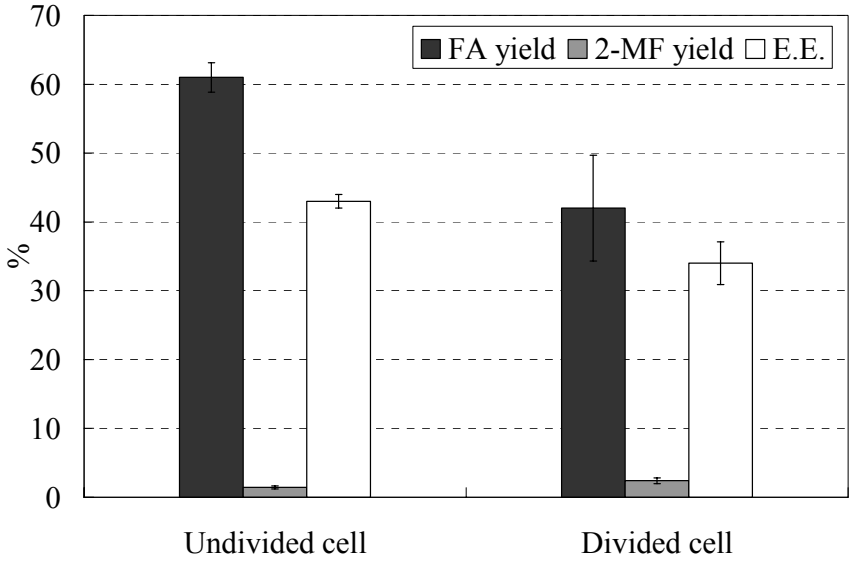

Figure 3.4 Product yield and electrochemical efficiency for ECH of furfural (100 mM) using Fe (cathode) and pure Ni (anode) in an undivided cell (50 mL water + methanol (4:1, V/V) with 0.2 M NH_4Cl) and a divided cell (both chambers: 50 mL water + methanol (4:1, V/V) with 0.2 M NH_4Cl). Current density: 600 mA/dm^2; pH: 5.0.

The effects of several additional cathode materials on product yields and electrochemical efficiency for furfuryl alcohol and 2-methylfuran formation were studied. These materials included Ni, Fe, Cu, 308 SS and Al. As can be seen in Figure 3.5, the furfuryl alcohol yield increased in the order: Al < 308 SS ≤ Cu < Ni ≤ Fe. As for 2-methylfuran, Ni, Cu and 308 SS were slightly better than Fe and Al, but the differences were small. Electrochemical efficiencies for different cathode materials were also calculated and increased in the same order as the yields (Figure 3.5). Vilar et al.[21] stated that the cathode had practically no effect on the electrochemical efficiency during ECH of cyclohexanone, isophorone and acetylcyclohexene using a Ni sacrificial anode, but the results for ECH of

furfural did show substantial differences. The reason for this difference was that Vilar et al. used pre-electrolysis to deposit nickel on the cathode material before adding organic compounds. In this investigation, pre-electrolysis was not used; instead, furfural was added to the solution at the beginning of the electrolysis. Without pre-electrolysis, there was no nickel deposited at the onset of reaction, and the unmodified cathode material contributed to the catalytic effect on the ECH of furfural. Later, when deposition of nickel had taken place for some time, the deposited nickel became the predominant catalyst for converting furfural. Over the course of ECH of furfural in the undivided cell, both the naked cathode and the deposited nickel contributed to the observed product yield and efficiency.

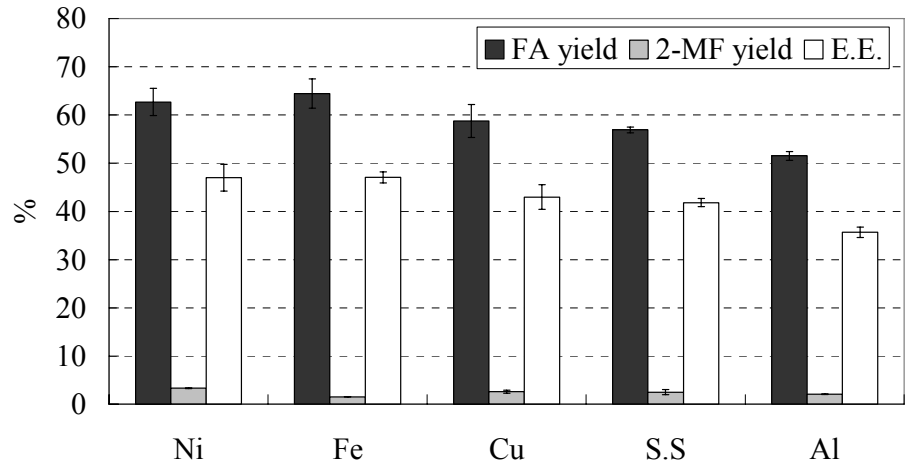

Figure 3.5 Product yields and electrochemical efficiency for ECH of furfural (100 mM) in 50 mL water + methanol (4:1, V/V) with 0.2 M NH_4Cl using different cathode materials. Current density: 600 mA/dm^2; pH: 5.0.

3.3.3 pH effect

Besides changing the electrode materials, the pH of the experimental solution was another important parameter affecting the ECH of furfural. It is expected that pH should affect the competition between hydrogenation of furfural (Eqs 3 to 5) and desorption of H_{ads} (hydrogen evolution: Eqs 6 and 7). The pH should have little effect on the thermal desorption

of H_{ads} (Eq. 6) but should have a pronounced effect on its electrochemical desorption (Eq. 7) because it involves H_2O (neutral and alkaline pH) or H_3O^+ (acidic pH) in the process.

Different pH conditions (pH=1.0, 5.0 and 9.5) were investigated for ECH of furfural (100 mM) using pure nickel as cathode and anode. The standard solution of water, methanol and NH_4Cl used in these experiments has a pH =5.0. HCl was added to the above solution to change the pH to 1.0, while NH_4OH (aqueous ammonia) was used to adjust the solution to pH=9.5.

The effect of pH on furfural conversion, product selectivity, yield, electrochemical efficiency and the material balance are shown in Table 3.3. The conversion of furfural at pH 1.0 was much lower than that at pH 5.0 and 9.5. As shown in Eq. 7, lowering pH (i.e. raising hydronium ion concentration) should raise the hydrogen evolution rate at the expense of furfural conversion and electrochemical efficiency. It was interesting that the selectivity of 2-methylfuran was increased as pH=1.0. To further enhance selectivity to 2-methylfuran, even more acidic conditions than pH 1.0 could be employed, but besides further loss of current to H_2 formation, acid catalyzed polymerization of furfuryl alcohol would then be expected.

Table 3.3 ECH of furfural (100 mM) using pure nickel for cathode and anode under different pH conditions

pH	Conversion	Selectivity (FA) (%)	Selectivity (2-MF) (%)	Yield (FA) %	Yield (2-MF) %	E.E. %	Mass balance %
1.0	66±3.0	86±1.3	14±1.3	39±3.1	6.4±0.2	39±2.1	79±5.9
5.0	80±1.7	95±0.0	5.0±0.0	63±2.8	3.3±0.1	56±2.2	86±1.3
9.5	74±2.3	93±0.1	7.0±0.1	24±0.7	1.9±0.0	23±0.5	53±1.6

Solvent and electrolytes: 0.2 M NH_4Cl in 50 mL water + methanol (4:1, V/V). Current density: 600 mA/dm^2.

The overall electrochemical efficiency based on the two products was highest at pH=5.0. At lower pH, the competitive reaction (Eq. 6 and 7) for hydrogen evolution was favored because of the high hydronium ion concentration. At higher pH 9.5, the hydrogenation reaction should be favored over the hydrogen evolution. However, the pH of the solution changed from 9.5 to 11 during the electrolysis. Furfural was not stable at this alkaline condition and the concentration of furfural decreased, which has been examined using control experiments (data not shown here). The decrease of furfural concentration lowered the reaction rate of furfural hydrogenation, thus resulting in lower furfural conversion and electrochemical efficiency (Table 3.3), which can also be observed in Figures 3.6 and 3.7.

3.3.4 Influence of starting reactant concentration

Different starting concentrations of furfural were chosen to study their effects on the electrochemical efficiency, furfural conversion and product yield during ECH. As shown in Figure 6, the electrochemical efficiency was maximized when the starting concentration was 100 mM. As the concentration was reduced below 100 mM, the hydrogenation reaction (Eq. 4) became slower so that hydrogen evolution became more competitive. When the concentration of furfural is large, hydrogenation should be favored relative to the hydrogen evolution reaction. However, more precipitate was observed at larger furfural concentrations because more electrons were passed and more nickel ion was produced. Additionally, more organic species were adsorbed onto the precipitate particles, thus reducing material balance closure (Figure 6). Because of the loss of product species as evidenced by the mass balance, the calculated electrochemical efficiency at 200 mM was smaller than that at 100 mM.

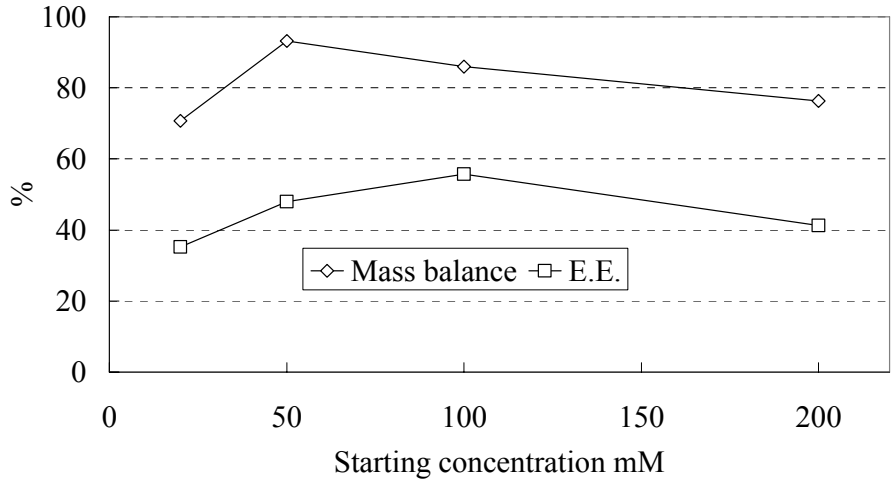

Figure 3.6 Effect of different starting concentrations of furfural on mass balance and electrochemical efficiency using Ni (cathode) and Ni (anode) in undivided cell. Solvent and electrolytes: 0.2 M NH_4Cl in 50 mL water + methanol (4:1, V/V); Current density: 600 mA/dm^2; pH: 5.0. 260% eq. of electrons based on the nominal starting concentration was passed.

As shown in Figure 3.7, furfural conversion increased slightly as the starting furfural concentration increased. Furfuryl alcohol and 2-methylfuran yields showed a maximum at 50 mM and 100 mM, respectively (Figure 3.7).

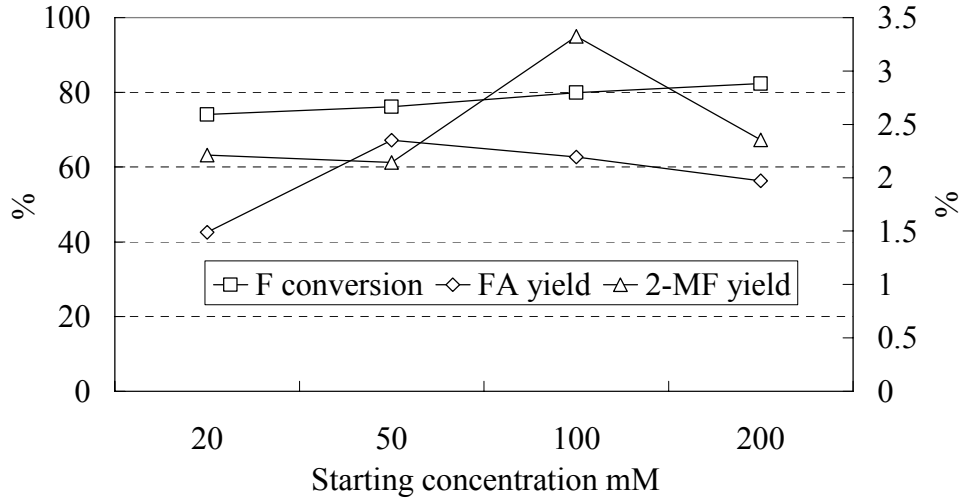

Figure 3.7 Effect of different starting concentrations of furfural on conversion, furfuryl alcohol yield (left y-axis) and 2-methylfuran yield (right y-axis) using Ni (cathode) and Ni (anode) in undivided cell. Solvent and electrolytes: 0.2 M NH_4Cl in 50 mL water + methanol (4:1, V/V); Current density: 600 mA/dm^2; pH: 5.0.

3.3.5 Effect of current density

Current density, directly related to the total reaction rate, may have an effect on the electrochemical efficiency and product yield. Several different current densities in the range of 300 -1200 mA/dm^2 were studied. Results showed that the electrochemical efficiency decreased when increasing the current density from 300 to 1200 mA/dm^2 (Figure 3.8). An optimum current density usually exists for ECH of organic compounds.[14, 18] When the current density is smaller than this optimum value, the surface coverage of the H_{ads} is smaller. The probability of the collision between H_{ads} and $(furfural)_{ads}$ is lower, and the electrochemical desorption of H_{ads} (Eq. 7) is important, resulting in a smaller electrochemical efficiency. When the current density is higher than the optimum value, the adsorption sites M are saturated with H_{ads}, so no matter how the current density is increased, the hydrogenation of furfural (Eq. 4) and thermochemical desorption of H_{ads} (Eq. 6) are not affected. However, higher current density would result in a more negative cathode potential, thus increasing the electrochemical desorption rate of H_{ads} (Eq. 7) and decreasing the electrochemical efficiency. The lowest current density 300 mA/dm^2 studied in this paper may exceed the optimum current density, thus a continuous decrease of electrochemical efficiency was observed.

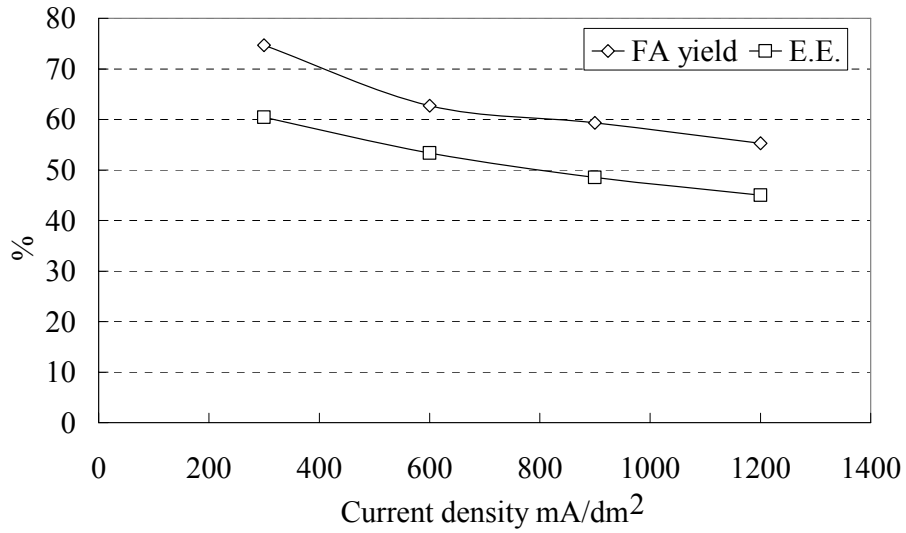

Figure 3.8 Effect of current density on electrochemical efficiency and furfuryl alcohol yield during ECH of furfural using nickel as cathode and anode in undivided cell. Solvent and electrolytes: 0.2 M NH_4Cl in 50 mL water + methanol (4:1, V/V); pH: 5.0.

3.3.6 Competitive reaction kinetics

Furfural is usually produced by acid hydrolysis of biomass residues such as corn cobs, corn stover, rice straw, wheat straw, forest slash and sawdust. Organic compounds derived from cellulose or lignin may compete with furfural hydrogenation. Competitive ECH of furfural with benzaldehyde, also an aromatic aldehyde, was therefore studied. Figure 3.9 shows reactant concentrations vs. time for the ECH of a mixture comprising 80 mM furfural and 80 mM benzaldehyde. Slopes of the resulting linear fits represent conversion rates on the nickel catalyst; these rates were very similar for furfural and benzaldehyde at 9.7 and 9.4 mM/h, respectively, consistent with their common character as aromatic aldehydes. The total of 19.1 mM/h conversion rate in the 50 mL sample volume was affected by a 133 mA current, yielding an overall electrochemical efficiency of 37.3%, similar to those found in the single substrate experiments. Thus, neither selectivity difference nor interference is seen between these two substrates.

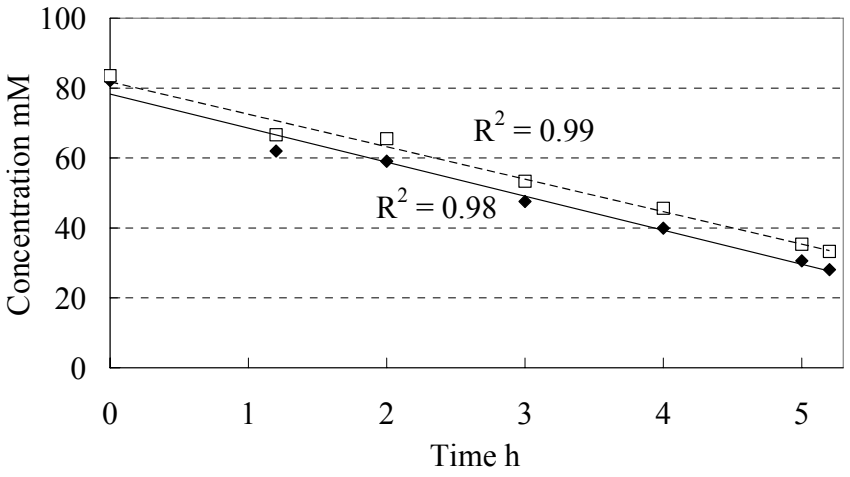

Figure 3.9 Concentrations of furfural (solid line) and benzaldehyde (dashed line) vs ECH reaction time using nickel as cathode and anode in an undivided cell. Reactant: mixture of 80 mM furfural and 80 mM benzaldehyde. Solvent and electrolyte: 0.2 M NH_4Cl in 50 mL water/methanol (3:2, v/v). Current density: 600 mA/dm^2; pH: 5.0.

3.4 Conclusions

Electrocatalytic hydrogenation of furfural was accomplished using an undivided electrolytic cell with a sacrificial anode immersed in aqueous solution. Furfuryl alcohol and 2-methylfuran were the major and minor products, respectively. Pure nickel and nickel alloy anode materials behaved similarly in terms of product selectivity. Conversely, the cathode material had a large effect on the electrocatalytic hydrogenation of furfural, with nickel and iron giving the best results among those studied. In this system, nickel deposition improved the activity and selectivity of the original cathode. Without pre-electrolysis during electrocatalytic hydrogenation of furfural, both the original cathode material and deposited nickel contributed to the catalytic effect. The pH of the solution also affected product selectivities and electrochemical efficiency. Furfuryl alcohol had an optimum yield at pH=5.0, while 2-methylfuran was favored at pH=1.0. As current density increased, furfuryl alcohol yield and electrochemical efficiency were decreased. In direct competition, ECH reaction

rates of furfural and of benzaldehyde were similar, with no signs of mutual interference.

Vaart et al.[22] stated that atomic hydrogen concentration at the catalyst surface can be controlled and maintained by the applied potential. This allows the operation of the ECH process at ambient pressures compared with the extremely high hydrogen pressure in catalytic hydrogenation. Based on this investigation, electrocatalytic hydrogenation of furfural using a sacrificial anode could be a very promising process for furfuryl alcohol production.

Acknowledgements

The authors would like to thank the Michigan State University Foundation and AgBioResearch for financial support. Assistance provided by Mr. Daniel L. Swanson and Mr. Ryan Black is also acknowledged.

REFERENCES

REFERENCES

1. J. Ebert. http://biomassmagazine.com/articles/1950/furfural-future-feedstock-for-fuels-and-chemicals. 2008.

2. M. J. Taherzadeh, L. Gustafsson, C. Niklasson and G. Liden, J. Biosci. Bioeng., 2000, **90**, 374-380.

3. R. S. Rao, R. T. K. Baker and M. A. Vannice, Catal. Lett., 1999, **60**, 51-57.

4. Y. L. Zhu, H. W. Xiang, Y. W. Li, H. J. Jiao, G. S. Wu, B. Zhong and G. Q. Guo, New J. Chem., 2003, **27**, 208-210.

5. H. Y. Zheng, Y. L. Zhu, B. T. Teng, Z. Q. Bai, C. H. Zhang, H. W. Xiang and Y. W. Li, J. Mol. Catal. A: Chem., 2006, **246**, 18-23.

6. D. B. Chu, Y. Y. Hou, J. G. He, M. Xu, Y. Q. Wang, S. X. Wang, J. Wang and L. W. Zha, J. Nanopart. Res., 2009, **11**, 1805-1809.

7. S. G. Kulkarni, V. S. Bagalkote, S. S. Patil, U. P. Kumar and V. A. Kumar, Propell. Explos. Pyrot., 2009, **34**, 520-525.

8. S. Gouli, E. Lois and S. Stournas, Energ. Fuel, 1998, **12**, 918-924.

9. J. Yang, H. Y. Zheng, Y. L. Zhu, G. W. Zhao, C. H. Zhang, B. T. Teng, H. W. Xiang and Y. W. Li, Catal. Commun., 2004, **5**, 505-510.

10. J. Lessard, J. F. Morin, J. F. Wehrung, D. Magnin and E. Chornet, Top. Catal., 2010, **53**, 1-4.

11. C. M. Cirtiu, A. Brisach-Wittmeyer and H. Ménard, J. Catal., 2007, **245**, 191-197.

12. D. Tountian, A. Brisach-Wittmeyer, P. Nkeng, G. Poillerat and H. Ménard, J. Appl. Electrochem., 2009, **39**, 411-419.

13. B. Mahdavi, J. M. Chapuzet and J. Lessard, Electrochim. Acta, 1993, **38**, 1377-1380.

14. D. Robin, M. Comtois, A. Martel, R. Lemieux, A. K. Cheong, G. Belot and J. Lessard, Can. J. Chem., 1990, **68**, 1218-1227.

15. P. Parpot, A. P. Bettencourt, G. Chamoulaud, K. B. Kokoh and E. M. Beigsir, Electrochim. Acta, 2004, **49**, 397-403.

16. G. Chamoulaud, D. Floner, C. Moinet, C. Lamy and E. M. Belgsir, Electrochim. Acta, 2001, **46**, 2757-2760.

17. D. Navarro and M. Navarro, J. Chem. Educ., 2004, **81**, 1350-1352.

18. D. S. Santana, G. O. Melo, M. V. F. Lima, J. R. R. Daniel, M. C. C. Areias and M. Navarro, J. Electroanal. Chem., 2004, **569**, 71-78.

19. M. V. F. Lima, F. D. Menezes, B. de Barros and M. Navarro, J. Electroanal. Chem., 2008, **613**, 58-66.

20. A. P. da Silva, S. D. C. Mota, L. W. Bieber and M. Navarro, Tetrahedron, 2006, **62**, 5435-5440.

21. M. Vilar, J. L. Oliveira and M. Navarro, Appl. Catal. A: Gen., 2010, **372**, 1-7.

22. V.D. Vaart, Electrocatalytic Hydrocracking, Virginia Polytechnic Institute and State University, Blacksburg, 1992, pp. 1.

Chapter 4 Mild Electrocatalytic Hydrogenation and Hydrodeoxygenation of Bio-oil Derived Phenolic Compounds using Ruthenium Supported on Activated Carbon Cloth

A paper published in *Green Chemistry*

Zhenglong Li[a,b], Mahlet Garedew[a], Chun Ho Lam[c], James E. Jackson[c], Dennis J. Miller[b], Christopher M. Saffron[a,b,d,*]

Abstract

Electrocatalytic hydrogenation (ECH) is an option for stabilizing or upgrading bio-oil that employs mild conditions (<=80°C and ambient pressure) compared to hydrotreatment. In this study, phenol, guaiacol (2-methoxyphenol), and syringol (2,6-dimethoxyphenol) were chosen as model lignin-like substrates because of their abundance in bio-oil and their high resistance to hydrogenation relative to the carbonyl compounds. Cathodic reduction was catalyzed by ruthenium supported on activated carbon cloth (Ru/ACC), a novel electrocatalyst. Incipient wetness impregnation and cation exchange methods were employed to prepare the electrocatalyst using three different ruthenium precursors. Scanning electron microscopy revealed that ruthenium nanoparticles within the range of 10 to 20 nm were deposited on the support by both catalyst synthesis methods. Catalysts prepared by cation exchange were more active than those prepared using incipient wetness impregnation, presumably because of support surface functionalization by the oxidation pretreatment. When using incipient wetness impregnation, catalysts synthesized with precursor

a. Department of Biosystems & Agricultural Engineering, East Lansing, MI 48824, US
b. Department of Chemical Engineering & Materials Science, East Lansing, MI 48824, US
c. Department of Chemistry, Michigan State University, East Lansing, MI 48824, US
d. Department of Forestry, East Lansing, MI 48824, US
*Corresponding author, Tel.: +1 517 432 7414; fax: +1 517 432 2892. E-mail address: saffronc@egr.msu.edu (C.M. Saffron).

hexaammineruthenium (III) chloride showed the best activity and electrochemical efficiency, followed by catalysts prepared with ruthenium (III) chloride and ruthenium (III) nitrosyl nitrate. The Ru/ACC electrocatalyst reduced guaiacol, phenol and syringol with similar electrochemical efficiencies, but temperature was an important variable; the electrochemical efficiency for guaiacol reduction increased from 8% at 25°C to 17% at 50°C, but then dropped back to 10% at 80°C. Solution pH also affected catalyst activity and product selectivity, with acidic conditions favoring guaiacol conversion, electrochemical efficiency and cyclohexanol selectivity.

4.1 Introduction

Bio-oil, the liquid product from fast pyrolysis of biomass, is a promising sustainable material for transportation fuel production. However, the raw bio-oil is not ready for end use because of its tendency to polymerize and to corrode metal containers and pipes. This reactivity is largely due to the presence of unsaturated oxygenates such as aldehydes, ketones, carboxylic acids and phenols.[1, 2] Thus, for long-term storage and any further upgrading, bio-oil must first be stabilized in order to minimize downstream coke formation, catalyst deactivation and carbon loss to the gas phase.[3]

Catalytic hydrogenation has been shown to be a good method for bio-oil stabilization, converting most aldehydes, ketones, phenols and sugars to saturated alcohols and polyols.[3, 4] However, such hydrogenation is typically run at temperatures over 100°C,[3, 5, 6] high enough to cause accelerated bio-oil polymerization.[7] We propose instead electrocatalytic hydrogenation (ECH) which operates at less than 80°C and ambient pressure; these mild conditions minimize both polymerization and catalyst deactivation by coke formation. During

ECH, reduction of protons from solution forms atomic hydrogen *in situ* on the catalytic electrode surface where it is needed to hydrogenate organic substrates. This strategy simplifies processing and avoids the need for externally supplied, fossil-based hydrogen gas and associated handling equipment. Ideally, the needed electricity would come from carbon-free sources such as solar, wind, or even nuclear power. Electrocatalytic hydrogenation thus represents a green, carbon-retentive pathway for stabilization (and potentially further upgrading) of biomass-derived bio-oil to produce fuels and chemicals.

Lignin-derived phenolic compounds account for 25-30% of the raw bio-oil,[8, 9] but have a lower oxygen content (22-30 vs. 33-40 wt % for raw bio-oil, dry basis).[10] Compared to other bio-oil components such as aldehydes and ketones, phenolics are more resistant to hydrogenation.[11] Therefore, successful ECH of phenol is a significant step towards its application for raw bio-oil stabilization.

Previous research[12-17] on ECH of phenolic compounds has shown that large cathode surface areas are usually necessary to achieve high reaction rates. Electrodes made with pressed metallic powder particles have been successfully used,[18, 19] but their mechanical strength is weak without addition of a binding material[20] and much surface area is lost in the powder pressing step. To overcome the disadvantages of pressed electrodes, Menard and co-workers developed a new electrode by entrapping catalytic powders into reticulated vitreous carbon (RVC).[12, 21-23] This is an effective system to test different classical catalytic hydrogenation catalysts using electrochemistry.[12, 24] However, the catalyst powders are mobile, so the amount of active catalysts involved in the actual hydrogenation is difficult to measure and the mechanically fragile electrode may be destroyed by strong stirring.

To develop a well-defined catalytic cathode, we immobilized ruthenium onto activated carbon cloth (ACC) using incipient wetness impregnation and cation exchange methods. As a catalyst support, the advantages of ACC include high rates of adsorption, high surface area (1000 to 2100 m^2/g)[25] and potential for easy *in situ* regeneration.[26] Ruthenium supported on carbon has been shown to be an efficient catalyst for classical chemical hydrogenation of various organics such as phenols,[27] organic acids,[28, 29] amino acids[30] and bio-oil itself[31].

In this investigation, ECH of guaiacol was assessed in terms of reactivity, product selectivity and electrochemical efficiency (E.E.) as functions of catalyst parameters (e.g. preparation methods, precursor types, ruthenium content, type of support) and reaction conditions (temperature and pH). In order to demonstrate chemical reduction on a range of phenolic compounds, the ECH of phenol and syringol were also investigated using the same conditions as for guaiacol ECH.

4.2 Experimental

4.2.1 Reagents and materials

Guaiacol (98+%) and 2-methoxycyclohexanol (99%) were obtained from Alfa Aesar. 2,6-Dimethoxyphenol (syringol) (99%) was purchased from Sigma-Aldrich and cyclohexanol (99+%) was from Mallinckrodt. All of these compounds were used as received without further purification. Phenol, from Mallinckrodt, was purified by sublimation to remove moisture.

Zorflex® ACC FM100 was obtained from the Calgon Carbon Co. Ruthenium (III) chloride ($RuCl_3$) hydrate (99.9% PGM basis, Ru 38% min), hexaammineruthenium (III)

chloride ($Ru(NH_3)_6Cl_3$, Ru 32.1% min) and ruthenium (III) nitrosyl nitrate ($Ru(NO)(NO_3)_3$, Ru 31.3% min) were bought from Alfa Aesar.

4.2.2 Catalyst preparation

Zorflex® ACC FM100 was chosen as the support for the ruthenium catalysts due to good conductivity and high surface area. For most of the experiments, ACC was washed in DI water; this material was labeled "original ACC." According to energy dispersive X-ray spectroscopy (EDX) analysis, there were some mineral impurities in the original cloth (Table 4.1). To probe the effects of the catalyst support, "washed ACC" was obtained by washing ACC in boiling concentrated HCl solution for three days, thoroughly rinsing with DI water to remove residual HCl, and then drying in the oven at 105°C. EDX of this material only showed C, O and small amounts of Cl, presumably a residue from the HCl washing, as there was no Cl in the original ACC.

Table 4.1 Energy dispersive X-ray analyses of the original ACC and washed ACC

	Weight %	
Element	Original ACC	Washed ACC
C	80.9±0.48	92.0±0.05
O	12.1±0.03	7.3±0.05
Cl	-	0.8±0.01
Al	2.6±0.16	-
S	0.3±0.06	-
Zn	4.1±0.29	-

Two methods were used for the catalyst preparation: incipient wetness impregnation and cation exchange. For incipient wetness impregnation, three precursors were used, including $Ru(NH_3)_6Cl_3$, $Ru(NO)(NO_3)_3$ and $RuCl_3$. For $Ru(NH_3)_6Cl_3$ and $Ru(NO)(NO_3)_3$, two ruthenium loadings (nominal 3 wt% and 5 wt%) were prepared, while only 3 wt% (nominal) ruthenium content was used for $RuCl_3$ because of its relatively low solubility in

water. A piece of ACC (1.3cm × 3.0cm) was first soaked in ruthenium precursor solution to saturate the ACC pores. Kimwipes® were then used to remove the excess solution after the ACC was soaked. The wet ACC was dried under room conditions, then vacuum dried at room temperature, and finally reduced with H_2 in a Parr pressure reactor (model 452HC) at 500 psi and 220 °C for more than 12 hrs. During the reduction, hydrogen was supplied continuously and the reactor was purged occasionally to remove the product gases.

$Ru(NH_3)_6Cl_3$ was used as the precursor for cation exchange preparation and five ruthenium loadings (nominal 1 wt%, 1.5 wt%, 3 wt%, 5 wt% and 6.6 wt%) were prepared. A piece of ACC was first pre-oxidized using boiling 1 mol/dm^3 HNO_3 solution for 24 hours.[32] The pretreated ACC was then washed thoroughly with DI water to remove the residual HNO_3 and dried under vacuum at room temperature. After drying, it was soaked in $Ru(NH_3)_6Cl_3$ solution with 1 mol/dm^3 ammonia overnight to exchange $Ru(NH_3)_6^{3+}$ onto the cloth.[33] The ACC was removed, washed carefully with DI water, and then dried under vacuum at room temperature, and reduced as above with H_2 at 500 psi and 220°C.

4.2.3 Catalyst characterization

Ruthenium contents of the catalysts were measured on a Varian 710-ES inductively coupled plasma optical emission spectrometer (ICP-OES). The catalysts were digested using aqua regia in a boiling water bath for 4 hr, filtered and diluted with DI water. The standards prepared with $RuCl_3$ were used to quantify the ruthenium content over a concentration range of 0.08 ppm to 50 ppm.

Scanning electron microscopy (SEM) on a JEOL JSM-7500F and a JEOL 6400V were used to image the catalyst support and the morphology of ruthenium particles on the

support. The catalysts were mounted onto the aluminum stubs with carbon paste and then dried under vacuum overnight. Secondary electron imaging was used to obtain the images. Surface chemical composition was characterized by EDX coupled with the JEOL 6400V SEM.

Brunauer-Emmett-Teller (BET) surface area, micropore area and micropore volume of the samples were measured on a Micromeritics® ASAP 2010 system using a static volumetric adsorption and desorption method. Nitrogen was used as the adsorptive gas and the measurement was made at 77 K. Nitrogen pressure was increased until 99% of the nitrogen saturation pressure was reached. The total surface area of the sample was calculated using the BET method from the adsorption isotherm from 0.06 to 0.20 relative pressures. The micropore volume was calculated from the desorption isotherm using the BJH (Barrett, Joyner and Hallender) method.

A method devised by NREL[34] was used to analyze the ash content in the original ACC and in the HCl washed ACC. Samples of 0.5 to 2.0 g were weighed to the nearest 0.1 mg and transferred to dried crucibles. A muffle furnace set to 575 ± 25°C was used to ash the samples to constant weights. After cooling in a desiccator, the residue was weighed to determine the ash content.

4.2.4 Experimental setup

Electrochemical hydrogenation was carried out in a two-chamber glass H-cell,[35] separated with a DuPont® Nafion-117 membrane. Catholyte (30 mL) consisted of 0.2 mol/dm^3 HCl, 0.2 mol/dm^3 NaCl or 0.2 mol/dm^3 NaOH, depending on the experiments. Ru/ACC prepared as described above was used as the working electrode (cathode). Anolyte

(30 mL) consisted of 0.2 M phosphate buffer (pH=7), and a Pt wire was used as the counter electrode (anode). The whole cell was placed in a water bath for experiments at controlled temperatures such as 50°C and 80°C. ECH was carried out under galvanostatic control (100 mA) with a dual channel potentiostat from Lambda (Model: LPD 422A FM). Before the electrochemical hydrogenation, 10 minutes of pre-electrolysis (80 mA) was applied to activate the ruthenium catalyst. After the ruthenium was reduced, 1 mL 620 mmol/dm^3 guaiacol solution in isopropanol was added to the cathode chamber to make an initial concentration of guaiacol equal to 20 mmol/dm^3. For all the experiments, ECH was performed for 2 hours.

4.2.5 Product analysis

Chemical analysis proceeded by withdrawing 1 mL sample aliquots at discrete time intervals from the cathode and the anode chambers. The samples were further saturated with NaCl, acidified to pH=1 and then 1 mL chloroform was added to extract the organics.[12] After the experiments, the Ru/ACC catalyst was immersed in 5 mL chloroform and the solution was sonicated for 15 min to desorb any adsorbed organics into the solution. The solution was then filtered using a 0.22 μm syringe filter for GC/MS analysis.

All the samples were analyzed on a Shimadzu QP-5050A GC/MS. The GC used a Restek Rtx-1701 capillary column, 60 m × 0.25mm with a 0.25 μm film thickness, a 1.0 ml/min helium carrier gas flow rate, and a split ratio of 1:40. The injector temperature was set at 270°C. The GC oven program started at 40°C for 1 min, and then heated at 15°C/min to 260°C. Mass spectrometry was operated in the electron ionization (EI) mode at an ionization energy of 80 eV, a m/z ranging from 28 to 400, and a sampling interval of 0.34 s. Species

associated with each chromatographic peak were identified by comparing their observed mass spectrum with the NIST library and then confirmed by injection of authentic samples. External standards were also used to identify compounds and quantify the peaks.

4.2.6 Calculations

The conversion, selectivity and electrochemical efficiency were calculated according to the following equations:

$$\text{Conversion} = (\text{moles consumed of reactant} / \text{initial moles of reactant}) \quad (11)$$

$$\text{Selectivity} = (\text{moles of desired product} / \text{total moles of products}) \quad (12)$$

$$\text{E.E.} = (\text{Electrons used to generate products} / \text{Total electrons passed}) \quad (13)$$

4.3 Results and Discussion

4.3.1 Characterization of catalysts

As mentioned in the introduction, a high surface area cathode is necessary for the efficient reduction of guaiacol. The catalytic cathodes' BET surface area, micropore area and micropore volume were analyzed (Table 4.2). In order to assess the underlying support properties of the catalyst supports, ACC was pretreated in the same manner (designated the "blank ACC") as the catalyst, by washing with DI water and reducing with hydrogen at 220 °C and 500 psi. The blank ACC has a surface area of 1,010 m^2/g, very similar to the value reported in the literature.[36] Compared with other supports used for cathodes,[12] this kind of support has much larger surface area. The majority of the pores are micropores and the volume is 0.30 cm^3/g (Table 4.2). Upon loading with different ruthenium precursors, the supports' micropore volumes decreased, suggesting that some of the micropores were

blocked by ruthenium. As shown in Table 4.2, catalyst 6.6-CE-NH3*, prepared by cation exchange, has a very different surface area and micropore volume than the other catalysts because the support was pretreated in 1 mol/dm^3 boiling nitric acid for 24 hrs. According to Pradhan and Sandle,[32] oxidation with nitric acid generates surface oxygen moieties at the entrance of the pores, restricting access of N_2 molecules to the micropores. Thus this type of catalyst shows reduced surface area and micropore volume.

Table 4.2 BET surface area, micropore area and micropore volume of the blank ACCand the catalysts

Sample name	Preparation method	Precursor	BET surface area m^2/g	Micropore area m^2/g	Micropore volume cm^3/g
Blank ACC	DI water wash H_2 reduction at 220 °C and 500 psi	-	1010	685	0.30
3-IW-Cl	Incipient wetness	$RuCl_3$	904	599	0.27
3-IW-NH3	Incipient wetness	$Ru(NH_3)_6Cl_3$	800	551	0.26
3-IW-NO	Incipient wetness	$Ru(NO)(NO_3)_3$	879	612	0.28
6.6-CE-NH3	Cation exchange	$Ru(NH_3)_6Cl_3$	341	139	0.06

Figure 4.1 shows a SEM image of the blank ACC FM100. With its carbon fibers knitted together, the conductivity is very high,[37] making it a good electrocatalyst support. Because it is monolithic, filtration or decantation is not needed after the reaction. This

* Catalyst codes are used to refer to each type of catalyst and catalyst preparation method. In 6.6-CE-NH3, the number "6.6" is the ruthenium weight percent, "CE" is the method cation exchange and "NH3" means the precursor is $Ru(NH_3)_6Cl_3$. For incipient wetness impregnation, "IW" is used to indicate the method. Designations for the other two precursors, $RuCl_3$ and $Ru(NO)(NO_3)_3$, are "Cl" and "NO" respectively. For the catalysts (3 wt% Ru) prepared on HCl-washed ACC with $RuCl_3$ as precursor, the code 3-IW-Cl-AW was used, where "AW" stands for acid washed.

flexible support can conveniently be cut and shaped to fit into different kinds of reactors.

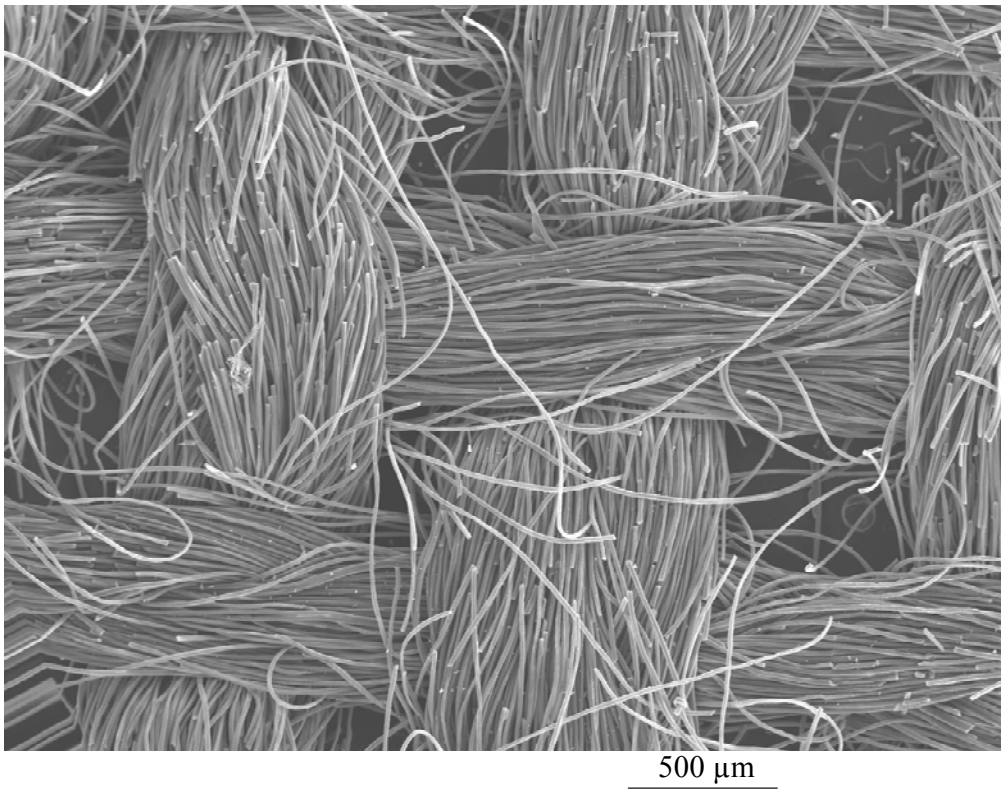

Figure 4.1 SEM image of the blank ACC FM100. Scale bar: 500 µm.

SEM images of the catalysts (IW series) prepared by incipient wetness impregnation with precursor $Ru(NH_3)_6Cl_3$ are shown in Figure 4.2 (a) and (b). As seen in Figure 4.2 (a), most of the ruthenium was distributed into white spots larger than 100 nm. Figure 4.2 (b) shows that the white spots were made of accumulated ruthenium particles. For the cation exchange (CE series) preparations, the HNO_3 pre-oxidation of the ACC fiber surface forms oxygenated functional groups such as carboxylic acid, lactone, phenolic hydroxyl and quinone groups.[32] When loading the ACC in the ruthenium salt solution, metal cations ion pair with the surface anionic sites. After catalyst reduction under hydrogen, white spots are observed on the ACC fiber (Figure 4.2 (c)). Magnification of these white spots reveals nanoparticles in the 10-20 nm range. Compared with the IW preparation, these nanoparticles

tend to be isolated from each other as opposed to forming a continuous sheet. (Figure 4.2 (d)).

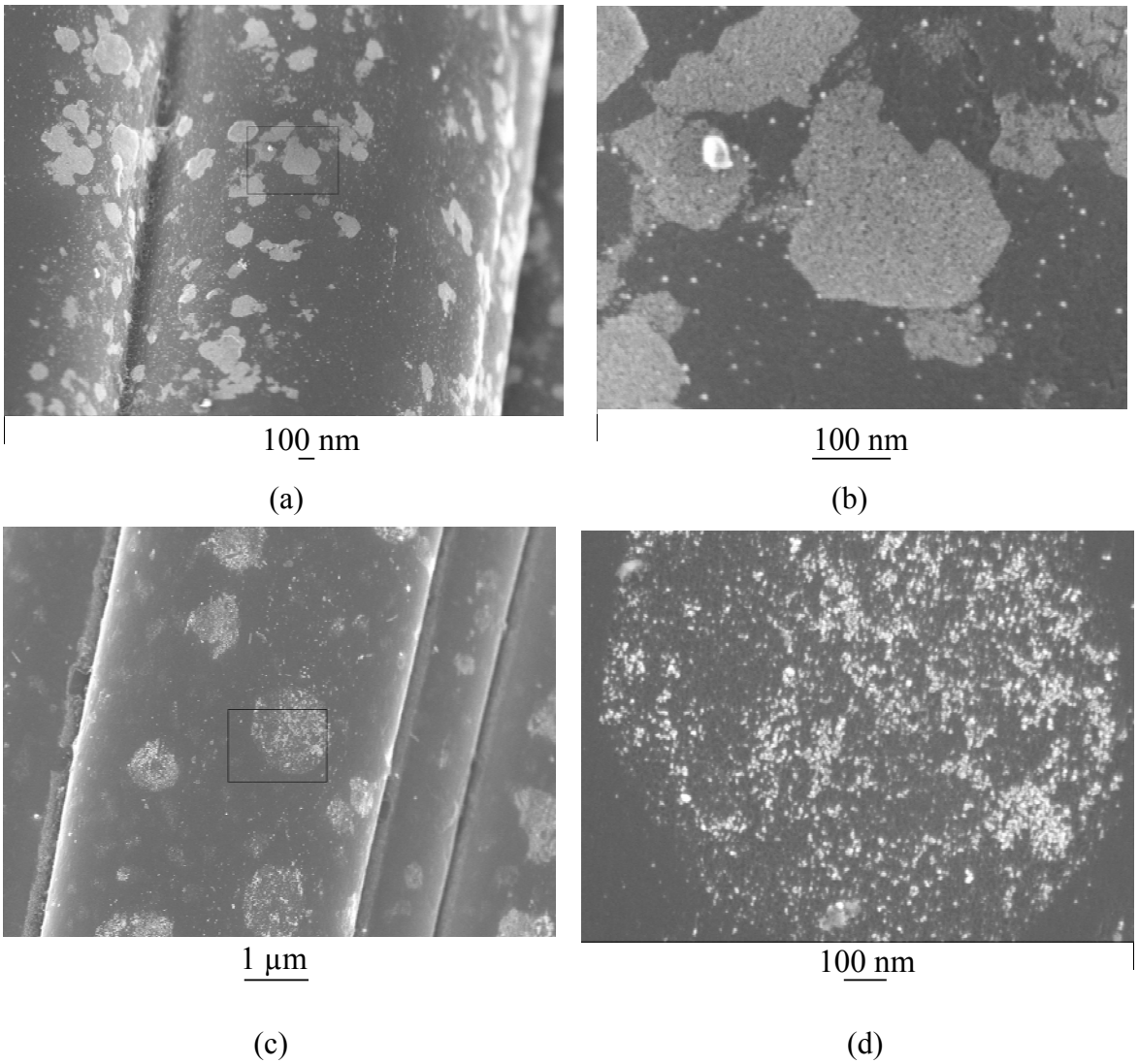

Figure 4.2 (a) and (b) SEM images of 3-IW-NH3 prepared with incipient wetness impregnation using $Ru(NH_3)_6Cl_3$ as precursor; (c) and (d) SEM images of 5-CE-NH3 prepared with cation exchange method using $Ru(NH_3)_6Cl_3$ as precursor. Scale bar: (a) 100 nm; (b) 100 nm; (c) 1 μm; (d) 100 nm.

4.3.2 Mechanism of guaiacol electrocatalytic hydrogenation with Ru/ACC

According to Sergeev and Hartwig,[38] a detailed reaction mechanism remains unclear, even for an aryl ether hydrogenolysis catalyzed by a well-defined nickel complex. For the present guaiacol cleavage, effected by heterogeneous Ru/ACC catalysts, we follow the lead

of Dabo et al. [21] and simply outline the transformation in a manner analogous to that of pi-bond hydrogenation (Scheme 4.1). Reactions involved in ECH of guaiacol include: formation of adsorbed atomic hydrogen (Eq. 1), adsorption of guaiacol (Eq. 2), reactions between adsorbed guaiacol and adsorbed hydrogen (Eq. 3), demethoxylation of guaiacol (Eq. 4), hydrogenation of phenol to cyclohexanone (Eq. 5) and cyclohexanol (Eq. 6), and desorption of the products (Eqs. 7 and 8).[28, 39]

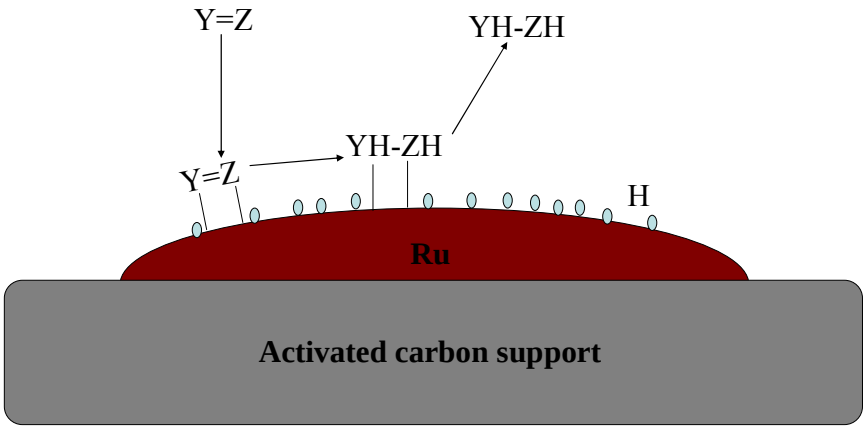

Scheme 4.1 Schematic representation of the electrocatalytic hydrogenation mechanism with Ru/ACC, where Y=Z is the unsaturated organic compound, YH-ZH is the hydrogenated product.

$$H_3O^+ + e^- + M \rightarrow M(H) + H_2O \quad (1)$$

$$M + \text{Guaiacol} \rightarrow (\text{Guaiacol})M \quad (2)$$

$$6M(H) + (\text{Guaiacol})M \rightarrow (\text{2-Methoxycyclohexanol})M + 6M \quad (3)$$

$$2M(H) + (\text{Guaiacol})M \rightarrow (\text{Phenol})M + (\text{Methanol})M + M \quad (4)$$

$$4M(H) + (\text{Phenol})M \rightarrow (\text{Cyclohexanone})M + 4M \quad (5)$$

$$2M(H) + (\text{Cyclohexanone})M \rightarrow (\text{Cyclohexanol})M + 2M \quad (6)$$

$$(\text{2-Methoxycyclohexanol})M \rightarrow \text{2-Methoxycyclohexanol} + M \quad (7)$$

$$(\text{Cyclohexanol})M \rightarrow \text{Cyclohexanol} + M \quad (8)$$

Here, M is the metal active site for hydrogen or organic compounds, M(H) is the

chemisorbed atomic hydrogen. Besides the reactions listed above, hydrogen desorption via the Tafel (Eq. 9) or Heyrovsky (Eq. 10) processes competes with the desired hydrogenation (Eq. 3-Eq. 6) decreasing its electrochemical efficiency (E.E.).[40, 41] As a practical matter, for bio-oil upgrading, this byproduct hydrogen could potentially be captured and used as a valuable reducing agent for further hydrotreatment.

$$M(H) + M(H) \rightarrow H_2 + 2M \quad (9)$$

$$M(H) + H^+ + e^- \rightarrow H_2 + M \quad (10)$$

4.3.3 Control experiments

The first control experiment used only blank ACC as cathode material; at 80°C and ambient pressure, no hydrogenation of guaiacol was observed. For this control experiment, there were no metal active sites for atomic hydrogen, and no catalyst for the hydrogenation reaction. Therefore, ACC alone cannot hydrogenate guaiacol.

The second control experiment used 3-IW-NH3 catalyst at 80°C and ambient pressure, with no current passed. No guaiacol was converted, showing that hydrogen is essential for hydrogenation.

The third control experiment was performed on 3-IW-NH3, with no current passed through the electrochemical cell. However, H_2 gas was supplied by bubbling through the solution at 80°C and ambient pressure. No conversion of guaiacol was observed either. Catalyst surface-bound atomic hydrogen forms differently in chemical catalytic hydrogenation vs. ECH. For ECH, atomic hydrogen directly forms on the cathode surface (Eq. 1), so reduction can occur at ambient pressure. For catalytic hydrogenation, H_2 gas must dissolve first, but it is poorly soluble in water, so high pressure is usually needed for aqueous

reactions. However, under ambient pressure, the H_2 concentrations in solution and on the catalyst surface would be low. Furthermore, the temperatures used here are much lower than the 125°C reported by Vispute[11] as the lowest temperature where guaiacol starts to be chemically reduced.

4.3.4 ECH of guaiacol using different catalysts: preparation methods and precursor effects

ECH of guaiacol was studied with several different catalysts prepared using two methods (incipient wetness impregnation and cation exchange) with different precursors. Various conditions were employed, including different reaction temperatures, electrolytes and currents. The results were summarized in Table 4.3. The effects of these conditions on guaiacol conversion, electrochemical efficiency and product selectivities are discussed in detail in the following text.

Table 4.3 Guaiacol conversion, electrochemical efficiency and product selectivities for ECH of guaiacol at various conditions. CH: cyclohexanol; Cis-2-MCH: Cis-2-methoxycyclohexanol; Trans-2-MCH: Trans-2-methoxycyclohexanol; P: phenol

Catal.	T °C	Electr-olyte 0.2 mol/ml	Cur. mA	Conv. %	E.E. %	Product selectivity %			
						CH	Cis-2-MCH	Trans-2-MCH	P
3-IW-Cl	80	HCl	100	52±0.4	10±2.1	65±7.1	31±4.8	4.4±2.3	--
3-IW-NH3	80	HCl	100	69±1.3	31±2.9	58±3.1	25±3.2	12±0.3	3.7±0.4
5-IW-NH3	80	HCl	100	48±8.7	19±4.3	59±11	29±3.1	9.8±6.4	2.4±2.8
3-IW-NO	80	HCl	100	38±0.5	9.8±0.5	47±0.9	36±0.0	12±1.0	5.9±0.1
5-IW-NO	80	HCl	100	53±1.6	19±0.4	72±1.3	22±0.4	5.2±0.8	--
1-CE-NH3	80	HCl	100	52±6.2	19±3.5	48±2.3	37±5.0	14±2.7	--

Table 4.3 (cont'd)

3-CE-NH3	80	HCl	100	75±3.9	30±4.3	53±1.4	36±2.3	11±2.0	--
3-IW-Cl	25	HCl	100	13±0.4	7.7±1.8	26±0.3	62±6.5	12±6.9	--
3-IW-Cl	50	HCl	100	36±12	17±1.6	30±1.4	56±1.4	14±0.0	--
1.5-CE-NH3	25	HCl	100	51±0.8	19±6.6	25±8.4	59±9.3	16±0.9	--
1.5-CE-NH3	50	HCl	100	60±13	31±4.9	38±0.5	47±2.8	15±2.2	--
3-CE-NH3	80	NaCl	100	64±8.8	20±2.2	42±3.3	42±1.3	17±2.0	--
3-CE-NH3	80	NaOH	100	62±2.4	28±1.0	48±0.2	38±0.5	13±0.6	--
3-IW-NH3	80	NaOH	100	45±2.3	20±1.2	46±3.8	36±2.3	11±1.9	6.6± 0.4
3-IW-NH3	80	HCl	40	71±3.3	27±0.1	61±1.9	28±1.2	11±0.7	--
3-IW-NH3	80	HCl	70	69±0.0	28±3.9	57±0.5	30±0.4	13±0.1	--
3-IW-NH3	80	HCl	130	65±4.2	23±0.6	45±1.3	38±0.8	14±0.5	2.1± 0.0
3-IW-NH3	80	HCl	160	60± <0.01	22± <0.01	49± <0.01	37± <0.01	14± <0.01	--

Products detected using GC/MS include cyclohexanol, cis-2-methoxycyclohexanol, trans-2-methoxycyclohexanol, methanol, phenol, cyclohexanone, 2-methoxycyclohexanone, cyclohexyl methyl ether and cyclohexane. Cyclohexanol, cis-2-methoxycyclohexanol, trans-2-methoxycyclohexanol and methanol are major products, but methanol was not included in the product selectivity calculation. Phenol, cyclohexanone, 2-methoxycyclohexanone, cyclohexyl methyl ether and cyclohexane are minor products. They are reported only when the quantities are measurable. The reaction pathway for ECH of guaiacol to the major products is shown in Scheme 4.2. While demethylation is one of the major reactions in traditional catalytic deoxygenation of guaiacol,[42] it is not observed during ECH; demethoxylation dominates instead. Thus ECH of bio-oil retains more carbon in the

liquid products than conventional upgrading.

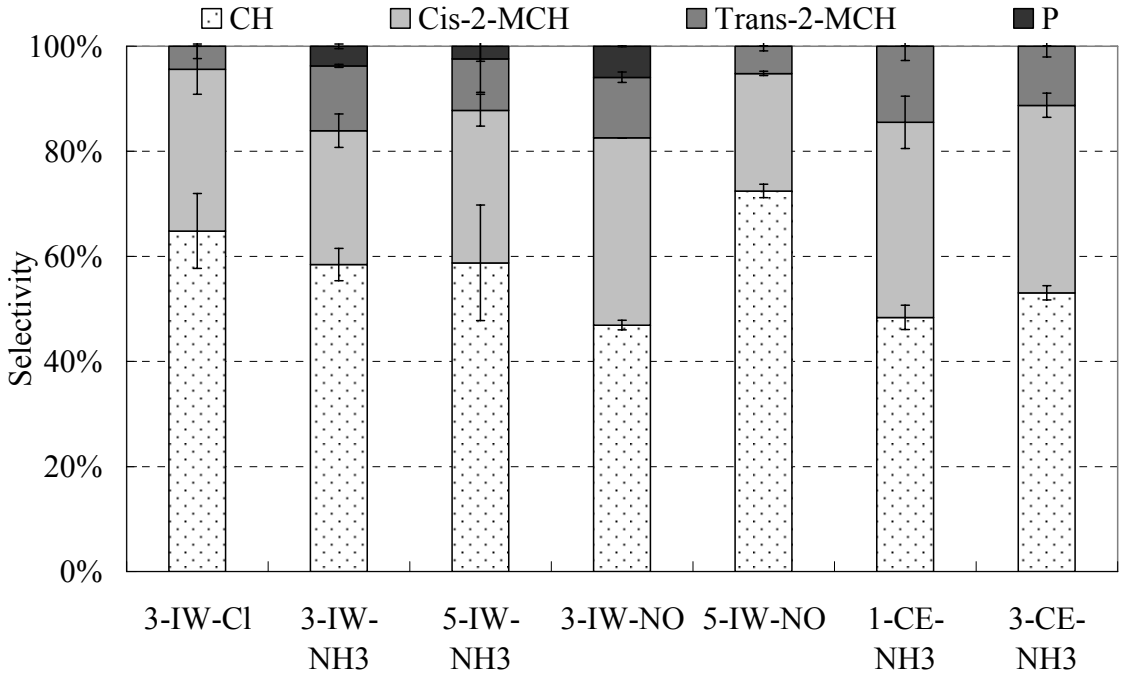

Figure 4.3 Product selectivities for ECH of guaiacol at 80°C and ambient pressure using different catalysts with 0.2 mol/dm^3 HCl as catholyte.

Deoxygenation of oxygenated compounds is one ultimate goal for bio-oil upgrading. Though deoxygenation is difficult at such mild conditions, partial deoxygenation of guaiacol was observed, resulting in two products, cyclohexanol and phenol. Cyclohexanol is a major product while phenol is only an intermediate. Among the catalysts studied, 5-IW-NO and 3-IW-Cl gave the greatest selectivity to cyclohexanol although their guaiacol conversion activities were relatively low (Figure 4.4).

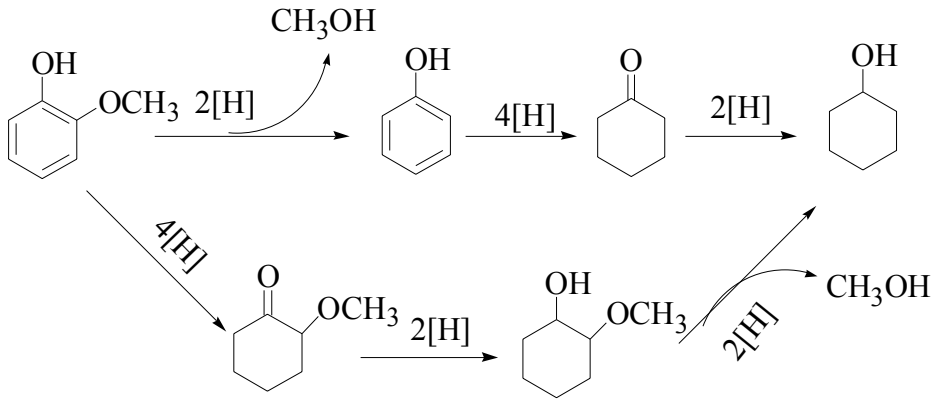

Scheme 4.2 Reaction pathway for ECH of guaiacol to the major products; 2-methoxycyclohexanol includes both cis and trans isomers.

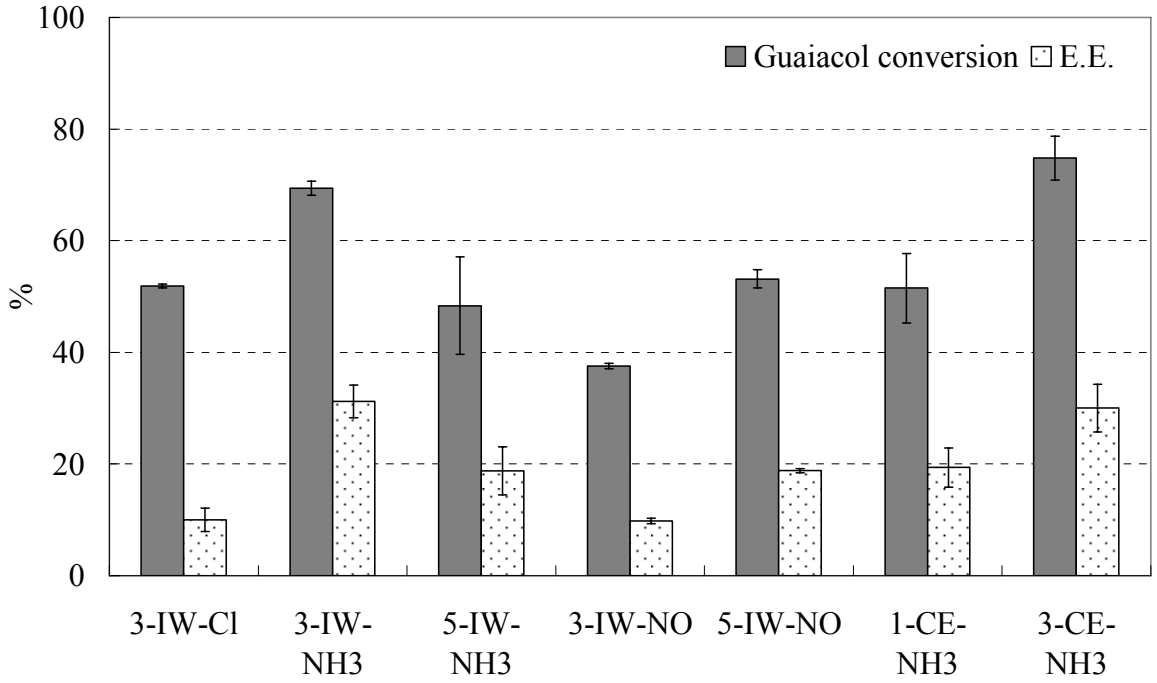

Figure 4.4 Guaiacol conversion and electrochemical efficiency for ECH of guaiacol at 80 °C and ambient pressure using different catalysts with 0.2 mol/dm^3 HCl as catholyte.

When we compared the catalysts with the same nominal ruthenium content (3 wt%), 3-CE-NH3 resulted in slightly higher guaiacol conversion than 3-IW-NH3 (Figure 4.4) even though the metal dispersions (measured from hydrogen chemisorption) are very similar. The pretreatment in the cation exchange method functionalizes the support surface by increasing acidic groups, which likely enhances guaiacol adsorption[43] and thus, electrocatalytic activity.

Ru/ACC catalysts prepared from different precursors using incipient wetness

impregnation showed different activities toward ECH of guaiacol. $Ru(NH_3)_6Cl_3$ exhibited the highest activity among the three precursors, followed by $RuCl_3$ and $Ru(NO)(NO_3)_3$. The presence of residual nitrogen on the catalyst and an uneven ruthenium distribution could be responsible for the reduced performance of the catalyst prepared with $Ru(NO)(NO_3)_3$.[44] This notion is supported by the blocky accumulations of ruthenium seen in Figure 4.5. Similarly, Nurunnabi et al.[45] showed low CO conversion during Fischer-Tropsch synthesis with catalysts prepared from $Ru(NO)(NO_3)_3$. Diaz et al.[46] also reported that Pd/C prepared with a nitrate precursor ($Pd(NO_3)_2$) showed a lower overall hydrogenation activity.

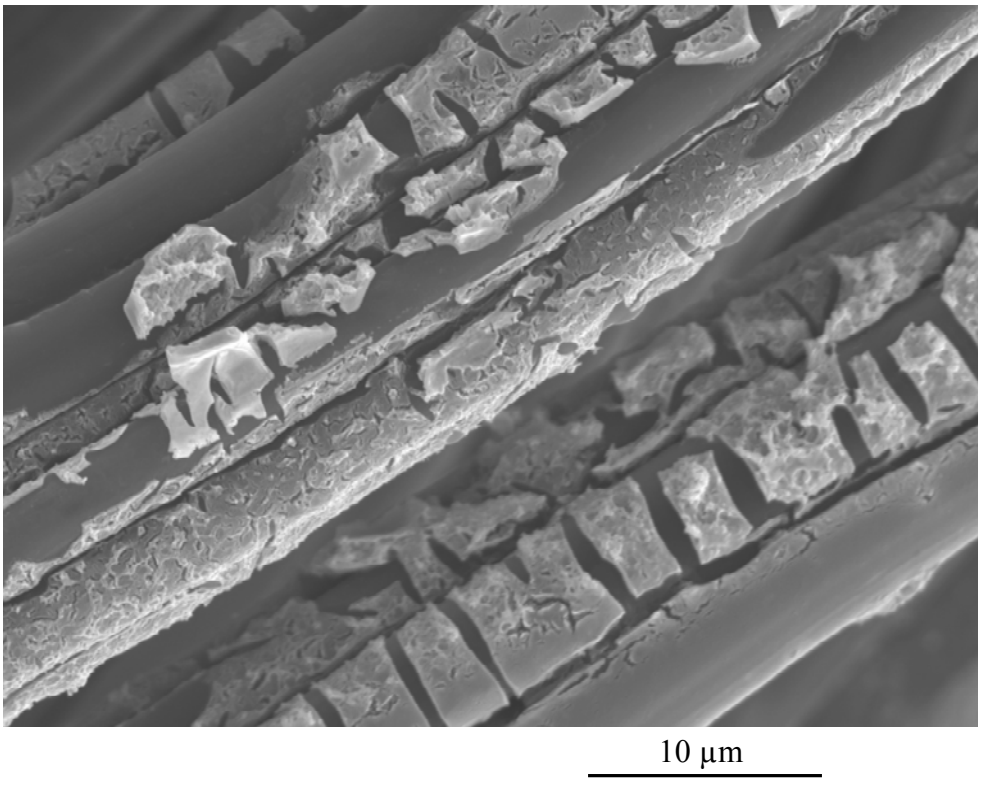

Figure 4.5 Ruthenium accumulation for the catalyst 3-IW-NO prepared with incipient wetness impregnation using $Ru(NO)(NO_3)_3$ as precursor. Scale bar: (a) 10 µm.

The electrochemical efficiencies of guaiacol ECH at 80°C using different catalysts were compared as summarized in Figure 4.4. Both 3-IW-NH3 and 3-CE-NH3 catalysts show >30% electrochemical efficiency, higher than the 26.3% maximum reported E.E. for phenol

ECH, obtained using a Pd catalyst.[12] One possible reason for these high E.E. values is that the present immobilization schemes achieve more intimate metal-support electrical contact.

4.3.5 Temperature effect

The effect of temperature on guaiacol ECH was studied with 0.2 mol/dm^3 HCl as catholyte for 2 hr under a constant current of 100 mA. Three different temperatures, 25, 50 and 80°C, were studied, all much lower than those used in classical catalytic conversion of phenolic compounds.[47, 48]

The E.E. is a function of the competition between electrocatalytic hydrogenation and hydrogen desorption. Raising the temperature from 25°C to 50°C increased E.E. (Figure 4.6) from 8% to 17% but further heating to 80°C dropped it back to 10%. This indicates that electrocatalytic hydrogenation was favored from 25°C to 50°C, while hydrogen desorption rates accelerated as temperature increased from 50°C to 80°C. Similar E.E. changes on the ECH of indigo to leuco indigo were observed by Roessler et al.[49], who found that E.E. rose as temperature was ramped up from 30°C to 60-80°C, but then dropped off above this range. However, Dabo et al.[21] found continuous E.E. improvement from 25°C to 75°C during ECH of 4-phenoxyphenol to phenol over 5% Pd/C in 1 mol/dm^3 NaOH. Amouzegar and Savadogo[50] also saw continuous E.E. increases from 5°C to 40°C to 60°C during ECH of phenol to cyclohexanol on platinum dispersed on graphite particles; the E.E. increase from 40°C to 60°C, however, was much smaller than that from 5°C to 40°C.

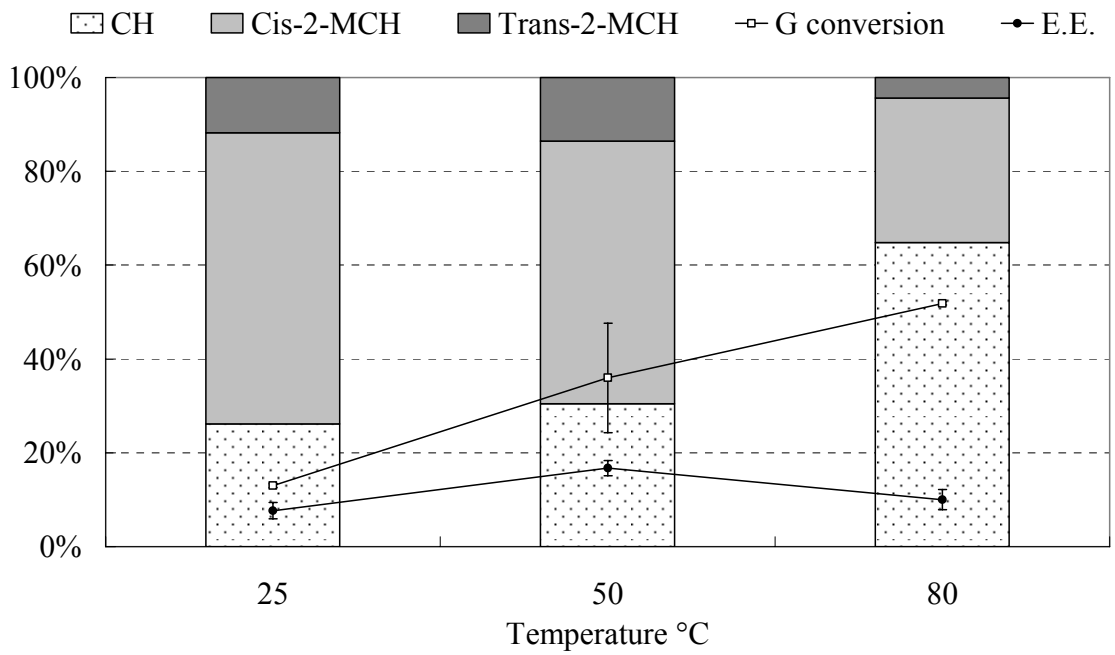

Figure 4.6 Product selectivities, guaiacol conversion and E.E. for ECH of guaiacol at different temperatures using 3-IW-Cl as cathode. Bars refer to product selectivities. G: guaiacol.

Cation exchange prepared catalyst shows good activity toward guaiacol conversion at 25°C, very similar to that at 50°C (Figure 4.7). However, guaiacol conversion for incipient wetness impregnation prepared catalyst decreased dramatically from 36% to 13% (Figure 4.6). Again, catalysts prepared by cation exchange show better performance than those prepared by incipient wetness impregnation.

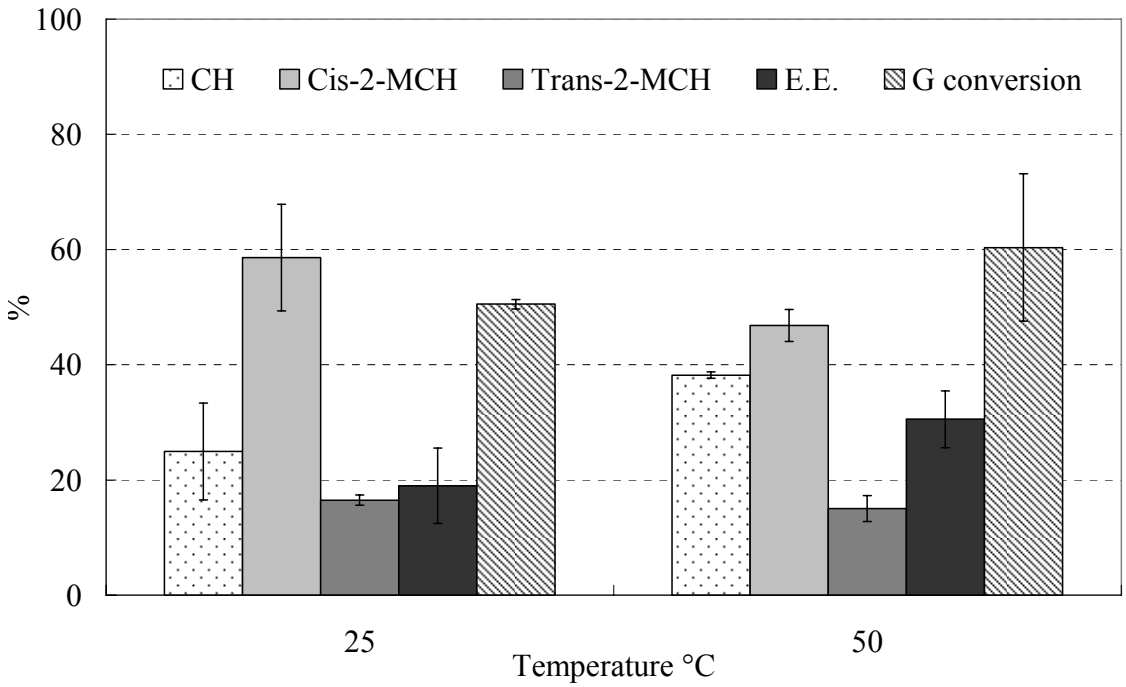

Figure 4.7 Product selectivities, guaiacol conversion and E.E. for ECH of guaiacol at different temperatures using 1.5-CE-NH3.

The effects of temperature on the product selectivities using 3-IW-Cl are shown in Figure 4.6. At 80°C, cyclohexanol was the dominant product, while cis-2-methoxycyclohexanol became the largest one at 25°C and 50°C. Though the trans-2-methoxycyclohexanol isomer was expected to be more stable, the cis isomer was always the major product at these studied temperatures. Presumably, during hydrogenation, the aromatic ring lies down on the ruthenium active surface and atomic hydrogens are added to the one face, thus forming cis-2-methoxyclohexanol. This phenomenon was also observed when using catalyst prepared by the cation exchange method (Figure 4.7). Solladié-Cavallo et al.[51] showed a similar result for hydrogenation of substituted phenols over Ru/Al_2O_3.

4.3.6 Catalyst support effect

Analysis by EDX reveals that there are other elements in the original ACC besides C and O, including Al, Zn and S (Table 4.1). Some elements, especially S, may have strong chemisorption with ruthenium, blocking active sites and moderating the hydrogenation

reaction.[52] Thus catalyst performance was assessed based on original and demineralized ACC. ACC was demineralized by washing in boiling hydrochloric acid for 3 days, resulting in the decrease of the ash content from 5 wt% to around 0.1 wt%. Catalysts made from original and demineralized ACC supports were compared during ECH of guaiacol using 0.2 mol/dm^3 HCl as catholyte at 25, 50 and 80 °C (Figure 4.8). The trivial differences found indicate that the extra elements in the original ACC do not interfere with the Ru catalytic activity.

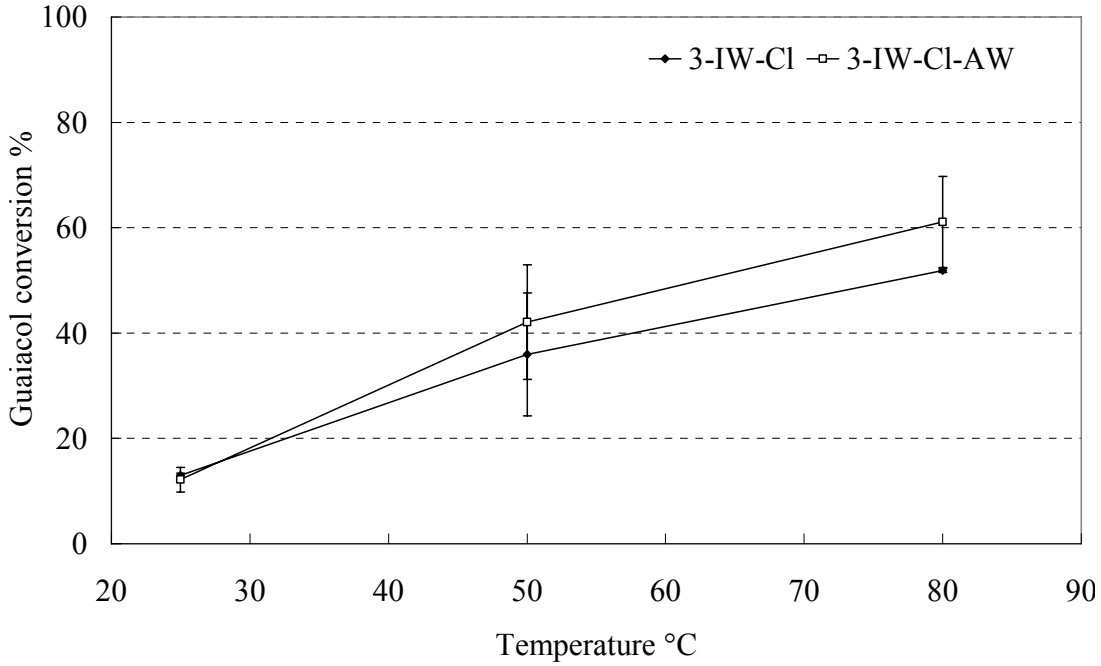

Figure 4.8 ECH of guaiacol using catalysts prepared on HCl washed ACC (3-IW-Cl-AW) and original ACC (3-IW-Cl) with 0.2 mol/dm^3 HCl as electrolyte at different temperatures.

4.3.7 pH effect

All experiments discussed above were carried out in 0.2 mol/dm^3 HCl solution. To probe pH effects, the performance of these catalysts in neutral (0.2 mol/dm^3 NaCl as catholyte) and basic solution (0.2 mol/dm^3 NaOH as catholyte) was examined here. All other conditions were the same as the runs with 0.2 mol/dm^3 HCl as electrolyte. When using

3-CE-NH3 and 3-IW-NH3 as catalysts, guaiacol conversion was favored under acidic conditions (Figure 4.9). Guaiacol adsorption onto catalyst sites (Eq. 2) is a key step in the hydrogenation reaction. The ionization state of guaiacol varies with solution pH, potentially affecting its adsorption characteristics. In acidic and neutral conditions, guaiacol (pKa=9.9)[53] is mainly a neutral molecule, while deprotonation of guaiacol to form phenolate anion occurs under alkaline conditions. As ionic forms prefer to remain in the polar solution and the carbon support preferentially adsorbs neutral species, adsorption onto the support is reduced. Furthermore, the resonance delocalization in the phenolate form shifts the thermodynamics and makes the ECH of guaiacol more difficult.[12] Thus, greater guaiacol conversion was observed in acidic than in alkaline solution. A similar effect on E.E. was observed, showing higher E.E. under acidic conditions. Likewise, selectivity to cyclohexanol was higher under acidic conditions, indicating a higher level of demethoxylation of guaiacol (Figure 4.9).

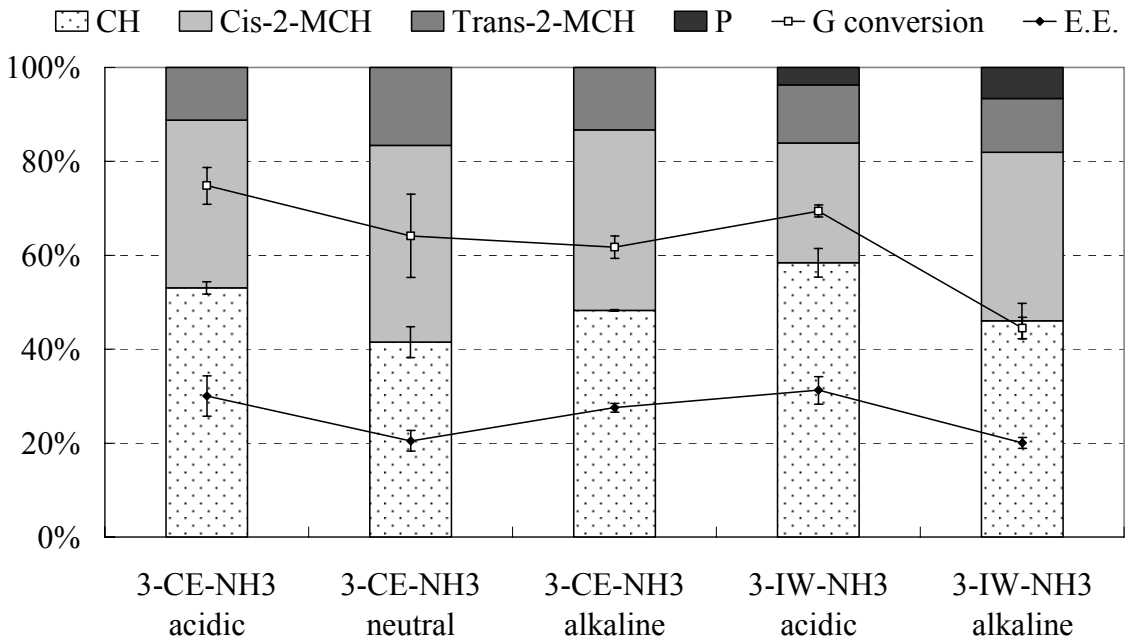

Figure 4.9 ECH of guaiacol using catalysts 3-CE-NH3 and 3-IW-NH3 under different pH conditions at 80 °C and ambient pressure. Bars refer to product selectivities.

4.3.8 Current density effect

Current density effects on guaiacol conversion, electrochemical efficiency and product selectivities were studied for guaiacol ECH at 80°C and ambient pressure with 0.2 mol/dm^3 HCl as catholyte. Because it was difficult to measure the actual effective electrode surface area, current is directly used without calculating current density. As shown in Figure 4.10, guaiacol conversion and electrochemical efficiency are invariant when current is in the range of 40 mA to 100 mA and above 100 mA, both decrease slightly. The current density effect on guaiacol conversion and E.E. is not very obvious for ECH of guaiacol using Ru/ACC as cathode because the surface area of the cathode is relatively high and the absolute change of the current density is very small. Additionally, product selectivities are only slightly affected. Selectivity for cyclohexanol formation is higher for the current range from 40 mA to 100 mA than 130 mA and 160 mA.

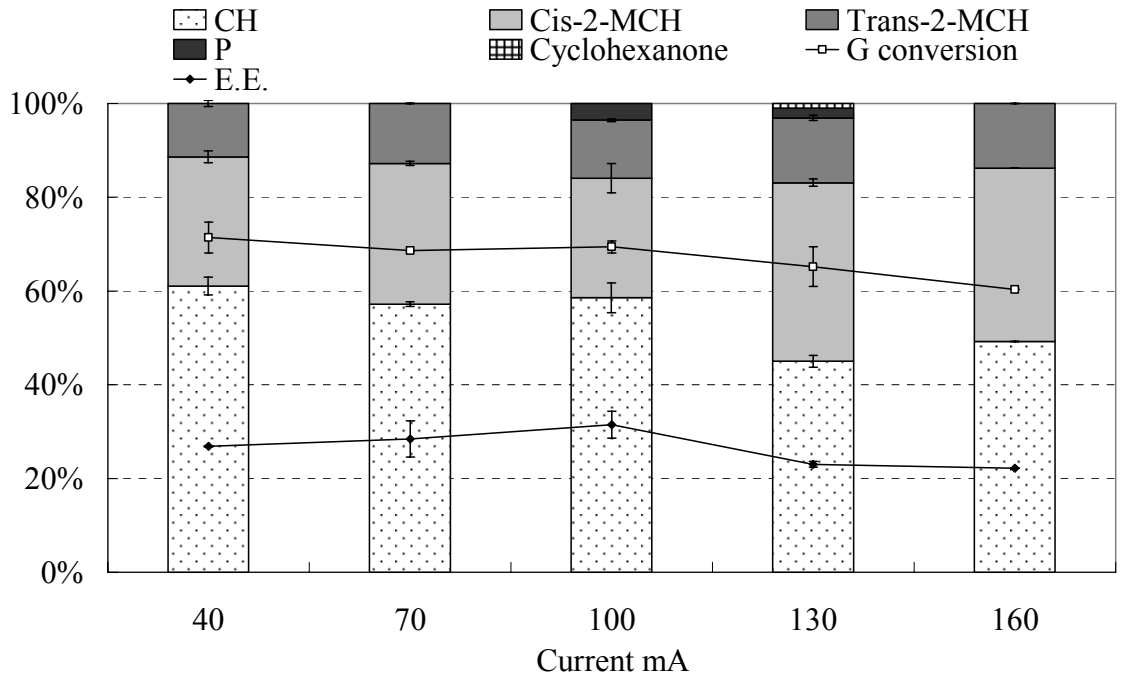

Figure 4.10 ECH of guaiacol using catalyst 3-IW-NH3 under different currents at 80°C and ambient pressure. Bars refer to product selectivities.

4.3.9 ECH of other phenolic compounds: phenol and syringol

In addition to guaiacol, both phenol and syringol served as lignin-derived model compounds. ECH of these two model compounds was carried out in 0.2 mol/dm^3 HCl catholyte solution at 80°C and ambient pressure. ECH of phenol generates two products, cyclohexanol and cyclohexanone (Table 4.4). Cyclohexanol is the major product, consistent with separate observations of rapid, efficient reduction of cyclohexanone to cyclohexanol. Five major products are obtained from ECH of syringol: cyclohexanol, cis-2-methoxycyclohexanol, trans-2-methoxycyclohexanol, 2-methoxycyclohexanone and guaiacol (Table 4.4); these products are similar to those obtained from ECH of guaiacol and point to demethoxylation as the first step from syringol.

Table 4.4 ECH of phenol and syringol using 1.5-CE-NH3 at 80°C and ambient pressure with 0.2 mol/dm^3 HCl as catholyte

			Product selectivity %					
Reactants	Conversion %	E.E. %	CH	CHO	Cis-2-MCH	Trans-2-MCH	2-MCHO	G
Phenol	89	29	99	1	--	--	--	--
Syringol	58	29	35	0	27	9	13	16

CHO: cyclohexanone; 2-MCHO: 2-methoxy-cyclohexanone.

Equal amounts of charge were passed for ECH of phenol and syringol, but ECH of phenol requires fewer electrons than ECH of syringol, resulting in higher conversion of phenol. The π-system's electron density increases as the methoxylation degree increases from phenol to syringol, so syringol should be more difficult to reduce. However, similar E.E. values were obtained for ECH of both model compounds.

4.4 Conclusions

This work shows that Ru/ACC is an efficient catalyst for electrocatalytic hydrogenation and partial hydrodeoxygenation of phenolic compounds under mild

conditions compared to other catalytic reductions, including other ECH schemes. Catalyst comparisons demonstrated that Ru/ACC catalysts prepared via the cation exchange method show much better activity than those prepared by incipient wetness impregnation. When using incipient wetness impregnation, $Ru(NH_3)_6Cl_3$ showed the highest activity among the three precursors studied. Within the range 25-80°C, higher temperature was found to favor guaiacol conversion and deoxygenation. Lower pH resulted in higher guaiacol conversion and electrochemical efficiencies. Furthermore, phenol and syringol can be hydrogenated using Ru/ACC catalysts, showing electrochemical efficiencies similar to those found for guaiacol. Based on the results from this investigation, electrocatalytic hydrogenation with Ru/ACC is a potential strategy for ambient pressure hydrogenation of phenolic compounds at low temperatures, and it may offer significant advantages for future bio-oil stabilization and upgrading.

Acknowledgements

The authors would like to thank the Michigan State University Foundation and AgBioResearch for financial support. Assistance provided by Dr. Ambareesh Murkute, Dr. Lars Peereboom and Mr. Xianfeng Ma with BET analysis is warmly acknowledged.

REFERENCES

REFERENCES

1. R. H. Venderbosch, A. R. Ardiyanti, J. Wildschut, A. Oasmaa and H. J. Heeres, J. Chem. Technol. Biotechnol., 2010, **85**, 674-686.

2. L. Moens, S. K. Black, M. D. Myers and S. Czernik, Energy Fuels, 2009, **23**, 2695-2699.

3. T. P. Vispute and G. W. Huber, Green Chem., 2009, **11**, 1433-1445.

4. F. H. Mahfud, F. Ghijsen and H. J. Heeres, J. Mol. Catal. A: Chem., 2007, **264**, 227-236.

5. L. Busetto, D. Fabbri, R. Mazzoni, M. Salmi, C. Torri and V. Zanotti, Fuel, 2010, **90**, 1197-1207.

6. F. H. Mahfud, S. Bussemaker, B. J. Kooi, G. H. Ten Brink and H. J. Heeres, J. Mol. Catal. A: Chem., 2007, **277**, 127-136.

7. A. Oasmaa and E. Kuoppala, Energy fuels, 2003, **17**, 1075-1084.

8. S. Czernik and A. V. Bridgwater, Energy Fuels, 2004, **18**, 590-598.

9. C. Zhao, J. He, A. A. Lemonidou, X. Li and J. A. Lercher, J. Catal., 2011, **280**, 8-16.

10. B. Scholze and D. Meier, J. Anal. Appl. Pyrolysis, 2001, **60**, 41-54.

11. T. Vispute, Ph.D. Dissertation, University of Massachusetts - Amherst, 2011.

12. F. Laplante, L. Brossard and H. Ménard, Can. J. Chem., 2003, **81**, 258-264.

13. D. Tountian, A. Brisach-Wittmeyer, P. Nkeng, G. Poillerat and H. Ménard, J. Appl. Electrochem., 2009, **39**, 411-419.

14. A. Brisach-Wittmeyer, N. A. Bouchard, R. Breault and H. Ménard, Can. J. Chem., 2006, **84**, 1640-1647.

15. H. Ilikti, N. Rekik and M. Thomalla, J. Appl. Electrochem., 2004, **34**, 127-136.

16. H. Ilikti, N. Rekik and M. Thomalla, J. Appl. Electrochem., 2002, **32**, 603-609.

17. K. Amouzegar and O. Savadogo, J. Appl. Electrochem., 1997, **27**, 539-542.

18. B. Mahdavi, P. Chambrion, J. Binette, E. Martel and J. Lessard, Can. J. Chem., 1995, **73**, 846-852.

19. A. Cyr, F. Chiltz, P. Jeanson, A. Martel, L. Brossard, J. Lessard and H. Menard, Can. J.

Chem., 2000, **78**, 307-315.

20. J. Lalancette, H. Menard, E. Potvin. *US Pat.,* 4 886 591, 1989.

21. P. Dabo, A. Cyr, J. Lessard, L. Brossard and H. Menard, Can. J. Chem., 1999, **77**, 1225-1229.

22. C. M. Cirtiu, A. Brisach-Wittmeyer and H. Menard, J. Catal., 2007, **245**, 191-197.

23. P. Dube, F. Kerdouss, F. Laplante, P. Proulx, L. Brossard and H. Menard, J. Appl. Electrochem., 2003, **33**, 541-547.

24. A. Cyr, F. Chiltz, P. Jeanson, A. Martel, L. Brossard, J. Lessard and H. Ménard, Can. J. Chem., 2000, **78**, 307-315.

25. J. R. Rangel-Mendez and M. Streat, Water Res., 2002, **36**, 1244-1252.

26. J. Aumo, S. Oksanen, J. P. Mikkola, T. Salmi and D. Y. Murzin, Ind. Eng. Chem. Res., 2005, **44**, 5285-5290.

27. C. Zhao, Y. Kou, A. A. Lemonidou, X. Li and J. A. Lercher, Angewandte Chemie, 2009, **121**, 4047-4050.

28. T. S. Dalavoy, J. E. Jackson, G. M. Swain, D. J. Miller, J. Li and J. Lipkowski, J. Catal., 2007, **246**, 15-28.

29. Z. Zhang, J. E. Jackson and D. J. Miller, Appl. Catal., A, 2001, **219**, 89-98.

30. K. P. Pimparkar, D. J. Miller and J. E. Jackson, Ind. Eng. Chem. Res., 2008, **47**, 7648-7653.

31. J. Wildschut, F. H. Mahfud, R. H. Venderbosch and H. J. Heeres, Ind. Eng. Chem. Res., 2009, **48**, 10324-10334.

32. B. K. Pradhan and N. K. Sandle, Carbon, 1999, **37**, 1323-1332.

33. M. Besson, P. Gallezot, A. Perrard and C. Pinel, Catal. Today, 2005, **102**, 160-165.

34. A. Sluiter, B. Hames, R. Ruiz, C. Scarlata, J. Sluiter and D. Templeton, *Determination of Ash in Biomass*, Report NREL/TP-510-42622, National Renewable Energy Laboratory, Golden, 2005.

35. Z. Li, S. Kelkar, C. H. Lam, K. Luczek, J. E. Jackson, D. J. Miller and C. M. Saffron, Electrochim. Acta, 2012, **64**, 87-93.

36. M. Perez, C. Salinas Martinez de Lecea and A. Linares Solano, Appl. Catal., A, 1997, **151**, 461-475.

37. A. Subrenat, J. N. Baleo, P. Le Cloirec and P. E. Blanc, Carbon, 2001, **39**, 707-716.

38. A. G. Sergeev and J. F. Hartwig, Science, 2011, **332**, 439-443.

39. C. M. Cirtiu, H. O. Hassani, N. A. Bouchard, P. A. Rowntree and H. Ménard, Langmuir, 2006, **22**, 6414-6421.

40. B. Mahdavi, J. M. Chapuzet and J. Lessard, Electrochim. Acta, 1993, **38**, 1377-1380.

41. D. Robin, M. Comtois, A. Martel, R. Lemieux, A. K. Cheong, G. Belot and J. Lessard, Can. J. Chem., 1990, **68**, 1218-1227.

42. T. Nimmanwudipong, R. C. Runnebaum, D. E. Block and B. C. Gates, Energy & Fuels, 2011, **25**, 3417-3427.

43. C. M. Cirtiu, H. O. Hassani, N. A. Bouchard, P. A. Rowntree and H. Menard, Langmuir, 2006, **22**, 6414-6421.

44. J. Wildschut, I. V. Melián-Cabrera and H. J. Heeres, Appl. Catal., B, 2010, **99**, 298-306.

45. M. Nurunnabi, K. Murata, K. Okabe, T. Hanaoka, T. Miyazawa and K. Sakanishi, J. Jpn. Pet. Inst., 2010, **53**, 75-81.

46. E. Diaz, A. F. Mohedano, L. Calvo, M. A. Gilarranz, J. A. Casas and J. J. Rodriguez, Chem. Eng. J., 2007, **131**, 65-71.

47. Y. C. Lin, C. L. Li, H. P. Wan, H. T. Lee and C. F. Liu, Energy Fuels, 2011, **25**, 890-896.

48. A. Gutierrez, R. K. Kaila, M. L. Honkela, R. Slioor and A. O. I. Krause, Catal. Today, 2009, **147**, 239-246.

49. A. Roessler, O. Dossenbach and P. Rys, J. Electrochem. Soc., 2003, **150**, D1-D5.

50. K. Amouzegar and O. Savadogo, Electrochim. Acta, 1994, **39**, 557-559.

51. A. Solladié-Cavallo, A. Baram, E. Choucair, H. Norouzi-Arasi, M. Schmitt and F. Garin, J. Mol. Catal. A: Chem., 2007, **273**, 92-98.

52. B. J. Arena, Appl. Catal., A, 1992, **87**, 219-229.

53. M. Ragnar, C. T. Lindgren and N. O. Nilvebrant, J. Wood Chem. Technol., 2000, **20**, 277-305.

Chapter 5 Electrocatalytic Upgrading of a Bio-oil Derived Phenolic Compound over Ruthenium Catalyst: Preliminary Study on the Reaction Network and Catalyst Deactivation

Zhenglong Li[a,b], Mahlet Garedew[a], James E. Jackson[c], Dennis J. Miller[b], Christopher M. Saffron[a,b,d,*]

Abstract

Electrocatalytic hydrogenation and hydrodeoxygenation (ECH) of guaiacol using ruthenium supported on activated carbon cloth (Ru/ACC) catalyst was performed at 80°C and ambient pressure. Several products were detected, including cyclohexanol, cis-2-methoxycyclohexanol, trans-2-methoxycyclohexanol, methanol, phenol, cyclohexanone, 2-methoxycyclohexanone, cyclohexane and cyclohexyl methyl ether. The reaction network for the ECH of guaiacol with Ru/ACC catalyst was assembled from the products formed and this network was compared with that for catalytic hydrodeoxygenation (HDO) of guaiacol. Two major routes were identified for guaiacol reduction: demethoxylation (partial hydrodeoxygenation) and direct hydrogenation of the aromatic ring. An assessment of catalyst reusability shows that guaiacol conversion did not significantly change upon two cycles of reuse. Only mild product selectivity changes were observed, resulting from the deposition of metal contaminants on the catalyst. With Pt wire directly connecting the catalyst to the electrical power source, this catalyst contamination can be avoided. Furthermore, Cl^-

a. Department of Biosystems & Agricultural Engineering, East Lansing, MI 48824, US
b. Department of Chemical Engineering & Materials Science, East Lansing, MI 48824, US
c. Department of Chemistry, Michigan State University, East Lansing, MI 48824, US
d. Department of Forestry, East Lansing, MI 48824, US
*Corresponding author, Tel.: +1 517 432 7414; fax: +1 517 432 2892. E-mail address: saffronc@egr.msu.edu (C.M. Saffron).

was not found to poison the ruthenium electrocatalyst during the ECH of guaiacol even when a high concentration HCl solution was used as catholyte.

5.1 Introduction

Upgrading biomass-derived pyrolysis oil is one strategy for producing renewable transportation fuels. However, several barriers limit bio-oil upgrading, including severe coke formation, catalyst deactivation and low carbon recovery into the liquid fuels.[1-3] Because high temperatures and pressures are responsible for these limitations, upgrading methods that use mild conditions are urgently needed. Recently, we developed a mild electrocatalytic hydrogenation (ECH) method for bio-oil upgrading,[4] which can be carried out at temperature lower than 100 °C and atmospheric pressure. During the ECH process, atomic hydrogen is formed *in situ* on the catalytic electrode surface as opposed to an external hydrogen source.. Electricity is employed as the reducing agent, making this method greatly applicable in locales where molecular hydrogen is not available, such as rural biomass production areas. Using ECH under mild conditions reduced coke formation, reduced catalyst deactivation and decreased carbon loss to the gas phase were observed.

Guaiacol is a model substrate used by many researchers to simulate bio-oil upgrading and to test the efficacy of catalysts. Hurff and Klein [5] studied hydrodeoxygenation of guaiacol over a $CoO\text{-}MoO_3/\gamma\text{-}Al_2O_3$ hydrotreating catalyst from 250 °C to 325 °C at 34.5 bar hydrogen pressure. Kallury et al.[6] used $MoO_3\text{-}NiO\text{-}Al_2O_3$ for hydrodeoxygenation of guaiacol from 350°C to 500°C. Elliott and Hart [7] also showed that hydrodeoxygenation of guaiacol can be done using palladium or ruthenium catalyst over a temperature range from 150°C to 300 °C at 13.8 MPa. Most of these studies are related to classical catalytic

hydrodeoxygenation of guaiacol, however, the number of studies using electrocatalytic hydrogenation of guaiacol is very limited.[4, 8] Studies related to ECH of phenolic compounds were reported, including phenol, catechol and alkyl-substituted phenols.[9-14] Various electrodes were used in these studies, such as, electrodes made by entrapping catalyst powders in reticulated vitreous carbon,[15, 16] electrodes made with pressed metallic powder particles[8, 17] and dispersed Pt electrodes.[13, 14] We also previously reported that activated carbon cloth supported ruthenium (Ru/ACC) catalyst was active toward ECH of guaiacol at a temperature range of 25 °C to 80 °C and ambient pressure.[4] In this chapter, we are going to continue to show the results for ECH of guaiacol, mainly the reaction network and catalyst deavation.

Reaction network and catalyst deactivation studies are needed to suggest methods for process improvement. The results of reaction network studies may suggest ways to improve the process in terms of increasing the reaction rate and optimizing the product selectivities. Very few studies exist regarding the catalytic hydrodeoxygenation pathway for guaiacol,[18, 19] and no detailed research on the reaction pathway for guaiacol ECH has been reported. This paper will discuss the reaction network for aqueous ECH of guaiacol using Ru/ACC and compare the reaction pathways of ECH with the solid catalyst hydrodeoxygenation of guaiacol. Catalyst deactivation is another important aspect to be considered when developing catalysts for bio-oil upgrading. Many studies related to catalyst deactivation for classical catalytic hydrogenation have been reported,[20-22] while there are hardly any catalyst deactivation studies related to ECH of bio-oil and its model compounds. This study will evaluate the reusability of the catalyst during ECH of guaiacol and examine the catalyst

changes using different analytical techniques.

5.2 Materials and methods

5.2.1 Reagents and materials

Guaiacol (98+%) and 2-methoxycyclohexanol (99%) were obtained from Alfa Aesar. 2,6-Dimethoxyphenol (syringol) (99%) was purchased from Sigma-Aldrich and cyclohexanol (99+%) was from Mallinckrodt. Hexaammineruthenium (III) chloride ($Ru(NH_3)_6Cl_3$, Ru 32.1% min) was purchased from Alfa Aesar. All of the aforementioned compounds were used as received without further purification. Phenol, from Mallinckrodt, was purified by sublimation to remove moisture. Zorflex® ACC FM100 was obtained from Calgon Carbon Co.

5.2.2 Catalyst preparation

A piece of ACC (1.3cm × 3.0cm) was first soaked into $Ru(NH_3)_6Cl_3$ solution, which was enough to saturate the ACC pores. After saturation, the ACC was removed and the excess solution was dried using Kimwipes®. The damp ACC was then dried on the lab bench, followed by vacuum drying at room temperature. The dry ACC was then chemically reduced with H_2 in a Parr pressure reactor (model 452HC) at 500 psi and 220 °C, unless otherwise stated. To facilitate the recognition of the catalyst, catalyst code 3-IW-NH3 is used, where "3" is the nominal ruthenium content, "IW" stands for incipient wetness impregnation and "NH3" refers to the $Ru(NH_3)_6Cl_3$ precursor.

5.2.3 Catalyst characterization

Ruthenium contents of the catalysts were measured on a Varian 710-ES inductively coupled plasma optical emission spectrometer (ICP-OES). The catalysts were digested using

aqua regia in a boiling water bath for 4 hr, then filtered and diluted with DI water. The standards prepared with $RuCl_3$ were used to quantify the ruthenium content over a concentration range of 0.08 ppm to 50 ppm.

Scanning electron microscopy (SEM) was performed using a JEOL JSM-7500F and a JEOL 6400V to image the catalyst support and the morphology of ruthenium particles on the support. The catalysts were mounted onto aluminum stubs with carbon paste and then dried under vacuum overnight. Secondary electron imaging was used to obtain the images. In addition to imaging morphology, the surface chemical composition was characterized by EDX coupled with the JEOL 6400V SEM.

Brunauer-Emmett-Teller (BET) surface area, micropore area and micropore volume of the samples were measured with a Micromeritics® ASAP 2010 system using a static volumetric adsorption and desorption method. Nitrogen was used as the adsorptive gas and the measurement was made at 77 K. Nitrogen pressure was increased until 99% of the nitrogen saturation pressure was reached. The total surface area of the sample was calculated using the BET method from the adsorption isotherm from 0.06 to 0.20 relative pressures. The micropore volume was calculated from the desorption isotherm using the BJH (Barrett, Joyner and Hallender) method.

5.2.4 Experimental setup

The electrocatalytic hydrogenation was carried out in a two-chamber glass H-cell,[23] separated with a Dupont® Nafion-117 membrane. The catholyte (30 mL) was 0.2 M HCl. Catalyst 3-IW-NH3 prepared as described above was used as the working electrode (cathode). The anolyte (30 mL) was 0.2 M phosphate buffer (pH=7), and a Pt wire was used as the

counter electrode (anode). The whole cell was placed in a water bath to control the temperature at 80°C. The ECH was carried out under galvanostatic control (100 mA) with a dual channel potentiostat from Lambda (Model: LPD 422A FM). Before the electrocatalytic hydrogenation, a 10 minute pre-electrolysis (80 mA) was applied to activate the ruthenium catalyst. Then 1 mL 620 mM guaiacol solution in isopropanol was added to the cathode chamber to make an initial concentration of guaiacol equal to 20 mM.

5.2.5 Product analysis

Chemical analysis proceeded by withdrawing 1 mL sample aliquots at discrete time intervals from the cathode and the anode chambers. The samples were further saturated with NaCl, acidified to pH=1 and then 1 mL chloroform was added to extract the organics.[24]

All the samples were analyzed on a Shimadzu QP-5050A GC/MS. The GC used a Restek Rtx-1701 capillary column, 60 m × 0.25 mm with a 0.25 μm film thickness, a 1.0 ml/min helium carrier gas flow rate, and a split ratio of 1:40. The injector temperature was set at 270°C. The GC oven program started at 40°C for 1 min, and then heated at 15°C/min to 260°C. The mass spectrometer was operated in the Electron Ionization (EI) mode at an ionization energy of 80 eV, a m/z ranging from 28 to 400, and a sampling interval of 0.34 s. Species associated with each chromatographic peak were identified by comparing their observed mass spectrum with the NIST library and then confirmed by injection of authentic samples. External standards were also used to identify compounds and quantify the peak responses.

5.2.6 Calculations

The conversion, selectivity and electrochemical efficiency were calculated according

to the following equations:

$$\text{Conversion} = \frac{\text{moles consumed of reactant}}{\text{initial moles of reactant}} \quad (1)$$

$$\text{Selectivity} = \frac{\text{moles of desired product}}{\text{total moles of products}} \quad (2)$$

$$\text{E.E.} = \frac{\text{Electrons used to generate products}}{\text{Total electrons passed}} \quad (3)$$

Heats of formation were used in this chapter to verify the reaction network for ECH of guaiacol and they were calculated using T1 method. This method "follows the G3(MP2) recipe, by substituting an HF/6-31G* for the MP2/6-31G* geometry, eliminating both the HF/6-31G* frequency and QCISD(T)/6-31G* energy and approximating the MP2/G3MP2 large energy using dual basis set RI-MP2 techniques."[25]

5.3 Results and discussion

Electrocatalytic hydrogenation and hydrodeoxygenation of guaiacol were previously carried out in an aqueous solution with Ru/ACC at 80°C and ambient pressure.[4] Several different catalysts were prepared with three different precursors ($RuCl_3$, $Ru(NH_3)_6Cl_3$ and $Ru(NO)_3(NO_3)$) using incipient wetness impregnation. Among those catalysts, 3-IW-NH3 showed better activity and electrochemical efficiency, so it was chosen as the catalytic cathode in this investigation.

5.3.1 Reaction network for ECH of guaiacol

ECH of guaiacol produces four major products, namely cyclohexanol, cis-2-methoxycyclohexanol, trans-2-methoxycyclohexanol and methanol. Several minor products were also detected using GC/MS and verified with standard chemicals. Phenol, cyclohexanone, 2-methoxycyclohexanone, cyclohexane and cyclohexyl methyl ether are five minor products during ECH of guaiacol with 3-IW-NH3 at 80°C. The identification and

quantification techniques of these products are shown in Table 5.1.

Based on the major and minor products, a reaction network for ECH of guaiacol is proposed in Scheme 5.1. Two major routes for ECH of guaiacol were identified: demethoxylation (partial hydrodeoxygenation) and direct hydrogenation of the aromatic ring.

Table 5.1 Major and minor products from ECH of guaiacol using 3-IW-NH3 as cathode at 80 °C and ambient pressure

Products	Classification based on product abundance[a]	Basis for identification of product	Basis for quantification of product
Cyclohexanol	Major	Standard	Standard
Cis-2-methoxy-cyclohexanol	Major	NIST library	Standard (trans-2-methoxy -cyclohexanol)
Trans-2-methoxy-cyclohexanol	Major	Standard	Standard
Methanol	Major	NIST library	b
Phenol	Minor	Standard	Standard
Cyclohexanone	Minor	Standard	Standard
2-Methoxyclohexanone	Minor	Standard	Standard
Cyclohexyl methyl ether	Minor	NIST library	Standard
Cyclohexane	Minor	Standard	c

a. Major products are referred to those with yield larger than 3% (molar base) when guaiacol conversion is 90%; and minor products are those with yield smaller than 3%.
b. Methanol was not quantified, but calculated from the yield of cyclohexanol and phenol. c. Cyclohexane was not quantified.

In the first route, guaiacol is first demethoxylated to form phenol and then phenol is hydrogenated to cyclohexanone and cyclohexanol. Cyclohexanol can be further dehydrated and hydrogenated to form cyclohexane. From the kinetics study (Figure 5.1), we can see that the yield of cyclohexanol reached the maximum at 240 min, and then it decreased gradually, indicating conversion of cyclohexanol to cyclohexane. During the 2nd route, the aromatic ring of guaiacol is first hydrogenated to produce 2-methoxycyclohexanone and then to

2-methoxycyclohexanol. A control experiment using 2-methoxycyclohexanol as the reactant showed that 2-methoxycyclohexanol can be demethoxylated to cyclohexanol under these conditions, however, the conversion of 2-methoxycyclohexanol to cyclohexanol is very small, indicating a slow reaction rate for this step. Observation of cyclohexyl methyl ether indicates dehydration and hydrogenation of 2-methoxycyclohexanol. Decrease of 2-methoxyclohexanol (Figure 5.1) also shows that 2-methoxyclohexanol is either further converted to cyclohexanol or cyclohexyl methyl ether. We can find that the reaction types involved in the ECH of guaiacol include demethoxylation (hydrodeoxygenation), hydrogenation and dehydration.

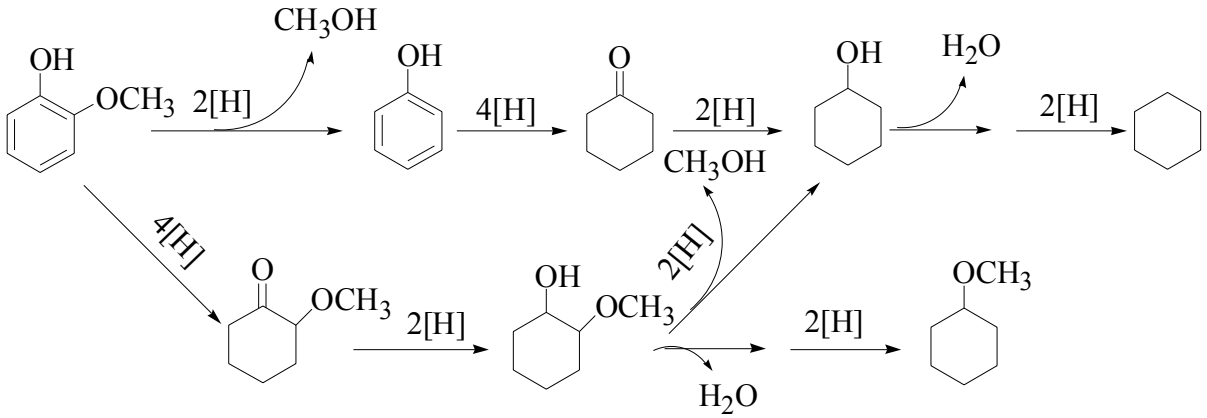

Scheme 5.1 Reaction network for ECH of guaiacol using 3-IW-NH3 as cathode at 80°C and ambient pressure

The T1 method was used to calculate the heat of formation for most of the products and verify the reaction network for ECH of guaiacol.[25] Figure 5.2 (a) and (b) show the heat of formation changes along the 1st and the 2nd reaction routes for ECH of guaiacol (Scheme 5.1). As shown in Figure 5.2 (a), guaiacol conversion to cyclohexanol was favored as the heat of formation decreased from -252.88 KJ/mol to -443.80 KJ/mol. Dehydration of cyclohexanol to cyclohexene is an endothermic reaction, thus high temperature is desirable. Figure 5.2 (b) shows that guaiacol conversion to 2-methoxycylohexanol was also favored as

the heat of formation decreased from -252.88 KJ/mol to -442.46 KJ/mol. Again the dehydration of 2-methoxycylohexanol to cyclohexyl methyl ether required high temperature as the heat of formation increased. Demethoxylation of 2-methoxycylohexanol to cyclohexanol was also favored as the heat of formation decreased from -442.46 KJ/mol (cis-2-methoxycyclohexanol) to -487.92 KJ/mol (cyclohexanol + methanol).

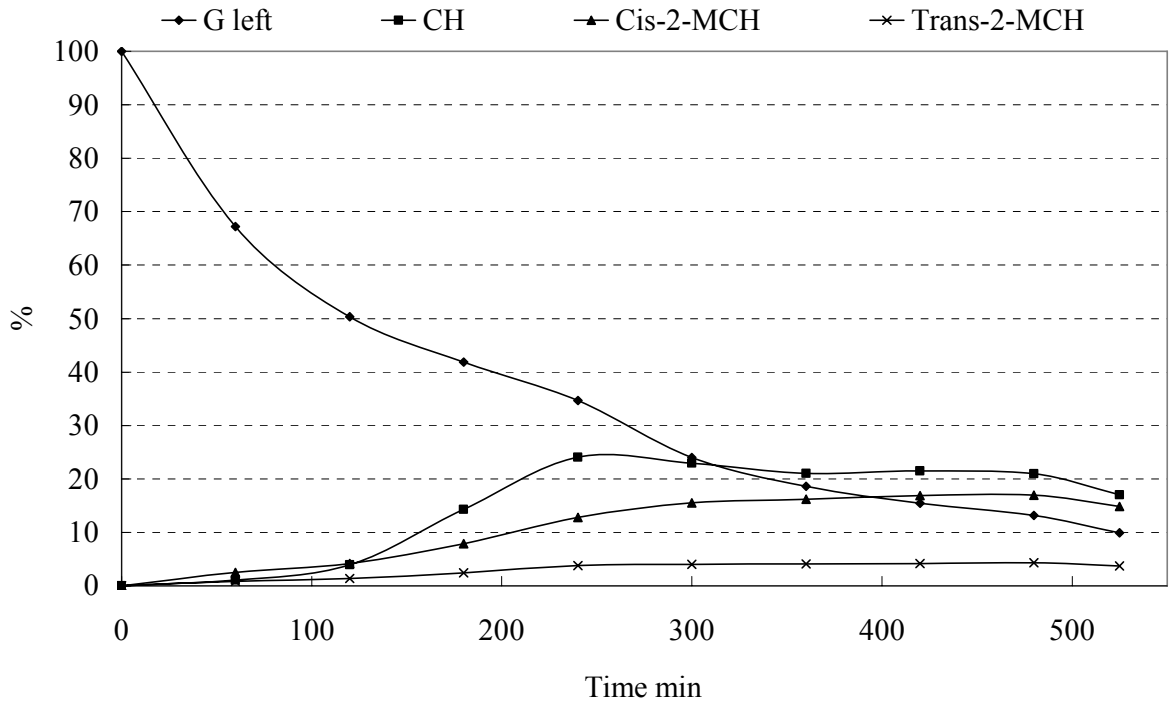

Figure 5.1 Reactant left and major product yields with respect to time during ECH of guaiacol in 0.2 M HCl catholyte at 80 °C and ambient pressure

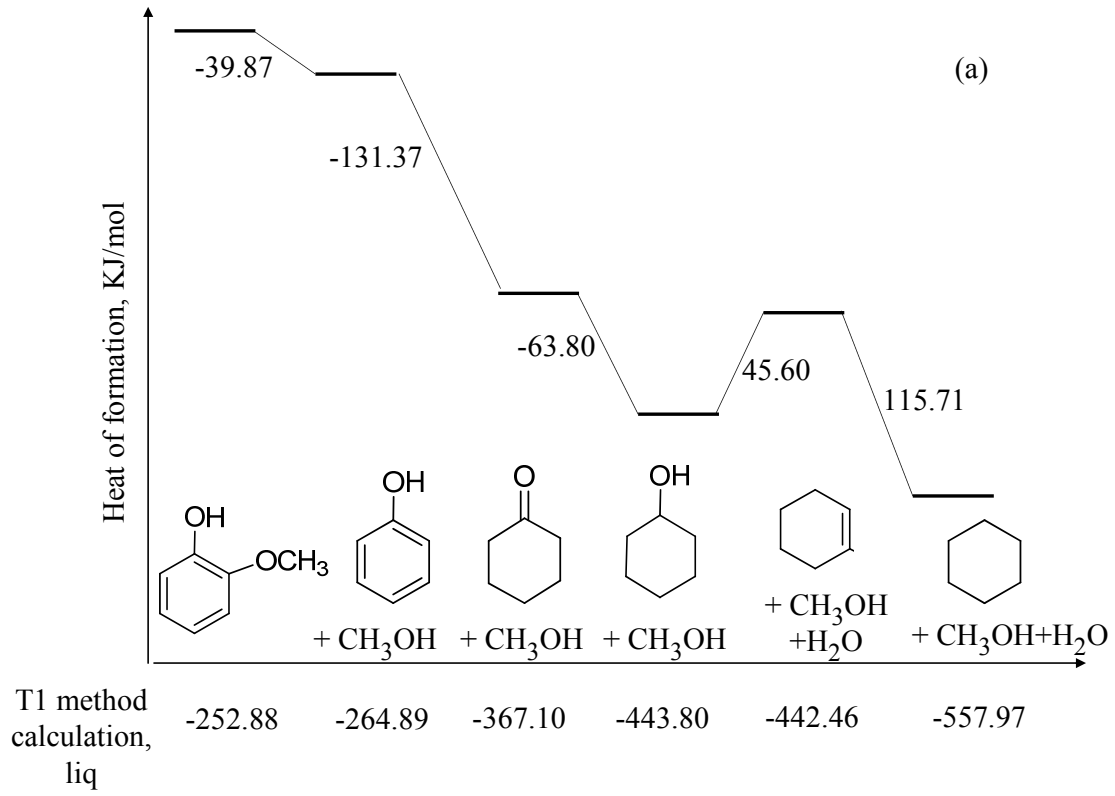

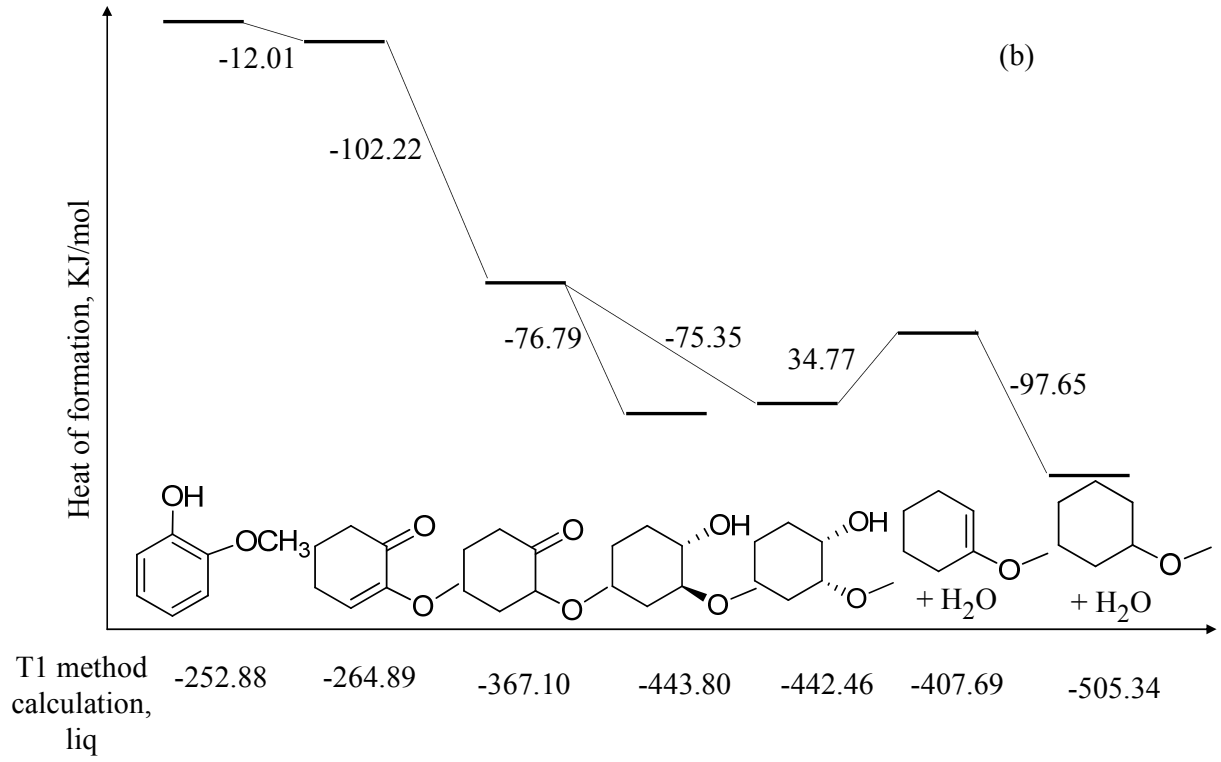

Figure 5.2 Heat of formation calculated using T1 method

The reaction network for classical catalytic conversion of guaiacol is very different from ECH of guaiacol because of different reaction conditions. Compared to the mild

conditions of ECH, catalytic conversion of guaiacol is usually carried out over a temperature range of 150°C to 500°C,[19, 26] under pressures up to 13.8 MPa.[7]

Sulfided CoMo and NiMo are two commonly used catalysts for catalytic hydrodeoxygenation (HDO) of guaiacol. Lin et al.[18] showed that the major products during hydrodeoxygenation of guaiacol included methoxybenzene, methylphenol, phenol, benzene, and cyclohexene using sulfided CoMo and NiMo catalysts at 400°C and 50 bar. They proposed a mechanism where demethylation of guaiacol to catechol, demethoxylation to phenol and deoxygenation to methylphenol proceed simultaneously (Scheme 5.2). During ECH of guaiacol, demethylation to catechol and deoxygenation to methylphenol were not identified mainly because of the mild conditions used in ECH. Besides these reaction routes, Bui et al.[19] also observed methyl substitution during HDO of guaiacol using alumina-supported CoMoS catalyst at 300 °C and 4 MPa. Benzene, a major HDO product from phenol, was also observed in this investigation (Scheme 5.3). Similar reaction network was identified by Zhao et al.[27] using transition metal phosphide catalysts.

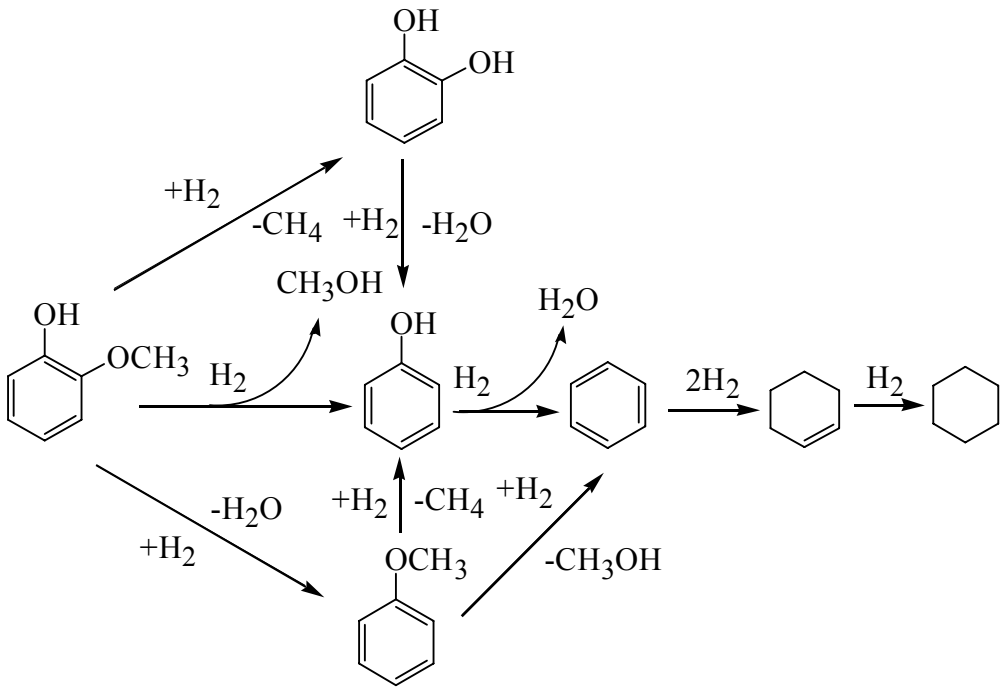

Scheme 5.2 Hydrodeoxygenation of guaiacol using sulfided CoMo and NiMo. (Data was taken from ref.18)

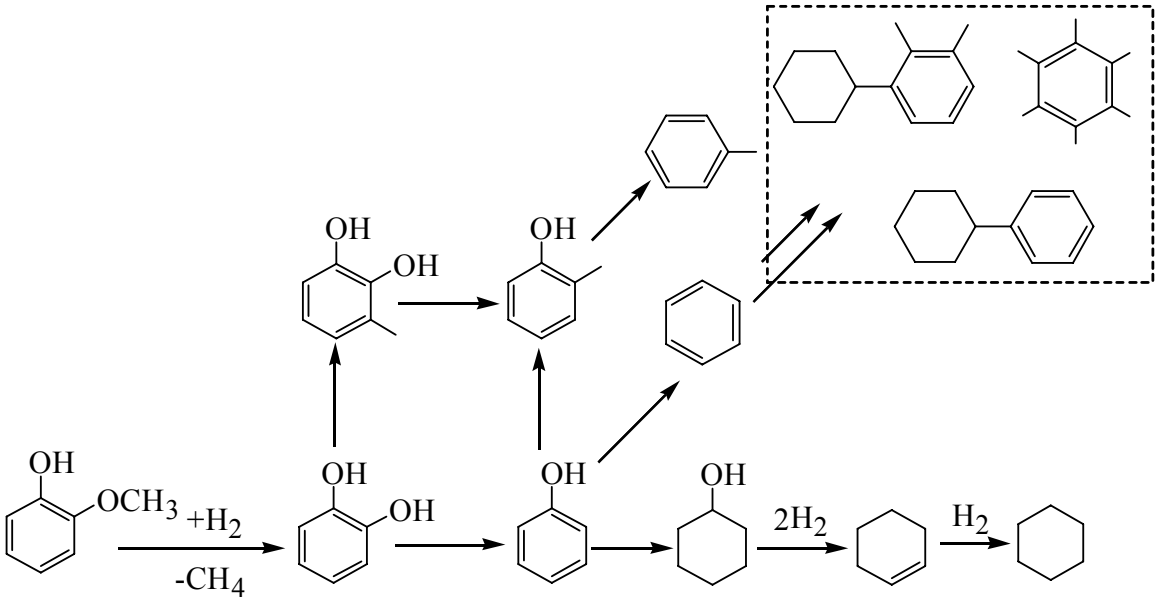

Scheme 5.3 General reaction scheme for hydrodeoxygenation of guaiacol using alumina-supported CoMoS catalyst (Data was taken from ref. 19)

Supported precious metals, such as Ru, Pt, Rh, have also been shown to be active for HDO of guaiacol. Elliott and Hart [7] showed very similar products as ECH of guaiacol when using carbon supported ruthenium and palladium catalysts at 150-250°C and 13.8 MPa. 1,2-cyclohexanediol is the only different product. A Rh-based catalyst showed a similar

reaction pathway as the 2nd route of ECH of guaiacol, being that the aromatic ring is hydrogenated first.[18] However, Nimmanwudipong et al.[28] showed a very different result when using platinum supported on alumina in the presence of H_2 at 300 °C and 140 kPa. More than 30 products were obtained and the most abundant products included phenol, catechol and 3-methylcatechol. The kinetically important reactions were demethylation, demethoxylation, hydrogenation and transalkylation, while there were no demethylation and transalkylation for ECH of guaiacol.

From the above discussion, we can see that demethylation is one of the major reactions during catalytic HDO of guaiacol and this is a big difference from ECH of guaiacol. The product from demethylation reaction, methane, is not desirable because carbon is lost to the gas phase. However, during ECH, most of the carbon is retained in the liquid phase as demethylation is not taking place under the ECH conditions.

5.3.2 Reusability of the catalyst 3-IW-NH3

Catalyst deactivation is a big concern during catalytic bio-oil upgrading because bio-oil tends to polymerize and form coke on the catalyst surface at high temperatures.[29] Even though ECH of guaiacol was carried out at relatively mild conditions, catalyst deactivation still needs to be carefully evaluated. To perform catalyst deactivation study, catalyst 3-IW-NH3 was reused two times. After each use of the catalyst, it was washed overnight using DI water, followed by drying under vacuum in the dessicator. At the beginning of the next experiment, pre-electrolysis was carried out at 80 mA for 10 min. The time course of guaiacol conversion for each experiment is shown in Figure 5.3. From the comparisons of the guaiacol conversion during the reuse experiments, we can see that the

catalyst activity is very stable during two reuses of the catalyst. Compared with other ruthenium catalysts used in catalytic hydrogenation, catalyst 3-IW-NH3 shows better stability. A significant catalyst activity loss was observed when recycling Ru/SiO_2 for liquid-phase hydrogenation of butan-2-one to butan-2-ol even though a lower temperature was used.[30] Ru/MCM-41 was also reported to deactivate gradually during hydrogenation of cinnamaldehyde.[31] The conversion of levulinic acid decreased from 92% to 61% after two reuse of the Ru/C catalyst during hydrogenation of levulinic acid at 130°C and 1.2 MPa.[32]

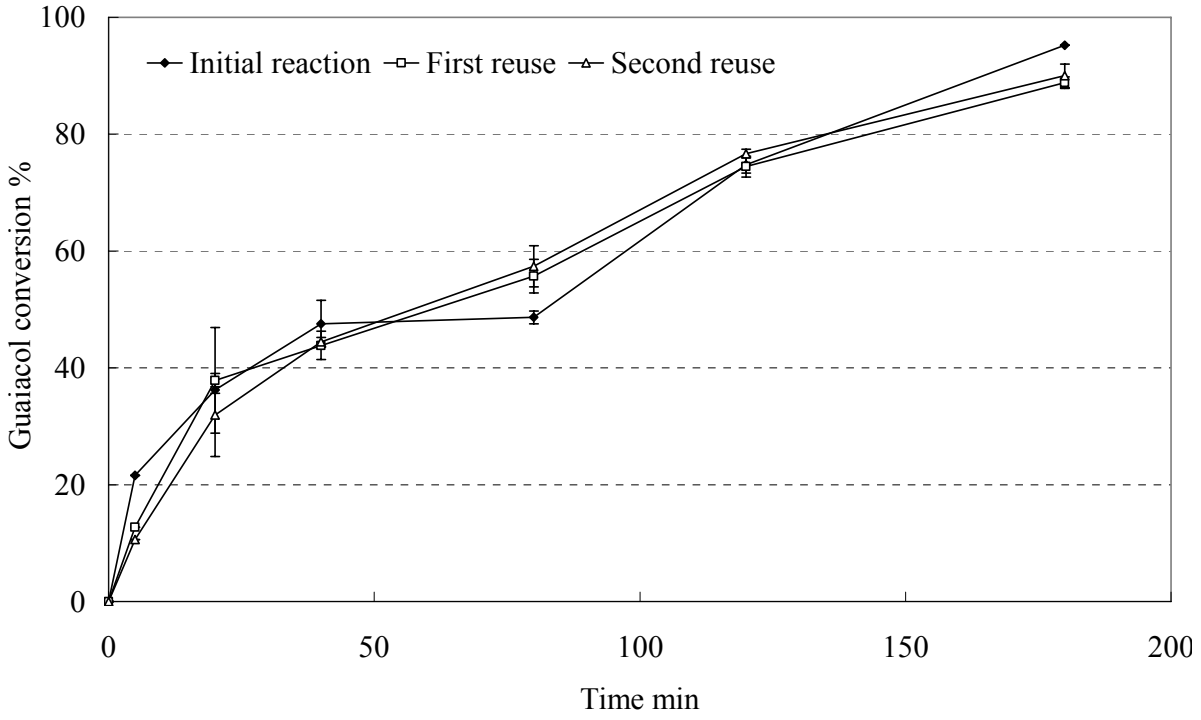

Figure 5.3 Guaiacol conversion for (i) the initial reaction, (ii) the first and (iii) the second reuse of the catalyst 3-IW-NH3 using 0.2M HCl as catholyte at 80 °C and ambient pressure

Product selectivity changes were also examined during the reuses of the catalyst. After 80 min, selectivity of cyclohexanol decreased from the initial experiment to the second reuse of the catalyst (Figure 5.4 (a)), while the selectivity of 2-methoxycyclohexanol increased (Figure 5.4 (b)). According to the reaction network (Scheme 5.1), as the catalyst was reused, hydrogenation of the aromatic ring was more favorable.

2-Methoxycyclohexanone and cyclohexanone were two intermediates during ECH of guaiacol. For the initial reaction, they were not detected during the whole reaction period (Figure 5.4 (c) and (d)). This indicates that the conversions of 2-methoxycyclohexanone and cyclohexanone are very fast for the fresh catalyst. However, as the catalyst was reused, some amount of 2-methoxyclohexanone and cyclohexanone were detected during the reaction period, indicating mild catalyst change and slowing of these conversion steps.

In order to find out the reason for this mild change, several aspects were considered, including active phase transformation, catalyst fouling and poisoning.[31] Sintering and leaching are two common ways for the active phase transformation. Because the reaction temperature is lower than 100°C, sintering can be considered negligible. ICP-OES was used to examine any ruthenium leaching. After the reaction, the cathode solution was evaporated under flowing nitrogen and aqua regia was added to dissolve any remaining solid residues at 100°C. The solution was then diluted with DI water and subjected to ICP analysis. No significant ruthenium leaching was detected during ECH of guaiacol using 3-IW-NH3 as cathode.

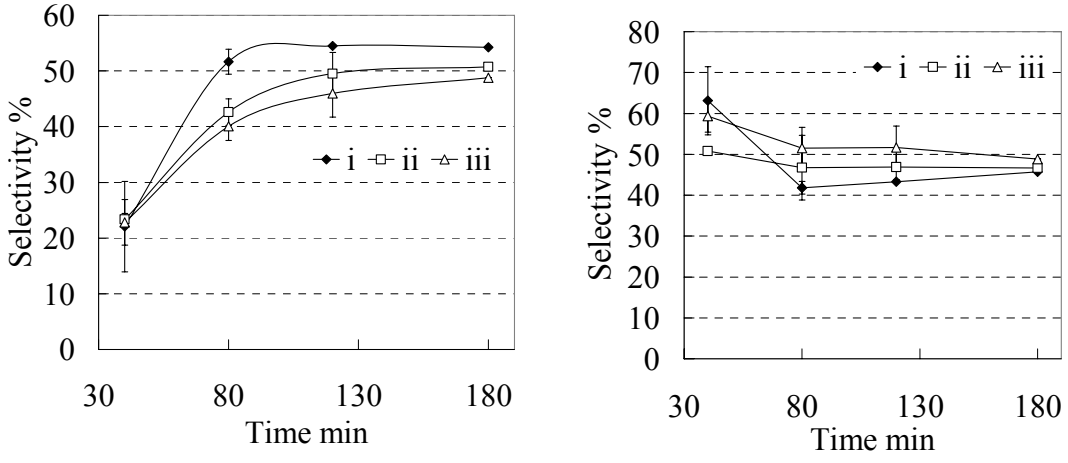

Figure 5.4 (a) Cyclohexanol, (b) 2-methoxycyclohexanol, (c) 2-methoxycyclohexanone and

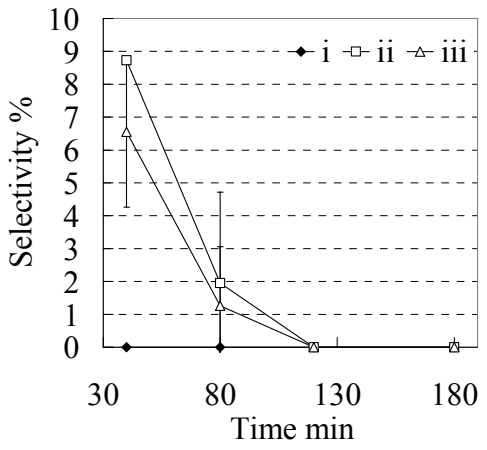

(c)

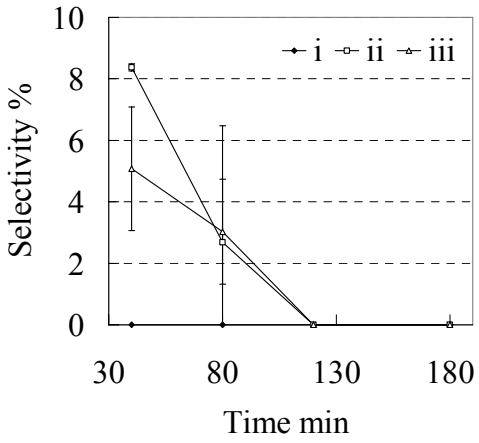

(d)

Figure 5.4 (cont'd)
(d) cyclohexanone selectivities with respect to time during (i) the initial reaction, (ii) the first and (iii) the second reuse of the catalyst 3-IW-NH3 using 0.2M HCl as catholyte

According to Hájek et al.[31], catalyst fouling is one possible reason for catalyst deactivation if selectivity changes are observed. Surface area is usually a good indication of catalyst fouling, thus BET surface areas of the catalyst for the initial reaction and after reuses were measured. As shown in Table 5.2, BET surface area decreased from 800 to 600 m^2/g after the initial reaction. Micropore volume also decreased from 0.26 to 0.17 cm^3/g. After the first reuse of the catalyst, BET surface area increased slightly perhaps because some of the contaminant was washed out. The surface area of the catalyst from the second reuse continues decreasing. Surface area decrease indicates that deposition occurred during the reaction, such as coke formation and metal deposition. Especially for electrocatalytic hydrogenation, reduction of metal cation and deposition onto the cathode surface may happen if there are any metal cation contaminants. To better understand deposition, the fresh catalyst and reused catalyst were analyzed using SEM and EDX. Figure 5.5 (b) shows some deposition on the fiber surface after the 2^{nd} reuse. EDX analyses of the fresh catalyst and the reused catalyst (Table 5.3) shows that there are some new elements in the reused catalyst, including nickel, iron and molybdenum, which are very likely from stainless steel. Stainless steel clips and

wires were used in these experiments. Leaching of these elements into solution and deposition onto the catalyst provides an explanation for the catalyst fouling, which may be the reason for the mild product selectivity changes. To maintain constant product selectivities, platinum wire can be used to directly connect the catalyst to the power supply. On the other side, this finding also suggests that other metals could be in incorporated with ruthenium to tune the product selectivities.

Table 5.2 BET surface area, micropore area and micropore volume of the fresh and the reused catalyst

	BET surface area m^2/g	Micropore area m^2/g	Micropore volume cm^3/g
Fresh	800	551	0.26
After first use	600	361	0.17
After first reuse	640	449	0.21
After second reuse	88	52	0.02

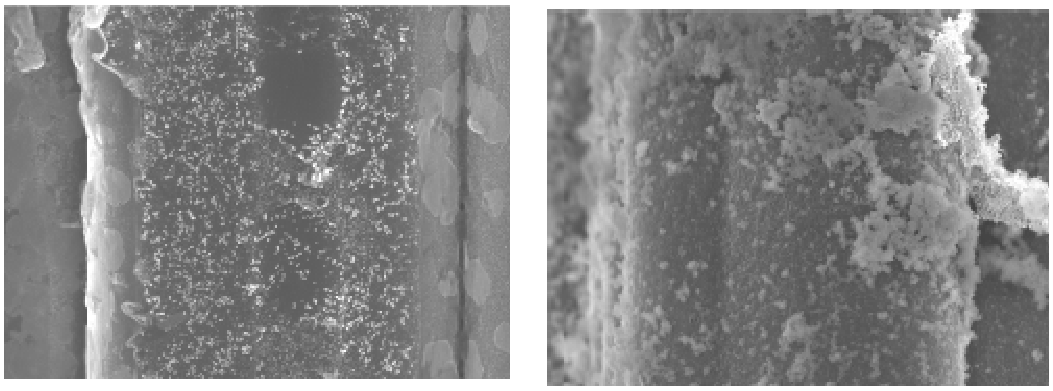

(a) (b)

Figure 5.5 SEM images of (a) the fresh catalyst 3-IW-NH3 and (b) that after the second reuse. (a) scale bar: 1 μm; (b) scale bar: 1 μm.

Table 5.3 EDX analyses of fresh catalyst 3-IW-NH3 and that after the second reuse

	Weight %	
Element	Fresh	Used
C	71.49	32.72
O	11.04	20.36
Al	4.97	0.79
Si	0.52	1.11

Table 5.3 (cont'd)

Fe	-	9.56
Ni	-	11.94
Mo	-	5.45
Ru	6.56	18.08
Cl	2.09	-
Zn	3.32	-

Catalyst poisoning due to strong chemisorption of Cl is very common for classical catalytic hydrogenation.[21] The inhibition of Cl on the catalyst performance is also examined here since HCl was used as the catholyte. Two other acids, $HClO_4$ and H_2SO_4, were used as the catholytes to avoid the use of Cl^- in the cathode solution. As shown in Figure 5.6, there is no significant difference for the overall guaiacol conversion among these three electrolytes, indicating the presence of Cl^- is not inhibiting the ruthenium electrocatalyst. Dalavoy et al.[33] also state that Cl is not harmful for ECH using ruthenium catalyst during the electrocatalytic hydrogenation of lactic acid to lactaldehyde and propylene glycol.

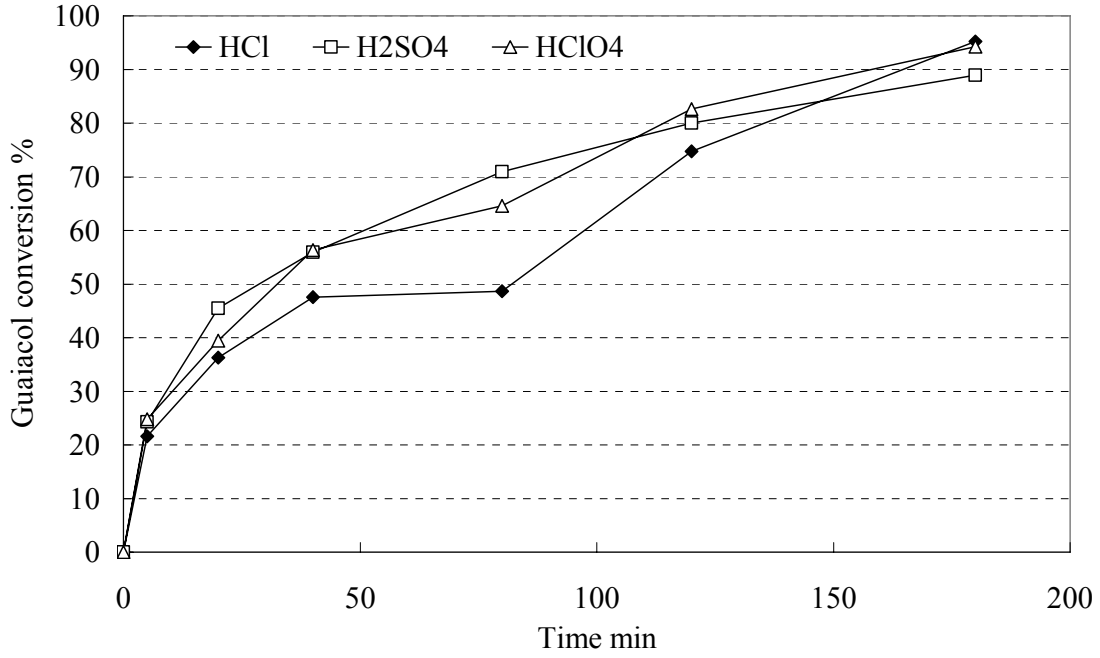

Figure 5.6 Guaiacol conversion with respect to reaction time using HCl, H_2SO_4 and $HClO_4$ as electrolytes during ECH of guaiacol at 80°C and ambient pressure

5.4 Conclusions

The reaction network for the ECH of guaiacol with Ru/ACC catalyst was discussed. Two reaction routes were proposed, with the 1st route to be demethoxylation to form phenol and hydrogenation of phenol for cyclohexanol, and the second route involving the direct hydrogenation of the aromatic ring to form 2-methoxycylohexanol. Demethylation was found to be the major difference between catalytic deoxygenation of guaiacol and the ECH of guaiacol. Guaiacol conversion did not change significantly after two reuses of the catalyst. Only mild product selectivity changes were observed, and the deposition of metal contaminants on the catalyst was presumably the reason for this change.

Acknowledgements

The authors would like to thank the Michigan State University Foundation and AgBioResearch for financial support. Assistance provided by Dr. Lars Peereboom and Mr. Xianfeng Ma with BET analysis and hydrogen chemisorption analysis is warmly acknowledged.

REFERENCES

REFERENCES

1. D. C. Elliott, Energy & Fuels, 2007, **21**, 1792-1815.

2. P. M. Mortensen, J. D. Grunwaldt, P. A. Jensen, K. G. Knudsen and A. D. Jensen, Applied Catalysis a-General, 2011, **407**, 1-19.

3. T. Vispute, Doctor of Philosophy, University of Massachusetts - Amherst, 2011.

4. Z. Li, M. Garedew, C. H. Lam, J. E. Jackson, D. J. Miller and C. M. Saffron, Green Chemistry, 2012, **DOI: 10.1039/c2gc35552c**.

5. S. J. Hurff and M. T. Klein, Industrial & Engineering Chemistry Fundamentals, 1983, **22**, 426-430.

6. R. Kallury, W. M. Restivo, T. T. Tidwell, D. G. B. Boocock, A. Crimi and J. Douglas, Journal of Catalysis, 1985, **96**, 535-543.

7. D. C. Elliott and T. R. Hart, Energy & Fuels, 2009, **23**, 631-637.

8. A. Cyr, F. Chiltz, P. Jeanson, A. Martel, L. Brossard, J. Lessard and H. Menard, Canadian Journal of Chemistry-Revue Canadienne De Chimie, 2000, **78**, 307-315.

9. D. Tountian, A. Brisach-Wittmeyer, P. Nkeng, G. Poillerat and H. Ménard, Journal of applied electrochemistry, 2009, **39**, 411-419.

10. A. Brisach-Wittmeyer, N. A. Bouchard, R. Breault and H. Ménard, Canadian journal of chemistry, 2006, **84**, 1640-1647.

11. H. Ilikti, N. Rekik and M. Thomalla, Journal of applied electrochemistry, 2002, **32**, 603-609.

12. H. Ilikti, N. Rekik and M. Thomalla, Journal of applied electrochemistry, 2004, **34**, 127-136.

13. K. Amouzegar and O. Savadogo, Electrochimica acta, 1994, **39**, 557-559.

14. K. Amouzegar and O. Savadogo, Journal of applied electrochemistry, 1997, **27**, 539-542.

15. P. Dabo, A. Cyr, J. Lessard, L. Brossard and H. Menard, Canadian journal of chemistry, 1999, **77**, 1225-1229.

16. C. M. Cirtiu, A. Brisach-Wittmeyer and H. Menard, Journal of Catalysis, 2007, **245**,

191-197.

17. B. Mahdavi, P. Chambrion, J. Binette, E. Martel and J. Lessard, Canadian Journal of Chemistry-Revue Canadienne De Chimie, 1995, **73**, 846-852.

18. Y. C. Lin, C. L. Li, H. P. Wan, H. T. Lee and C. F. Liu, Energy & Fuels, 2011, **25**, 890-896.

19. N. B. Van, D. Laurenti, P. Afanasiev and C. Geantet, Applied Catalysis B-Environmental, 2011, **101**, 239-245.

20. M. Besson and P. Gallezot, Catalysis today, 2003, **81**, 547-559.

21. B. J. Arena, Applied Catalysis A: General, 1992, **87**, 219-229.

22. M. Burgener, R. Wirz, T. Mallat and A. Baiker, Journal of Catalysis, 2004, **228**, 152-161.

23. Z. Li, S. Kelkar, C. H. Lam, K. Luczek, J. E. Jackson, D. J. Miller and C. M. Saffron, Electrochimica Acta, 2012, **64**, 87-93.

24. F. Laplante, L. Brossard and H. Ménard, Canadian journal of chemistry, 2003, **81**, 258-264.

25. W. S. Ohlinger, P. E. Klunzinger, B. J. Deppmeier and W. J. Hehre, The Journal of Physical Chemistry A, 2009, **113**, 2165-2175.

26. J. Zakzeski, P. C. A. Bruijnincx, A. L. Jongerius and B. M. Weckhuysen, Chem. Rev, **110**, 3552-3599.

27. H. Y. Zhao, D. Li, P. Bui and S. T. Oyama, Applied Catalysis a-General, **391**, 305-310.

28. T. Nimmanwudipong, R. C. Runnebaum, D. E. Block and B. C. Gates, Energy & Fuels, 2011, **25**, 3417-3427.

29. R. K. Sharma and N. N. Bakhshi, Energy & fuels, 1993, **7**, 306-314.

30. H. G. Manyar, D. Weber, H. Daly, J. M. Thompson, D. W. Rooney, L. F. Gladden, E. Hugh Stitt, J. Jose Delgado, S. Bernal and C. Hardacre, Journal of Catalysis, 2009, **265**, 80-88.

31. J. Hájek, N. Kumar, V. Nieminen, P. Maki-Arvela, T. Salmi, D. Y. Murzin and L. Cerveny, Chemical Engineering Journal, 2004, **103**, 35-43.

32. Z. Yan, L. Lin and S. Liu, Energy & Fuels, 2009, **23**, 3853-3858.

33. T. S. Dalavoy, J. E. Jackson, G. M. Swain, D. J. Miller, J. Li and J. Lipkowski, Journal of Catalysis, 2007, **246**, 15-28.

Chapter 6 Electrocatalytic Stabilization and Upgrading of Water-soluble Bio-oil Using Ruthenium Catalyst Supported on Activated Carbon Cloth at Room Conditions

Zhenglong Li[a,b], Lauren Raycraft[a], Mahlet Garedew[a], Shantanu Kelkar[a,b], James E. Jackson[c], Dennis J. Miller[b], Christopher M. Saffron[a,b,d,*]

A paper to be submitted

Abstract

Electrocatalytic hydrogenation (ECH) was used as a new approach for bio-oil stabilization and upgrading. Water-soluble bio-oil, as generated by water separation, was hydrogenated using ECH under room temperature and ambient pressure. A new electrocatalyst, ruthenium supported on activated carbon cloth, was used as the cathode catalyst. After electrocatalytic hydrogenation, most of the aldehydes and ketones were hydrogenated to the corresponding alcohols or diols, which were thermochemically more stable. Carbon recovery into the liquid product was more than 80%, and only less than 0.1wt % solid was formed during ECH. An accelerated aging test was performed to evaluate the stability of ECH treated water-soluble bio-oil. Size exclusion chromatography (SEC) and viscosity measurements were used to analyze the aged bio-oil. SEC analysis indicated that ECH treated bio-oil was more stable than that without ECH treatment. Besides stabilization of the bio-oil, valuable products, such as hydrogen and diols, can be recovered during electrocatalytic hydrogenation. Material and energy balance calculations indicate that further

a.Department of Biosystems & Agricultural Engineering, Michigan State University, East Lansing, MI 48824, US; b. Department of Chemical Engineering & Materials Science, Michigan State University; c. Department of Chemistry, Michigan State University; d. Department of Forestry, Michigan State University.* Corresponding author at: saffronc@egr.msu.edu (C.M. Saffron).

reduction of the cell voltage and improvement of the electrochemical efficiency are required as future work to improve energy efficiency.

6.1 Introduction

Fast pyrolysis is a thermochemical method for converting biomass into a liquid product, known as bio-oil. Because bio-oil has a much higher bulk density than the original biomass, fast pyrolysis becomes an effective way to densify biomass. Locating this technique in the regional biomass processing depots (RBPDs), near the biomass harvesting area, can potentially reduce the cost of biomass transportation to the central refinery. However, high concentrations of carboxylic acids, mainly formic acid and acetic acid, make the bio-oil very corrosive to the storage materials. The other issue is the chemical instability of the bio-oil due to the presence of reactive carbonyl compounds (aldehydes and ketones) that readily undergo polymerization. To reduce the corrosiveness and improve the chemical stability, stabilization or mild upgrading is required before transporting bio-oil to the central refinery.

Recently, mild hydrotreatment scheme has been proposed by several groups.[1-4] Huber's group used a mild hydrogenation with Ru/C at 125-175°C and 52-100 bar.[1-3] After the hydrogenation, most of the functionalities (aldehydes, ketones, sugars) were reduced to the corresponding alcohols or polyols. The products showed better thermal stability compared with the reactants containing carbonyl functionalities, resulting in less coke formation during the following downstream upgrading.[3] Venderbosch et al.[4] applied mild hydrotreating at less than 250°C and over 200 bar using Ru/C catalyst. When the hydrotreatment temperature was 175°C, hydrogenation of carbon-carbon double bonds and aldehydes/ketones was observed. Polymerization of the sugar fraction was also detected under this condition. When the

temperature was increased to 225°C, phase separation occurred due to significant amount of water generation. Re-polymerization and hydrotreating reactions took place in parallel under this hydrotreating condition. Gagnon and Kaliaguine [5] also investigated the mild hydrogenating pretreatment in the presence of a Ru catalyst, with optimum conditions at a temperature of 80°C and a pressure of 600 psi. Even though coke formation can be reduced using these hydrotreatment methods, coking rate is still very large (18.9 wt%)[2] as bio-oil polymerizes quickly under these conditions, thus catalyst deactivation is still a problem. Therefore methods with even milder conditions should be investigated.

Homogeneous catalysis may provide such mild conditions for bio-oil upgrading, e.g., <100°C and 1-3 MPa. Huang et al.[6] developed a homogeneous catalyst $RuCl_2(PPh_3)_3$ to hydrogenate the aldehydes and bio-oil under mild conditions (55-90°C, 1.3-3.3 MPa). Results showed that the majority of the aldehydes were transformed to the corresponding alcohols, and some ketones and other compounds with C=C were also converted to more stable products. Mahfud et al. applied a homogeneous hydrogenation on bio-oil model compounds, water-soluble bio-oil fraction [7] and dichloromethane soluble fraction [8] in a two-phase aqueous organic system using ruthenium homogeneous catalysts. Reduction of aldehydes and ketones to alcohols was also observed. Shvo catalyst was used to hydrogenate bio-oil derived from pyrolysis of white poplar at the temperature range of 90-145°C and under pressure of 10 atm.[9] Significant chemical changes of the bio-oil were observed. Besides the hydrogenation of the aldehydes, ketones and non-aromatic double bonds, the catalytic system also promoted the hydrolysis of sugar oligomers into monomers. Separation of the homogeneous catalysts from the products and reuse of these catalysts are big challenges for homogeneous upgrading

of the bio-oil. Furthermore, the catalyst cost for the homogeneous catalyst is usually much higher compared to the related heterogeneous catalyst. Large amount of hydrogen consumption also poses a barrier to this method.

To facilitate fast pyrolysis application in the regional biomass processing depots, fast pyrolysis systems are limited in small or medium scales. Bio-oil upgrading with hydrotreatment is not economically practical in the small or medium scale. Furthermore, hydrogen is not always available in the regional biomass processing depots. Thus a new method with an alternative reducing agent is required to stabilize the bio-oil in the regional biomass processing depots.

In this context, this paper discussed a novel electrocatalytic hydrogenation (ECH) approach to stabilize or upgrade the bio-oil. Instead of molecular hydrogen, electricity, produced from renewable sources, such as solar and wind, will be used as the reducing agent. Atomic hydrogen is produced in situ on the catalytic electrode surface and reacts with the organic compounds absorbed on the catalyst surface.[10] The surface hydrogen atom concentration is controlled by the applied electrode potential, so the reaction can take place at very mild conditions, such as ambient pressure and temperature. Furthermore, the catalyst is heterogeneous and monolithic, so no catalyst separation is required in the downstream upgrading.

Water-soluble bio-oil was investigated as it contains most of the carboxylic acids and carbonyl groups from the bio-oil. This bio-oil fraction is also difficult to upgrade using the traditional hydrotreatment since water is detrimental to most of the catalysts at high temperatures. Sharma and Bakhshi [11] have reported that the presence of large amount of

water in the bio-oil had an adverse influence on the activity of HZSM-5 because the number of acid sites on the catalyst surface decreased. In this paper, we tried to accomplish reducing of the corrosiveness and improving of the chemical stability (reduce of the carbonyl groups) by performing electrocatalytic hydrogenation on the water-soluble bio-oil. Understanding the chemical reactions during ECH is the most important goal for this research. The properties for the bio-oil before and after the electrocatalytic hydrogenation were compared with several characterization methods, including GC/MS, size exclusion chromatography (SEC) and total organic carbon (TOC) analysis. Accelerated aging test was performed to evaluate the stability of the water-soluble bio-oil before and after ECH treatment. Viscosity measurement and SEC were employed to characterize the bio-oil after the aging test. Electrochemical efficiency was also calculated using the measured hydrogen generation and improvement of the electrochemical efficiency was carried out by adding surfactant into the bio-oil. Material and energy balance were calculated for the electrocatalytic hydrogenation of the water-soluble bio-oil process.

6.2 Material and Methods

6.2.1 Bio-oil

Bio-oil was obtained from pyrolysis of poplar DN34 in a bench-scale screw-conveyor fast pyrolysis reactor, as shown in chapter 2. It was stored at -3°C in the refrigerator right after its production. The properties of the bio-oil were shown in Table 6.1 and the major compounds were shown in Table 6.2.

Table 6.1 The properties of the bio-oil derived from fast pyrolysis of poplar DN34

		Weight %, a.r.
Elements	C	34.3
	H	8.2
	O	57.5
	N	<0.01
Solids (methanol insoluble)		0.7
pH		2.8
density		1.12 g/mL
HHV		10.4

a.r.: as received.

Table 6.2 Quantification of some major compounds in bio-oil with GC/MS and HPLC

Compounds in bio-oil	Group	Method	wt% in whole bio-oil
Cellulose/hemicellulose derived compounds			
Acetic acid	Acids	GC/MS	6.2
Acetol	Misc. Oxygenates	GC/MS	5.6
1-Hydroxy-2-butanone	Misc. Oxygenates	GC/MS	3.1
Furfural	Furans	GC/MS	0.4
Furfuryl alcohol	Furans	GC/MS	0.3
Cyclopentanone	Ketones	GC/MS	0.3
3-Methyl-2-cyclopentenone	Ketones	GC/MS	0.4
3-Methyl-1,2-cyclopentanedione	Ketones	GC/MS	1.1
Levoglucosan	Sugars	GC/MS	3
Glucose	Sugars	HPLC	0.3
Xylose	Sugars	HPLC	0.3
Lignin derived compounds			
Phenol	Phenols	GC/MS	1
2-Methylphenol	Phenols	GC/MS	0.3
Guaiacol	Phenols	GC/MS	0.5
Cresol	Phenols	GC/MS	0.5
4-Ethyl-guaiacol	Phenols	GC/MS	0.4
Eugenol	Phenols	GC/MS	0.2
Isoeugenol	Phenols	GC/MS	1.2
Methoxyeugenol	Phenols	GC/MS	2.3
Syringol	Phenols	GC/MS	1.4

6.2.2 Water-soluble bio-oil

Water-soluble bio-oil was obtained by mixing bio-oil with water, followed by half an

hour sonication. After that, the mixture was centrifuged and the top layer was decanted to use as the water-soluble bio-oil fraction. Before each experiment, another filtration was performed using a 0.22 μm syringe filter.

Water/bio-oil ratio will influence the phase separation and final recovery into the aqueous phase and affect the final bio-oil concentration in the aqueous layer. Mercader et al.[12] found that when water/bio-oil ratio was 1:10, there was no phase separation. As shown in Figure 6.1, when the ratio increased to 1:8, phase separation was observed. As the amount of water increased, more bio-oil will be recovered into the aqueous layer. However, the final bio-oil concentration in the aqueous layer will also decrease if more water was used. As a demonstration, a bio-oil/water ratio at 1:4 was used, with the final bio-oil concentration at 15 wt%. To reduce the electrocatalytic hydrogenation reaction time, two times dilution on this water-soluble bio-oil fraction was performed and the final water-soluble bio-oil fraction was used for the following experiments. Even though this highly diluted water-soluble bio-oil is not ideal for the bio-oil upgrading, the chemistry during ECH of this water-soluble bio-oil can be extended to the concentrated water-soluble bio-oil with smaller water content, such as bio-oil/water ratio 8:1. And this method is still useful for the concentrated bio-oil stabilization.

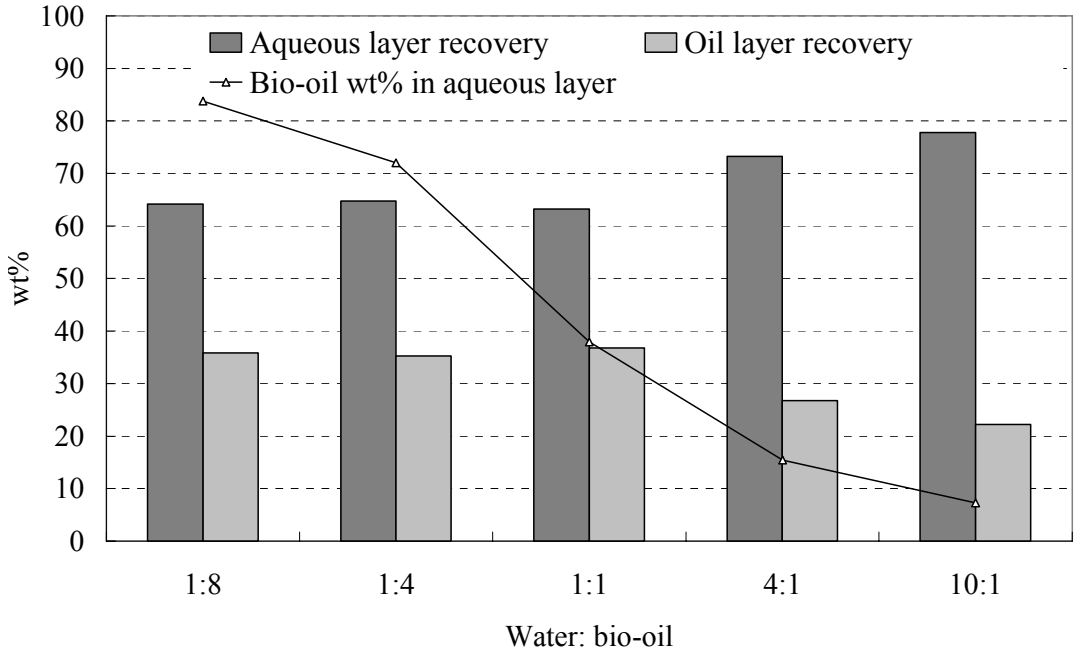

Figure 6.1 Separation of bio-oil using water with different water/bio-oil ratio

6.2.3 Catalyst preparation

A piece of activated carbon cloth (ACC) (1.3cm × 3.0cm) was first soaked into $Ru(NH_3)_6Cl_3$ solution, which was enough to saturate the ACC pores. After the ACC pores were saturated with the solution, it was taken out and extra solution was dried off using kimwipes®. The wet ACC was first dried at room condition and then dried under vacuum at room temperature. Finally, it was reduced with H_2 in a Parr pressure reactor (model 452HC) at 500 psi and 220 °C. To facilitate the recognition of the catalyst, a catalyst code 3-IW-NH3 is used, where "3" is the nominal ruthenium content, "IW" stands for incipient wetness impregnation and "NH3" means the precursor is $Ru(NH_3)_6Cl_3$.

6.2.4 Electrochemical cell setup

Electrochemical hydrogenation of the water-soluble bio-oil was carried out in a two-chamber glass H-cell,[10] separated with a DuPont® Nafion-117 membrane. Due to the heat formation during passing the current through the solution, running water was used to

cool down the cathode chamber (Figure 6.2). Water-soluble bio-oil with 0.2 M NaCl was used in the cathode side. 3-IW-NH3 prepared as described above was used as the working electrode (cathode). Anolyte (30 mL) consisted of 1 M sulfuric acid, and a Pt wire was used as the counter electrode (anode). ECH was carried out under galvanostatic control (480 mA) for 6.5 hr with Instek GPR-11H30D DC power supply. Due to the hydrogen production and bubbling through the bio-oil, to catch the organic compounds carried out by hydrogen, a trap with DI water was used to collect the evaporated organic compounds (Figure 6.2).

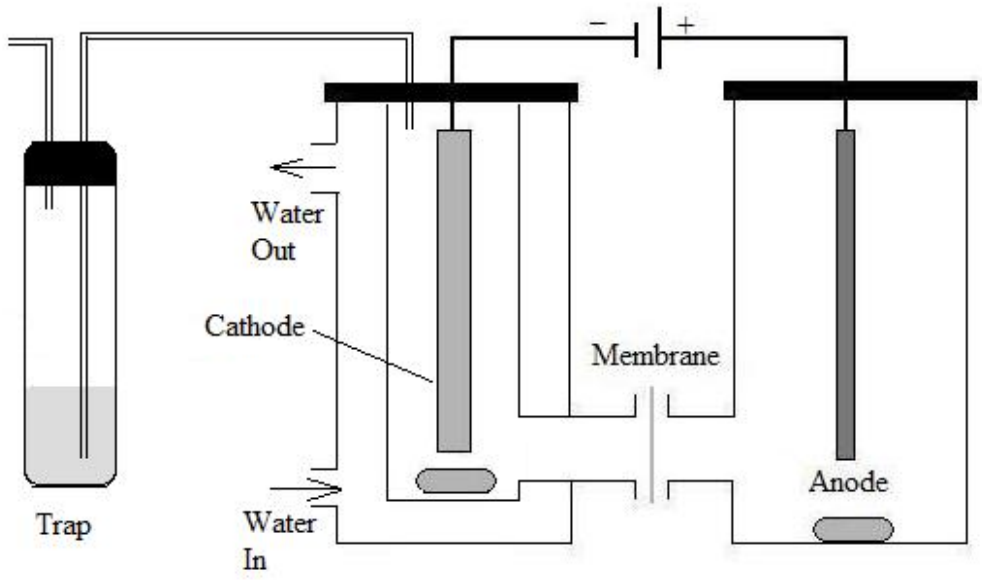

Figure 6.2 Electrochemical hydrogenation cell setup for ECH of water-soluble bio-oil

6.2.5 Products analysis

Pyroprobe-GC/MS Analytical pyrolysis experiments were conducted using a microscale pyrolysis unit, CDS Pyroprobe 5250 (CDS Analytical Inc, Oxford, PA) interfaced to a Shimadzu QP-5050A gas chromatograph/mass spectrometer (Shimadzu Corp, Columbia, MD). Approximately 0.5 mg of ground biomass sample was packed between quartz wool in a quartz tube with a filler rod. Three replicates of each sample were run. The pyroprobe was set at 600°C with a hold time of 10 s at a heating rate of 1000°C/s. The GC used a Restek

Rtx-1701 column (Restek, Bellefonte, PA), 60 m x 25 mm with a 0.25 mm film thickness. The column gas flow was 1 cm/s with a split ratio of 1:100. The GC oven temperature program began with a 1 minute hold at 40 °C followed by heating at 8 °C/min to 270 °C. The injector and detector temperature was set at 280 °C. The mass spectra were recorded in electron ionization mode for m/z 29 to 400. Identification of compounds was performed by comparing the mass spectra of the peaks with standard spectra of other compounds using the NIST library to obtain the most probable matches. Pure compounds (Sigma-Aldrich Co., St Louis, MO) were then used to confirm the peak identities based on matching of retention times and mass spectra.

GC/MS Liquid samples were analyzed using GC/MS (Shimadzu Corp, Columbia, MD), with the conditions same as above. Quantification was performed using external standards. A four-point calibration curve was constructed relating concentration to peak area response. The amount of a certain chemical produced was determined with the calibration curves.

Size exclusion chromatography Molecular weight distribution of the water-soluble bio-oil fraction was determined using an Agilent 1100 HPLC system equipped with a Waters Ultrahydrogel^{TM} 250 7.8×300mm column. Both diode array detector (DAD) detector (260, 280 and 340 nm) and refractive index detector were used. The mobile phase was 0.1M sodium nitrate and 0.01 M sodium hydroxide with a flow rate of 0.6 mL/min. Column temperature was set as 40°C for SEC analysis. Samples were dilute 2 times using the mobile phase. Dextran standards were used to identify the molecular weight peaks for the carbohydrates in bio-oil samples. No lignin standard was used, so the molecular weights were

unknown. Thus the signal of the DAD detector was plotted against the elution time. Larger molecules will elute out first and show up on the left side of the x-axis.

Total organic carbon (TOC) TOC of the water-soluble bio-oil was analyzed using a TOC analyzer. Each sample was analyzed by triplicate. Standards with concentrations from 6.25 ppm to 50 ppm were used to quantify the TOC in the samples. The samples were diluted to proper concentrations that can fit into the standard concentration range.

Electrochemical efficiency (E.E.) The amount of hydrogen generation was measured by water displacement using an inverted graduated cylinder. The E.E. was calculated according to the following equation:

$$E.E. = (I \times t - 2 \times n \times F) / (I \times t)$$

Where I is the current, t is the reaction time, n is the number of moles of hydrogen, F is faraday constant.

6.2.6 Bio-oil aging

Water-soluble bio-oil (10-20 g) was weighed into a pressure tube. Afterward, the tube was carefully capped and placed in an oven at a temperature of 80°C for 48 hr. After the aging, bio-oil was filtered with 0.22 μm syringe filter for various analyses.

6.3 Results and Discussion

6.3.1 ECH of water-soluble bio-oil

(1) Characterization of the bio-oil before and after ECH

Water-soluble bio-oil fractions before and after ECH were analyzed by GC/MS. As shown in Table 6.3, aldehydes and ketones were observed in the water-soluble bio-oil fraction before ECH, including formaldehyde, acetaldehyde, propanal, acetone, butanal,

2,3-butanedione, 2-butanone, glycolaldehyde, acetol, cyclohexanone and 3-methyl-1,2-cyclopentanedione. After the electrocatalytic hydrogenation, most of these compounds disappeared or reduced significantly. Hydrogenation of these compounds was one of the reasons for the decrease of these chemicals as many hydrogenation products were observed in the water-soluble fraction after 6.5 h ECH, such as ethanol, isopropanol, 2-propanol, 1-propanol, 2-butanol, tetrahydrofurfuryl alcohol, ethylene glycol and propylene glycol. Possible reaction schemes were shown in Scheme 6.1.

Table 6.3 Normalized GC/MS chromatogram areas (to internal standard, isobutanol) of the major compounds in the water-soluble bio-oil at t=0 h and t=6.5 h during ECH using 0.2 M NaCl as catholyte at room temperature and ambient pressure

Retention time min	Chemicals	Normalized area	
		Bio-oil in cathode chamber at t=0 h	Bio-oil in cathode chamber at t=6.5 h
3.81	Formaldehyde	0.21	0.00
3.99	Acetaldehyde	0.77	0.00
4.09	Methanol	2.96	2.19
4.41	Ethanol	0.01	0.52
4.49	Propanal	0.17	0.00
4.57	Acetone	0.74	0.09
4.63	Methyl acetate	0.47	0.00
4.65	2-Propanol	0.00	0.28
5.37	1-Propanol	0.00	0.09
5.41	Butanal	0.08	0.00
5.54	2,3-Butanedione	0.20	0.00
5.59	2-Butanone	0.52	0.03
5.77	2-Butanol	0.00	0.05
6.25	Isobutanol (Internal standard)	1.00	1.00
7.35	Glycolaldehyde	1.61	0.01
7.64	Acetic acid	6.90	3.09
8.39	Acetol	3.21	0.34
9.74	Cyclopentanone	0.08	0.06
10.34	Ethylene glycol	0.00	0.20
10.57	Propylene glycol	0.00	1.29
11.10	Butanedial	1.03	0.00

Table 6.3 (cont'd)

Retention time min	Chemicals	Normalized area	
		Bio-oil in cathode chamber at t=0 h	Bio-oil in cathode chamber at t=6.5 h
13.82	3-Methyl-cyclopentanone	0.29	0.00
15.90	3-Methyl-1,2-cyclopentanedione	0.57	0.18
16.35	Phenol	0.51	0.10
16.87	Guaiacol	0.12	0.02
22.44	Syringol	0.42	0.08
23.99	1,2,3-Trimethoxybenzene	0.30	0.11
27.91	Levoglucosan	1.61	0.95

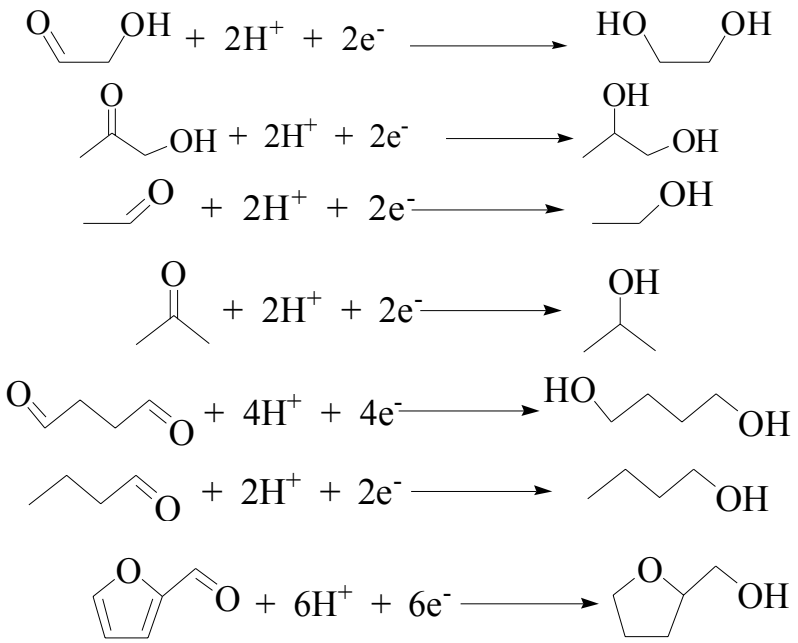

Scheme 6.1 Reaction schemes for ECH of organic compounds in water-soluble bio-oil

As shown in Table 6.3, acetic acid decreases by more than 50%, indicating corrosiveness is reduced during ECH since acetic acid is one of the major contributions to the bio-oil corrosiveness. No strong evidence showed the hydrogenation of acetic acid occurred during ECH since the conditions were very mild. Migration of acetic acid to the anode chamber through the membrane may be the major contribution to the decrease. This could be an alternative approach to reduce the carboxylic acids and the corrosiveness.

Some of the major products during ECH of water-soluble bio-oil were quantified by

GC/MS (Table 6.4). Besides the alcohols production, relatively larger amount of diols, such as ethylene glycol and propylene glycol, were also produced with the total carbon yield of 10%. Optimization of the pyrolysis or pyrolyzing proper biomass feedstock may increase the yields of glycoaldehyde and acetol. Thus the yields of ethylene glycol and propylene glycol can be greatly improved. Other diols or polyols may be produced during ECH, such as 1,2-butanediol, 1,4-butanediol and sorbitol, etc. Electrocatalytic hydrogenation upgrading of the water-soluble bio-oil fraction can be a great approach for production of the diols or the polyols at very mild conditions.

Table 6.4 GC/MS quantification of the major products after 6.5 hr ECH

Products	Concentration (t=0 hr)		Concentration (t=6.5 hr)	
	g/L	mmol-C/L (C%)	g/L	mmol-C/L (C%)
Ethanol	0.01	0.43 (0%)	0.28	12 (0.9%)
1-propanol	0	0	0.12	5.8 (0.4%)
1-butanol	0	0	0.06	3.4 (0.2%)
Tetrahydrofurfuryl alcohol	0	0	0.05	2.6 (0.1%)
Ethylene glycol	0	0	3.10	69 (5.0%)
Propylene glycol	0	0	1.7	68 (5.0%)
TOC		1857		1384

Besides the hydrogenation of the aldehydes and ketones, there may be other reasons contributing to the decrease of the compounds during ECH, including polymerization of the compounds, migration of the compounds to the anode chamber through the membrane and adsorption onto the catalyst. These reasons will be explained in the following discussion. Control experiments were performed in the electrochemical cell (Figure 6.2) without electricity, but the other conditions were same as the ECH experiments. As shown in Table 6.5, decrease of the reactants was observed in the control experiments, indicating that the

aforementioned reasons are possible.

Table 6.5 Normalized chromatogram areas (to internal standard, isobutanol) of the major compounds in the water-soluble bio-oil at the beginning and the end of the control experiments

Retention time min	Chemicals	Normalized area	
		Bio-oil in cathode chamber at t=0 h	Bio-oil in cathode chamber at t=6.5 h
3.81	Formaldehyde	0.21	0.16
3.99	Acetaldehyde	0.77	0.49
4.09	Methanol	2.96	1.52
4.49	Propanal	0.17	0.15
4.57	Acetone	0.74	0.47
4.63	Methyl acetate	0.47	0.34
5.41	Butanal	0.08	0.05
5.54	2,3-Butanedione	0.20	0.17
5.59	2-Butanone	0.52	0.38
6.25	Isobutanol (Internal standard)	1.00	1.00
7.35	Glycolaldehyde	1.61	0.47
7.64	Acetic acid	6.90	3.70
8.39	Acetol	3.21	2.51
11.10	Butanedial	1.03	0.40
13.82	3-Methyl-cyclopentanone	0.29	0.10
15.90	3-Methyl-1,2-cyclopentanedione	0.57	0.26
16.35	Phenol	0.51	0.11
16.87	Guaiacol	0.12	0.03
22.44	Syringol	0.42	0.07
23.99	1,2,3-Trimethoxybenzene	0.30	0.03
27.91	Levoglucosan	1.61	0.23

No coke formation was observed at these mild conditions, however, small amount of solid was precipitated out in the cathode chamber during the ECH. The solid was measured to be 8 mg after drying under vacuum (less than 0.1wt% of the 15 mL water-soluble bio-oil). Identification of the solid was performed using Py-GC/MS. The details of the peaks were shown in Figure 6.3. A few small peaks for ketones and furans can be observed at the beginning of the chromatogram, and lots of phenolic compound peaks are detected following that. The solid was also dissolved in methanol and analyzed directly in GC/MS, and no peaks

were observed. This indicates that the solid was made of phenolic and carbohydrate oligomers or polymers, formed from the polymerization reactions during ECH of the water-soluble bio-oil. Due to the fast consumption of the protons, it was expected that the local solution close to the catalyst had a high pH even though the bulk solution was still acidic. The basic condition favored the polymerization of the phenolic compounds. A strong stirring may help decrease the pH around the catalyst and reduce the polymerization.

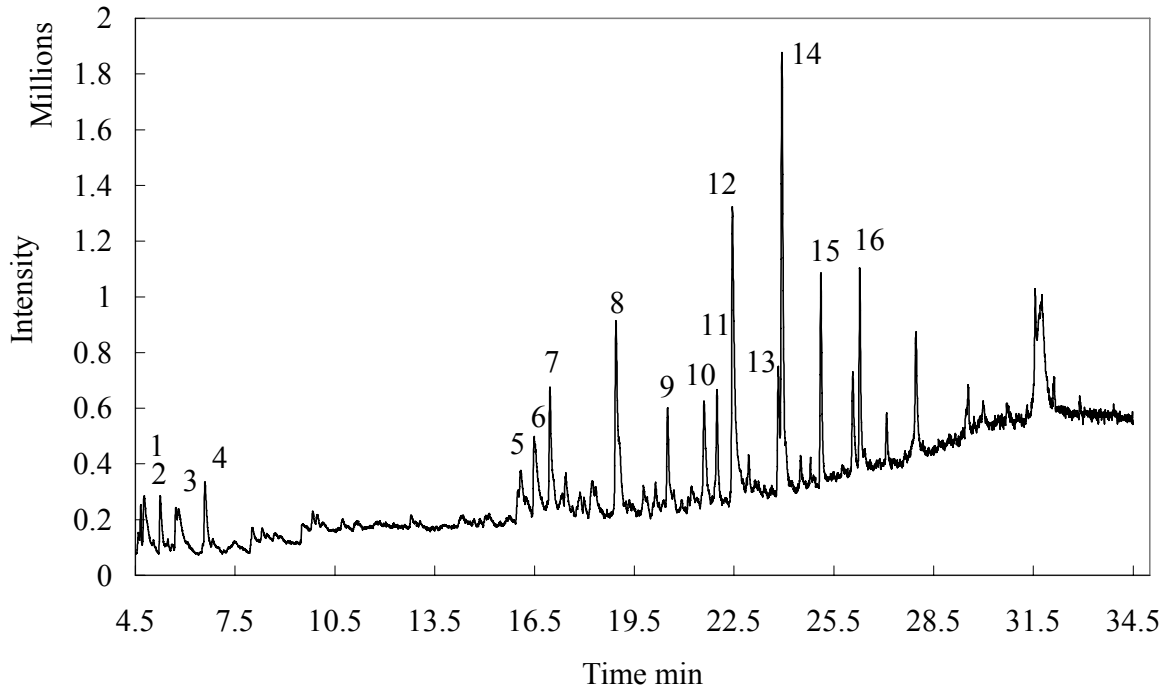

Figure 6.3 Pyrogram of the solids from ECH of water-soluble bio-oil. Possible compounds' names corresponding to the peaks: (1) acetone, (2) 2-methylfuran, (3) 2,3-butanedione, (4) 2,5-dimethylfuran, (5) 3-methyl-1,2-cyclopentanone, (6) phenol, (7) guaiacol, (8) 2-methoxy-4-methylphenol, (9) 4-ethyl-2-methoxyphenol, (10) 2-methoxy-4-vinylphenol, (11) 2-methoxy-4-propylphenol, (12) syringol, (13) 2-methoxy-4-(1-propenyl)-phenol, (14)1,2,4-trimethoxybenzene, (15) 5-tert-butylpyrogallol, (16) 4-Methyl-2,5-dimethoxybenzaldehyde

The solid formation indicates polymerization happened during ECH of water-soluble bio-oil. To examine the molecular weight changes for the water-soluble bio-oil, size exclusion chromatography was used to measure the molecular weight distribution. As shown in Figure 6.4 (a), the intensity of the peak around 1400 Da increased after electrocatalytic

hydrogenation. Figure 6.4 (b) also shows a significant increase at 16 min. Both of these increases indicate possible polymerization to form carbohydrates and phenolic oligmers during electrocatalytic hydrogenation. The molecular weight increase has also been observed in the catalytic stabilization of bio-oil. Gagnon and Kaliaguine [5] showed that the average molecular weight increased from 1775 to 3040 Da during stabilization of bio-oil using CuCr at 120°C and 1000 psi. More direct comparison of the molecular weight increase between electrocatalytic hydrogenation and catalytic hydrogenation should be made in the future.

The mild conditions employed in this investigation were expected to slow the polymerization of bio-oil during ECH, however, the pH increase of the local solution close to the cathode and the presence of large concentration of electrolyte may enhance the polymerization. Strong stirring can help to reduce the pH changes of the solution close to the cathode. Solid polymer electrolyte electrochemical cells can eliminate the use of electrolyte. With the improvement of these conditions, polymerization during ECH can be greatly reduced.

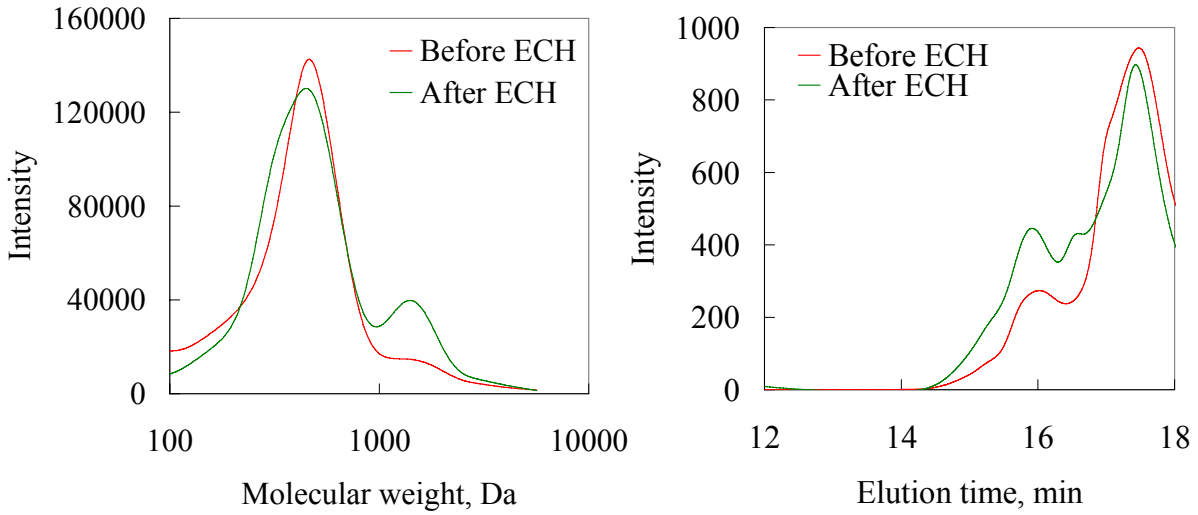

Figure 6.4 Size exclusion chromatographs of water-soluble bio-oil before and after ECH with (a) IR detector (left) and (b) DAD detector (260nm) (right)

The organic compounds migration and adsorption onto the cathode were examined by

analyzing the carbon distribution in different parts of the electrochemical cell with TOC analyzer (Table 6.6). Control experiments without electricity were first performed to check the carbon distribution. After 6.5 h, 81% was retained in the cathode chamber, however, 12% carbon was transferred to the anode chamber due to the organic concentration gradient. The catalytic cathode also adsorbed 4.0% carbon. And the other 3% carbon loss may be due to the organics trapped in the Nafion® membrane during the migration of the organic compounds to the anode chamber. Thus, organic compounds migration to the anode chamber and adsorption onto the catalyst are two major reasons for the decrease of the organic compounds in the control experiments (Table 6.5).

After 6.5 h ECH reaction, there was about 80% carbon retained in the cathode chamber, and 6.0% carbon was detected in the anode chamber due to the migration through the membrane. The cathode adsorbed about 2.6% carbon and 0.2% was trapped in the downstream water trapping system. The total carbon identified in the whole system was about 88.8%. The solid formed during ECH contributed to part of the carbon loss (about 2% by assuming the solid formula as "(C6H6O)" since most of the solid is phenolic polymer). Organics trapped in the membrane may be another source for the carbon loss as the membrane turned black after the ECH reaction. The other important carbon loss may be due to the oxidation of the organics on the anode as the carbon content in the anode was lower than that for the control experiments. Small organic compounds, such as methanol, ethanol, formic acid and acetic acid, can migrate through the membrane to the anode side.[13-16] These organic compounds can be oxidized to form carbon dioxide under the anode conditions [17, 18] (high overpotential and 1 M sulfuric acid). Modification of the membrane to reduce the

transport of small organic compounds to the anode chamber is possible for the future work. Even without any improvements, the carbon retention is still better than that in the catalytic hydrogenation. As shown by Vispute,[2] the carbon retentions in the liquid products were only 75% and 64% during low temperature hydrogenation of the water-soluble bio-oil at 150°C and 175°C.

Table 6.6 TOC changes for the bio-oil in the control experiments and during the electrocatalytic hydrogenation

	Control	ECH
Water-soluble bio-oil before ECH		100%
Water-soluble bio-oil (cathode) after ECH	81%	80%
Anode solution	12%	6.0%
Organics adsorbed on the cathode	4.0%	2.6%
Organics in the trapping system	-	0.2%
Total (after ECH)	97%	88.8%
Others	3%	11.2%

1. Carbon percent is based on the water-soluble bio-oil before ECH

(2) Stability test

The water-soluble bio-oil after ECH treatment should be more stable since the majority of the carbonyl groups were hydrogenated to more stable alcohols or diols. To confirm the stability of the ECH treated bio-oil, accelerated aging tests were performed at 80°C for 48 h. SEC and viscosity measurement were used to characterize the bio-oil before and after the aging tests.

Control aging test was first performed on the water-soluble bio-oil without ECH treatment. Size exclusion chromatography was used to analyze the molecular weight distribution before and after aging for the water-soluble bio-oil in the control aging experiment. The molecular weight of the carbohydrates did not change very much after aging (Figure 6.5 (a)), however, the molecular weight of lignin derived compounds increased

significantly as a big peak showed up before 14 min (Figure 6.5 (b)). Reactions of phenol or substituted phenols with aldehydes to form resin are possible reasons for the increase of large molecules.[19]

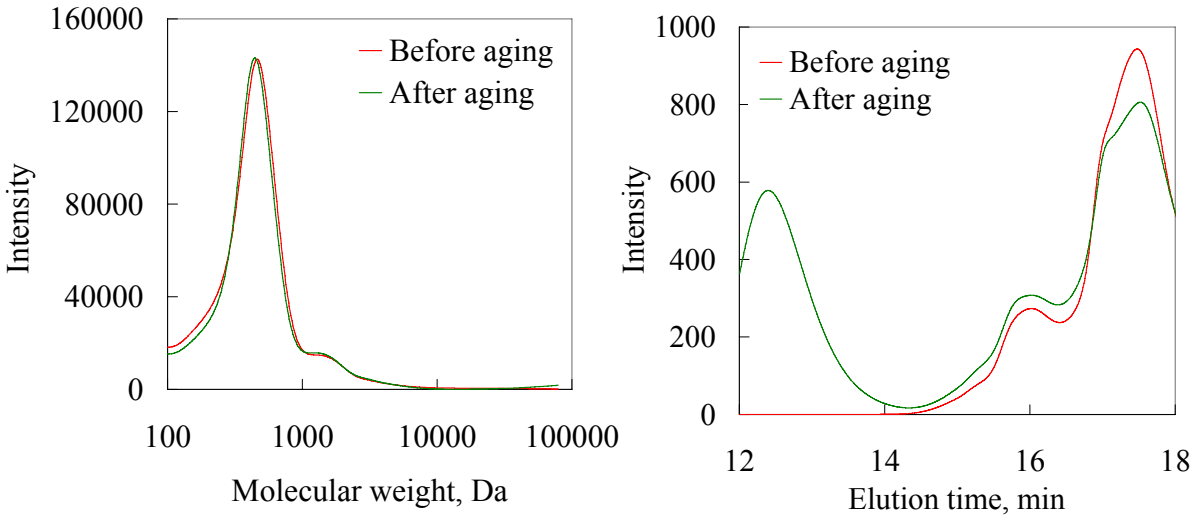

(a) (b)

Figure 6.5 Size exclusion chromatographs of water-soluble bio-oil without ECH treatment before and after aging with (a) IR detector and (b) DAD detector (260nm)

The ECH treated water-soluble bio-oil was also subjected to accelerated aging test. SEC analysis showed that the molecular weights of both the carbohydrates and lignin derived compounds increased slightly (Figure 6.6), however, compared with the water-soluble bio-oil without ECH treatment, the molecular weight of ECH treated bio-oil did not increase very much as no big peak showed up before 14 min for the lignin derived molecules. This indicates ECH treatment can slow bio-oil aging as the carbonyl groups are hydrogenated during the ECH process.

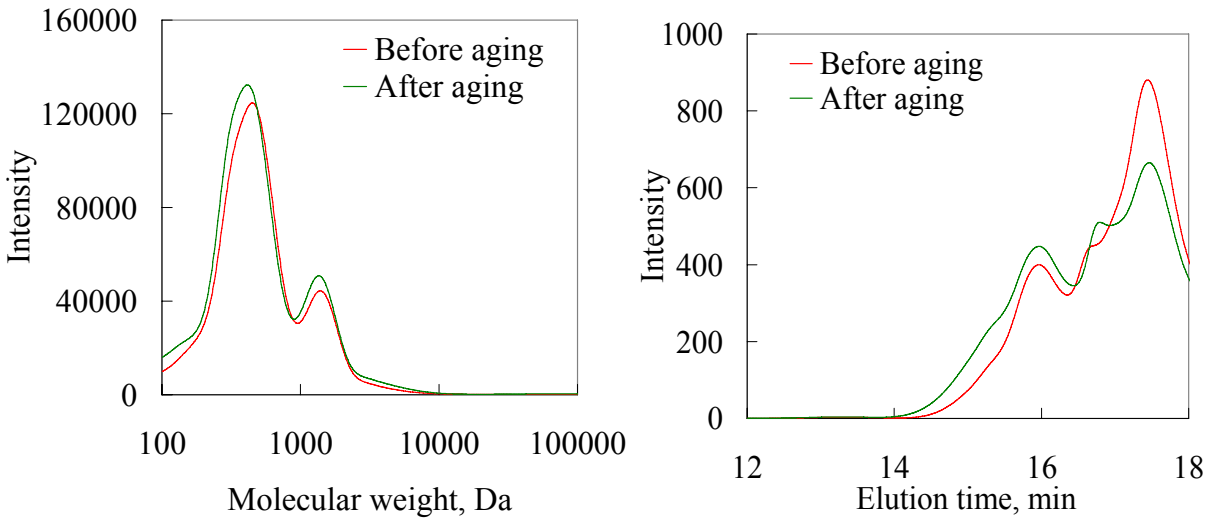

Figure 6.6 Size exclusion chromatographs of water-soluble bio-oil with ECH treatment before and after aging with (a) IR detector and (b) DAD detector (260nm)

Viscosity measurement is a common method to evaluate bio-oil aging. As polymerization takes place during aging, the viscosity will increase as shown in Chapter 2 (Figure 2.12). Figure 6.7 shows the viscosity changes before and after aging. For both bio-oil without and with ECH treatment, aging does not change the viscosity very much. Since the majority of this water-soluble bio-oil was water, some changes of the molecular weight did not affect the viscosity due to the dilution effect of water. Thus for very dilute bio-oil fraction, viscosity measurement may not be a good evaluation approach for aging test.

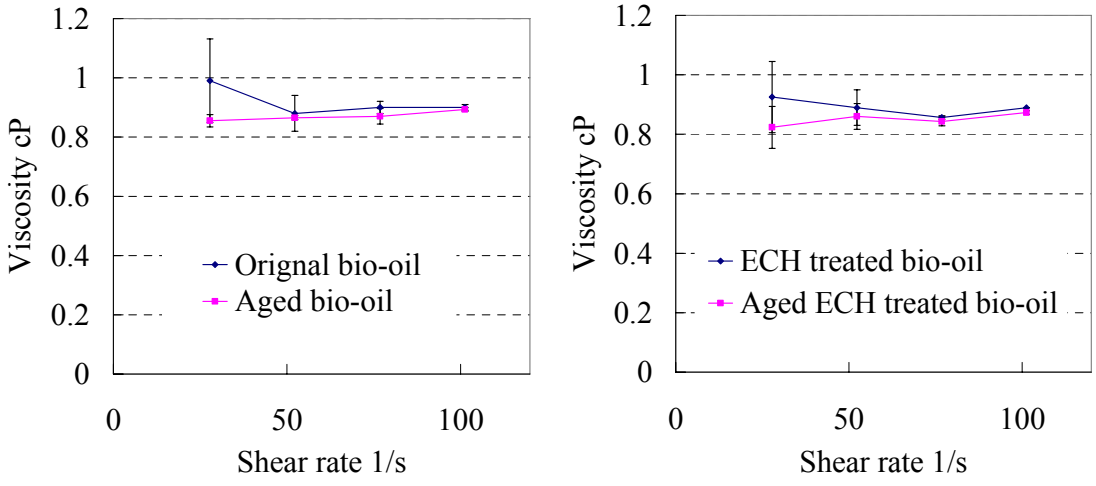

Figure 6.7 Viscosity change for original bio-oil and ECH treated bio-oil after aging for 48 h at 80°C

6.3.2 E.E. for ECH of water-soluble bio-oil and improvement of the E.E. by adding surfactant

Electrochemical efficiency is very important for electrocatalytic hydrogenation of bio-oil because it will influence the energy efficiency and the operation cost. Hydrogen production, a side reaction, is the reason for the low electrochemical efficiency. Water displacement method was used to measure the quantity of hydrogen produced during the 6.5 hr ECH reaction. The electrochemical efficiency was calculated by subtracting the hydrogen production from "100%". At the beginning of the electrocatalytic hydrogenation, the electrochemical efficiency was about 23%. However, it continued to decrease to 7% in the end of the 6.5 hr reaction. The reason for this decrease may be due to the coverage of the catalyst by solids formed during the ECH. As the active sites for the hydrogenation decrease, the hydrogenation rate decreased and the hydrogen production rate increased.

Various methods have been used to improve the E.E. during ECH of various organic compounds.[20,21] Amouzegar and Savadogo [20] showed that catalyst with smaller particle size can improve the electrochemical efficiency to 70% during ECH of phenol with Pt catalyst. Temperature, current density, electrolyte and pH also influence the electrochemical efficiency.[21, 22] Besides that, surfactant was also shown to strongly enhance the efficiency of ECH of unsaturated compounds.[23, 24] The incorporation of the organic substrate in a hydrophobic layer adsorbed on the electrode surface increased the local substrate concentration and this favored the hydrogenation reaction. Cetyltrimethylammonium bromide (CTAB), one cationic surfactant, has been shown to improve E.E. during ECH of limonene and carvone.[25] It was examined here to improve the E.E. for ECH of water-soluble bio-oil.

As seen in Figure 6.8, the E.E. can be improved by 4% to 10% when adding 2 mM CTAB. Further optimization of the CTAB concentration, reaction pH and temperature should be carried out in the future work in order to achieve the maximum improvement of the E.E. Even though the electrochemical efficiency is still not very high, hydrogen, as a valuable product, can be recovered and used in the downstream upgrading, improving the economics of this process.

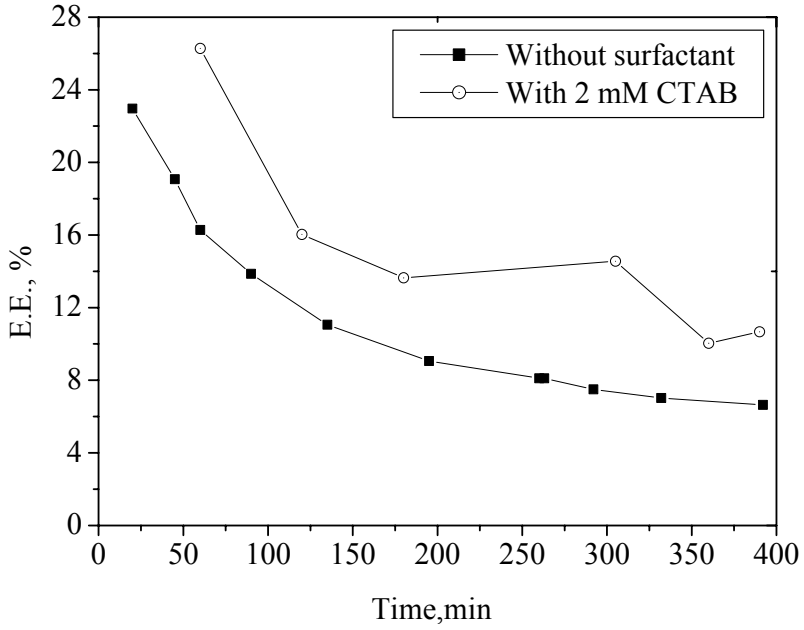

Figure 6.8 Electrochemical efficiency changes vs reaction time with and without surfactant (CTAB) during ECH of water-soluble bio-oil using 3-IW-NH3

6.3.3 Material and energy balance for ECH of water-soluble bio-oil

(1) Material balance

For the above experiments, bio-oil was first extracted using water (bio-oil: water ratio is 1:4), and then the water-soluble fraction was diluted for another two times before going into the ECH cell. The final bio-oil: water ratio is 1:8.73. The material balance is shown in Figure 6.9. According to Figure 6.1, 73% bio-oil is recovered into the water-soluble bio-oil (WSBO) and 27% is separated as pyrolytic lignin. Water-soluble bio-oil is hydrogenated in the cathode side of the two-chamber ECH cell by adding electrolyte 1 (0.2 M NaCl as

electrolyte 1 in the experimental section). Electrolytes are assumed to be stable under the ECH conditions. Water is added into the anode chamber with the mass equal to that of WSBO and water in the cathode chamber. After ECH, the amount of stabilized water-soluble bio-oil (SWSBO) changed compared to the WSBO, including the increase due to hydrogenation and the loss from the migration of small molecules to the anode chamber. The increase is equal to the hydrogen used for the hydrogenation (0.005 Kg), calculated by the difference between theoretical hydrogen yield and measured hydrogen yield (measured by water displacement). Loss of SWSBO is not known and assumed to be x percentage of WSBO. Thus the final SWSBO is (0.73(1-x%)+0.005) Kg (Figure 6.10). As the bio-oil loss increased from 0 to 20%, the final SWSBO decreased from 0.74 Kg to 0.59 Kg. Oxygen is also produced in the anode chamber (0.58 Kg) due to the oxidation of water, resulting in water decrease in the anode chamber. The water loss is calculated based on generated oxygen according to:

$2H_2O \rightarrow 2H_2 + O_2$

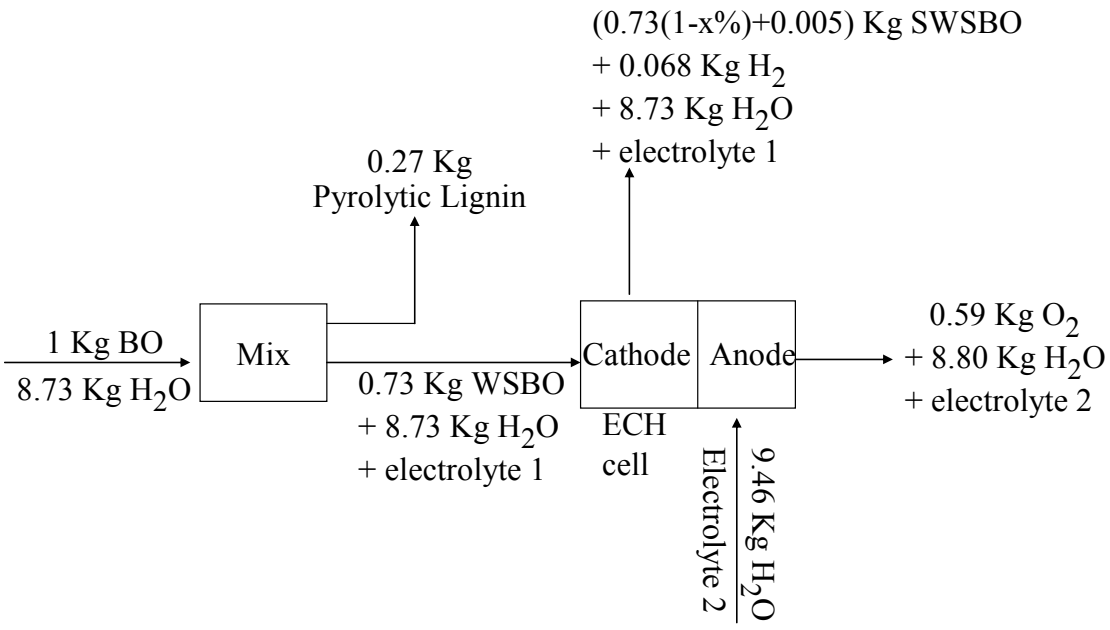

Figure 6.9 Material balance for ECH of water-soluble bio-oil with bio-oil: water at 1:8.73

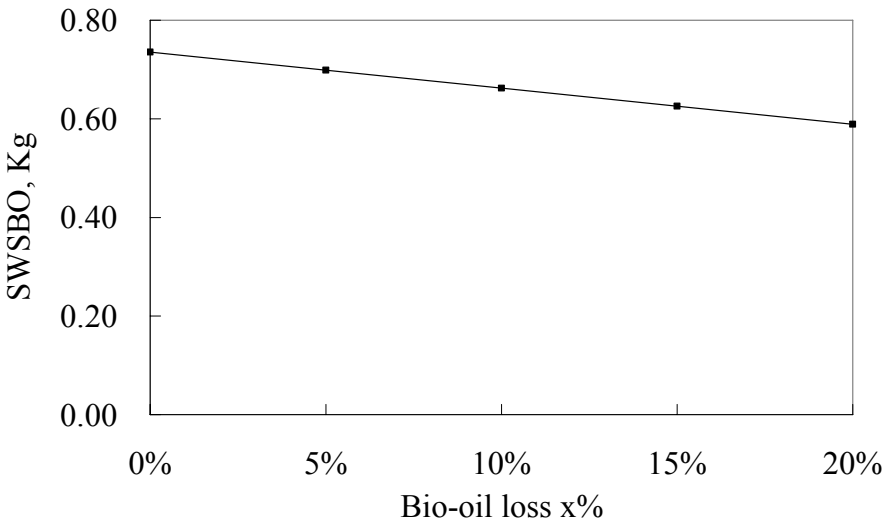

Figure 6.10 SWSBO weight changes with WSBO loss x%

(2) Energy balance

According to the first law of thermodynamics, energy balance for a batch reactor is:

$$\Delta E = \Delta Q - \Delta W$$

Assume there are no significant pressure and volume changes during ECH, the energy change for the ECH system is the change of energy content of the products vs the reactants. The energy balance for the ECH process is (Figure 6.11):

$$E_1 + W_e = E_2 + E_3 + Q_{loss}$$

Where E_1 is the energy content of the WSBO; W_e is the electrical energy input to the ECH system, and W_e can be calculated according to $W_e = U\ I\ t$, and U is the applied voltage, I is the current and t is the time for the ECH. The average voltage for our current two-chamber ECH cell is 30 volts with the current at 480 mA. For 15g WSBO (6.5 h reaction time), 0.34 MJ electrical energy is required, thus the electrical energy needed for 9.46 Kg BO is about 212.51 MJ. The energy content of SWSBO (E_2) is contributed by the loss of WSBO and hydrogenation, thus $E_2 = 5.6(1\text{-}x\%) + 0.7$, where 5.6 MJ is E_1, 0.7 MJ is the energy content of hydrogen added into the SWSBO.

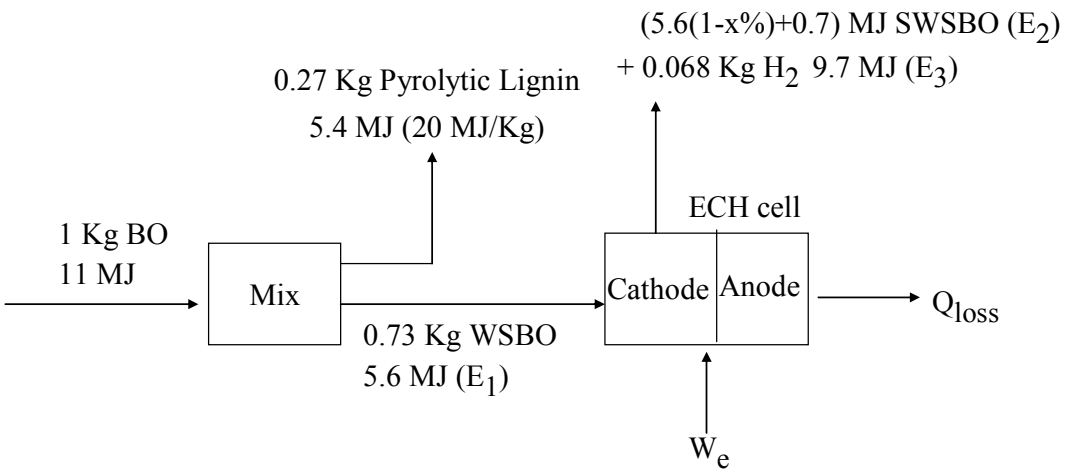

Figure 6.11 Energy balance for ECH of water-soluble bio-oil with bio-oil: water at 1:8.73

Two energy efficiencies were calculated to evaluate the ECH system. Energy efficiency 1 (η_1) = $(E_2-E_1)/W_e$; and Energy efficiency 2 (η_2) = $(E_2+E_3-E_1)/W_e$. These efficiencies were calculated and shown in Table 6.7. Both energy efficiencies are very low and Q_{loss} is the major reason, including the energy loss due to heating the solution and membrane (solution and membrane resistance), energy loss due to the electrode overpotential and WSBO loss. For the current two-chamber ECH cell design, solution resistance is regarded as an important resistance since the two electrodes are far away from each other. Solid polymer electrolyte ECH cell could be a method to reduce the solution resistance and the improvement of the energy efficiency by using different cell design will be discussed next.

Table 6.7 E_2, Q_{loss}, η_1 and η_2 change with WSBO loss

WSBO loss	E_2 MJ	Q_{loss} MJ	Energy efficiency 1 (η_1)	Energy efficiency 2 (η_2)
0%	6.33	202.10	0.3%	4.9%
5%	6.05	202.38	0.2%	4.8%
10%	5.77	202.66	0.1%	4.6%
15%	5.49	202.94	-0.1%	4.5%
20%	5.21	203.22	-0.2%	4.4%

6.3.4 Optimization of the ECH process

(1) Improvement of the energy efficiency

Solid polymer electrolyte ECH cell can be used to reduce the electrodes distance and decrease the solution resistance significantly. With the development of the optimized cell design, the applied voltage can be greatly reduced and the energy efficiencies will be increased. Figure 6.12 shows how the energy efficiencies change with the decrease of applied voltage. As the voltage decreases to 2 V, the energy efficiencies increased to 3.1% and 72% assuming WSBO loss is 5%. Energy efficiency 2 (η_2) is optimized to a very high level, however, energy efficiency 1 (η_1) is still very low. This is due to the low electrochemical efficiency, resulting in lots of hydrogen as byproduct.

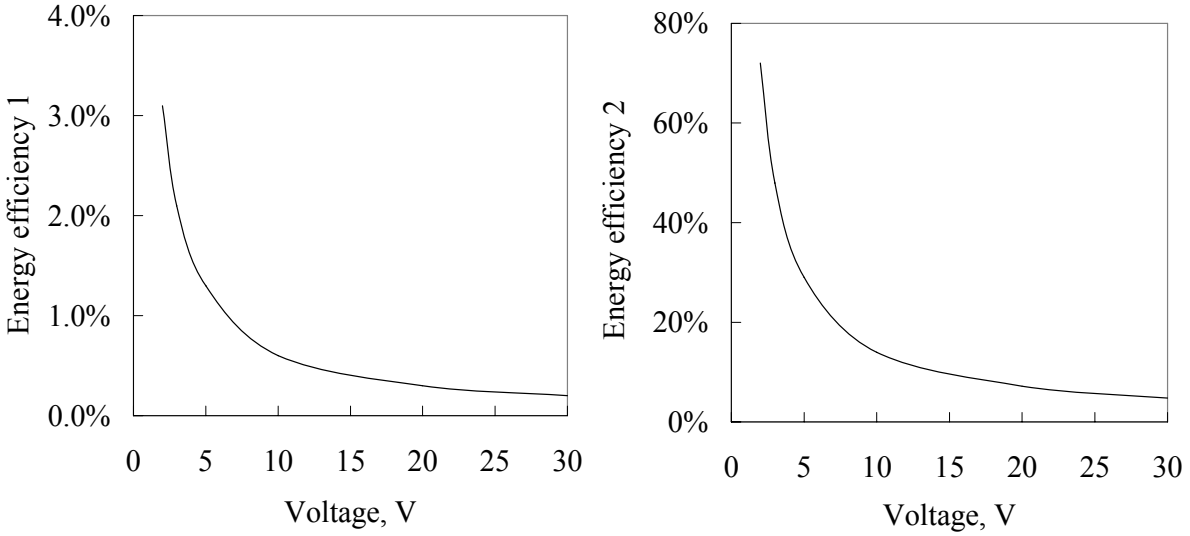

Figure 6.12 Energy efficiency 1 and 2 change with the applied voltage. (Assuming WSBO loss is 5%)

As mentioned in section 6.3.2, E.E. can be improved by optimization of the catalysts, reaction conditions (temperature, pH, electrolyte, current density) and by adding surfactants. Figure 6.13 shows how the energy efficiencies change with the electrochemical efficiency. Both of these energy efficiencies have linear relationships with E.E. As the E.E. increases

from 7% to 98%, energy efficiency 1 increased from 3.1% to 45%, while energy efficiency 2 decreased from 72% to 45%. As continuing to reduce the electrode overpotential and WSBO loss, the energy efficiencies can be further improved.

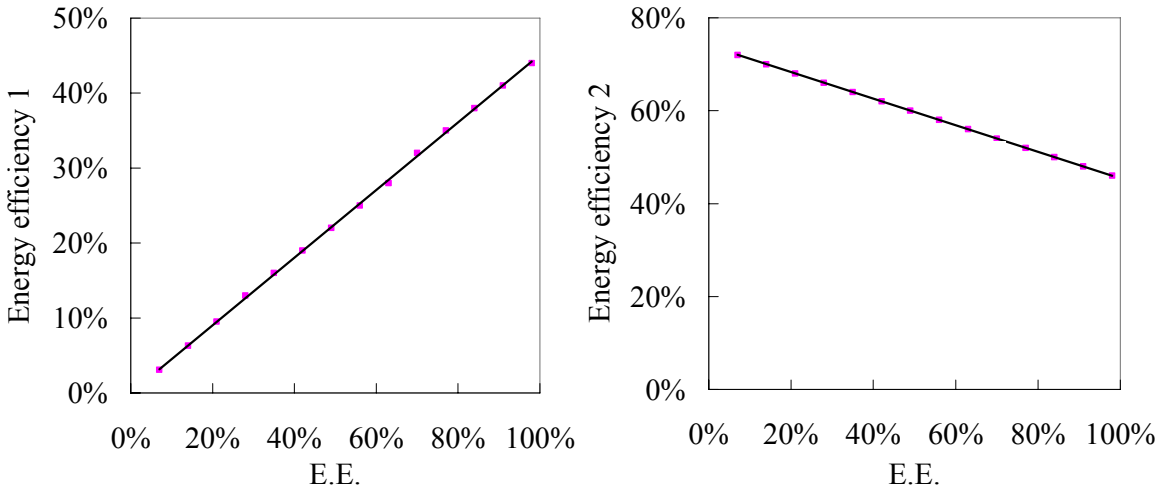

Figure 6.13 Energy efficiency 1 and 2 change with the E.E. (Assuming WSBO loss is 5% and applied voltage is 2 V.)

(2) Reduction of the water use

Large amount of water is used in the above scenario, resulting in a high cost for the downstream products separation and causing environmental concern. Much less water can be used to separate bio-oil as phase separation occurs when bio-oil: water ratio is 8:1. Figure 6.14 shows the material balance for ECH of water-soluble bio-oil with bio-oil: water at 8:1. Water use can be reduced from 18.19 Kg (bio-oil: water, 1:8.73) to 0.90 Kg (bio-oil: water, 8:1) per Kg of bio-oil. The final organics concentration can also be greatly increased and this will help to reduce the cost of the final products separation if needed.

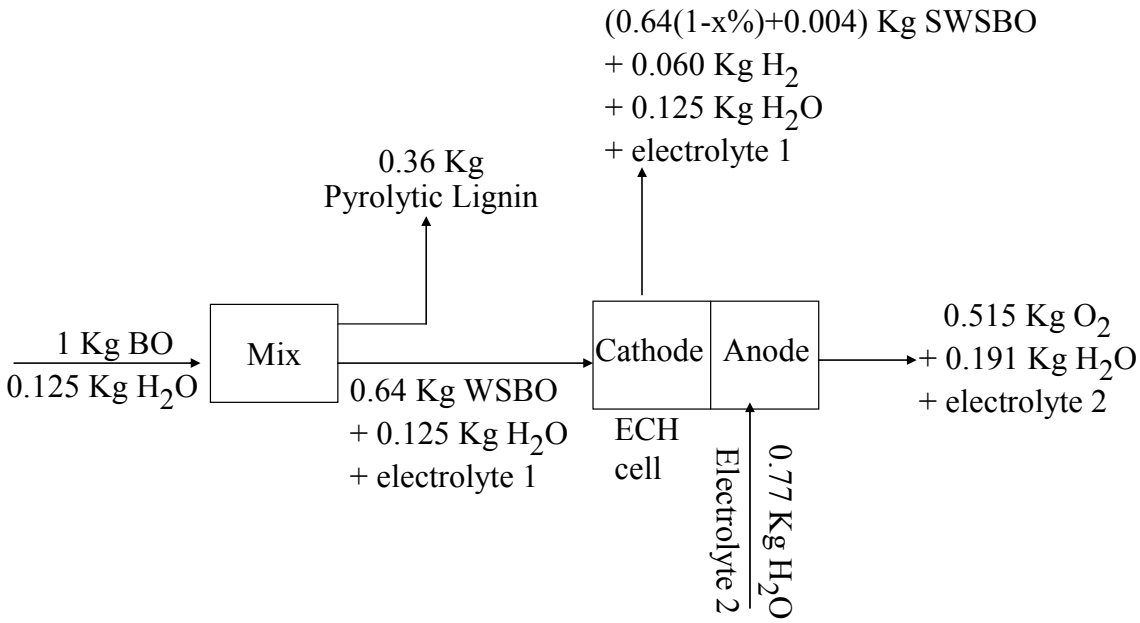

Figure 6.14 Material balance for ECH of water-soluble bio-oil with bio-oil: water at 8:1.

By performing the material and energy balance for ECH of water-soluble bio-oil, we can find out that the energy efficiencies are quite low due to the current two-chamber ECH cell design as this cell is just used to demonstrate the proof of concept. For the future work, optimization of the cell design and improvement of the catalyst and reaction conditions can be performed to reduce the applied voltage and improve the electrochemical efficiency, and then much better energy efficiencies can be achieved.

6.4 Conclusions

Electrocatalytic hydrogenation can convert most of the aldehydes and ketones in the bio-oil to the corresponding alcohols. SEC analyses showed that bio-oil with ECH treatment is more stable compared with bio-oil without ECH treatment. A better carbon recovery (>80%) into the liquid phase was also obtained during ECH of water-soluble bio-oil. Solids were observed during electrocatalytic hydrogenation, however, the amount of solid (less than 0.1 wt%) was much less compared with that from catalytic hydrogenation of bio-oil. Valuable

products, such as hydrogen, ethylene glycol and propylene glycol, can be recovered after electrocatalytic hydrogenation of water-soluble bio-oil. Thus, electrocatalytic hydrogenation can be one of the best approaches to upgrade this water-soluble bio-oil fraction into stable fuel intermediates and valuable chemicals. This method can be extended to other high concentration water-soluble bio-oils with much less water content. Whole bio-oil is also expected to be stabilized using ECH if proper electrolyte or cell design is used.

Acknowledgements

The authors would like to thank the Michigan State University Foundation and AgBioResearch for financial support. Assistance provided by Mr. Yan Lyang Pan with TOC analysis is warmly acknowledged.

REFERENCES

REFERENCES

1. T. P. Vispute and G. W. Huber, Green Chemistry, 2009, **11**, 1433-1445.

2. T. Vispute, Ph.D. Dissertation, University of Massachusetts - Amherst, 2011.

3. T. P. Vispute, H. Y. Zhang, A. Sanna, R. Xiao and G. W. Huber, Science, 2010, **330**, 1222-1227.

4. R. H. Venderbosch, A. R. Ardiyanti, J. Wildschut, A. Oasmaa and H. J. Heeres, Journal of Chemical Technology & Biotechnology, 2010, **85**, 674-686.

5. J. Gagnon and S. Kaliaguine, Industrial & engineering chemistry research, 1988, **27**, 1783-1788.

6. F. Huang, W. Z. Li, Q. A. Lu and X. F. Zhu, Chemical Engineering & Technology, 2010, **33**, 2082-2088.

7. F. H. Mahfud, F. Ghijsen and H. J. Heeres, Journal of Molecular Catalysis A: Chemical, 2007, **264**, 227-236.

8. F. H. Mahfud, S. Bussemaker, B. J. Kooi, G. H. Ten Brink and H. J. Heeres, Journal of Molecular Catalysis A: Chemical, 2007, **277**, 127-136.

9. L. Busetto, D. Fabbri, R. Mazzoni, M. Salmi, C. Torri and V. Zanotti, Fuel, **90**, 1197-1207.

10. Z. Li, S. Kelkar, C. H. Lam, K. Luczek, J. E. Jackson, D. J. Miller and C. M. Saffron, Electrochimica Acta, 2012, **64**, 87-93.

11. R. K. Sharma and N. N. Bakhshi, Energy & fuels, 1993, **7**, 306-314.

12. F. de Miguel Mercader, M. J. Groeneveld, S. R. A. Kersten, C. Geantet, G. Toussaint, N. W. J. Way, C. J. Schaverien and K. J. A. Hogendoorn, Energy Environ. Sci., 2011, **4**, 985-997.

13. S. K. Sikdar, Separation Science and Technology, 1986, **21**, 941-951.

14. S. K. Sikdar, Journal of membrane science, 1985, **23**, 83-92.

15. Q. M. Huang, Q. L. Zhang, H. L. Huang, W. S. Li, Y. J. Huang and J. L. Luo, Journal of Power Sources, 2008, **184**, 338-343.

16. D. W. Kim, H. S. Choi, C. Lee, A. Blumstein and Y. Kang, Electrochimica acta, 2004,

50, 659-662.

17. A. Kapaka, G. Foti and C. Comninellis, Journal of the Electrochemical Society, 2008, **155**, E27.

18. N. M. Markovic, H. A. Gasteiger, P. N. Ross, X. Jiang, I. Villegas and M. J. Weaver, Electrochimica acta, 1995, **40**, 91-98.

19. J. P. Diebold, I. Thermalchemie and L. National Renewable Energy, *A review of the chemical and physical mechanisms of the storage stability of fast pyrolysis bio-oils*, National Renewable Energy Laboratory Golden, CO, 2000.

20. K. Amouzegar and O. Savadogo, Journal of applied electrochemistry, 1997, **27**, 539-542.

21. A. Roessler, O. Dossenbach and P. Rys, Journal of the Electrochemical Society, 2003, **150**, D1-D5.

22. P. Dabo, A. Cyr, J. Lessard, L. Brossard and H. Menard, Canadian journal of chemistry, 1999, **77**, 1225-1229.

23. H. Ilikti, N. Rekik and M. Thomalla, Journal of applied electrochemistry, 2004, **34**, 127-136.

24. H. Ilikti, N. Rekik and M. Thomalla, Journal of applied electrochemistry, 2002, **32**, 603-609.

25. P. Chambrion, L. Roger, J. Lessard, V. Beraud, J. Mailhot and M. Thomalla, Canadian journal of chemistry, 1995, **73**, 804-815.

Chapter 7 Conclusions and Future Work

7.1 Conclusions

To apply fast pyrolysis in the RBPDs, a new screw-conveyor pyrolysis reactor was designed with several advantages, including no requirement for heating media and no need for large amount of inert gas, compactness and transportability. About 50 wt% bio-oil was produced from this reactor with poplar as biomass feedstock, and the temperatures for the three heating zones were set at 350°C, 450°C and 450°C. This bio-oil was characterized using GC/MS, HPLC, proximate analysis and ultimate analysis. Bio-oil stability was also investigated using accelerated aging test. Electrocatalytic hydrogenation was studied as an effective way for bio-oil stabilization. Model compound, furfural, was studied using a nickel sacrificial anode in an undivided cell. Catalytic cathode, pH, reactant concentration and current density were found to have great effects on furfural conversion and electrochemical efficiency. Phenolic compounds were also investigated using a newly designed electrocatalyst, ruthenium supported on activated carbon cloth. Incipient wetness impregnation and cation exchange methods were employed to prepare the electrocatalysts using three different ruthenium precursors. Catalysts prepared by cation exchange were more active than those prepared using incipient wetness impregnation, presumably because of support surface functionalization by the oxidation pretreatment. Temperature was an important variable for the electrochemical efficiency during guaiacol reduction. The E.E. increased from 8% at 25°C to 17% at 50°C, but then dropped back to 10% at 80°C. Solution pH also affected catalyst activity and product selectivity, with acidic conditions favoring guaiacol conversion, electrochemical efficiency and cyclohexanol selectivity. The Ru/ACC catalyst was chosen to

stabilize the real bio-oil, water-soluble bio-oil. After 6.5 h ECH at 480 mA, most of the carbonyl groups were converted to the corresponding alcohols. The hydrogenated water-soluble bio-oil showed better stability than that without ECH treatment. Based on these results, electrocatalytic hydrogenation was shown to be an effective alternative way for bio-oil stabilization/upgrading.

7.2 Future work

To further explore electrocatalytic hydrogenation as a promising bio-oil upgrading method, the following works are recommended for the future research:

(1) Currently the electrochemical efficiency is still low, especially for ECH of real bio-oil. The choice of metallic catalyst is very important for the E.E. Thus other metals should be investigated to prepare catalyst on the activated carbon cloth, such as Pd, Pt, Ni, Cu, etc.

(2) Bimetallic metals usually show better activity and product selectivity. Preparation of bimetallic catalysts by adding metals with high hydrogen overpotential may increase the electrochemical efficiency.

(3) Besides incipient wetness impregnation and cation exchange, other catalyst preparation methods should be explored to improve the metal dispersion, such as immobilizing metal nanoparticles onto electrode support.

(4) Modeling study for ECH of bio-oil model compounds should be performed to identify the rate-limiting step and set up kinetics model.

(5) Whole bio-oil without adding water should be studied by choosing proper solvent or carrying out in the solid polymer electrolyte electrochemical cells.

(6) Electrocatalytic upgrading with relatively high temperature and pressure should be explored to further upgrade the bio-oil to commercial hydrocarbon fuels; proper electrochemical cell should be designed.